Dissertation

SUBMITTED TO THE

Combined Faculties of the Natural Sciences and Mathematics
of the Ruperto-Carola-University of Heidelberg, Germany

FOR THE DEGREE OF

Doctor of Natural Sciences

Put forward by

Nicolas Teeny

born in Zahle, Lebanon

Oral examination: October 18th, 2016

Tunneling Time, Exit Time and Exit Momentum in Strong Field Tunnel Ionization

Referees:

Honorarprof. Dr. Christoph H. Keitel
Prof. Dr. Andreas Mielke

Zusammenfassung

Tunnelionisation gehört zu den grundlegenden Prozessen in der Atomphysik. Es ist bis heute noch nicht klar, wann ein Elektron ionisiert und wie lang dieser Tunnelprozess dauert. In dieser Arbeit lösen wir die zeitabhängige Schrödingergleichung und wenden *ab initio* Quantenberechnungen an, um diese Fragen zu beantworten. Zusätzlich, durch Nutzen von Quantengrundprinzipien, legen wir den Ausgangsimpuls vom tunnelionisierten Elektron fest. Dadurch finden wir heraus, dass die Annahmen des oft angewendeten two-step Modells unpräzis sind. Es wird in dem two-step Modell angenommen, dass das Elektron am Zeitpunkt des Maximums des elektrischen Feldes mit verschwindendem Impuls tunnelionisiert. Nach der Berechnung der Wahrscheinlichkeitsverteilung des Endimpulses zeigen wir, dass das two-step Modell nicht den korrekten Endimpuls voraussagen kann. Aus diesem Grund leiten wir ein modifiziertes two-step Modell her, das den korrekten Endimpuls voraussagen kann. Außerdem bestimmen wir einen Zeitpunkt, an dem die Tunnelionisation anfängt. Dieser Zeitpunkt unterscheidet sich von dem Zeitpunkt des Maximums des elektrischen Feldes. Durch die Bestimmung des wahrscheinlichsten Zeitpunktes, an dem das Elektron in die Tunnelbarriere eintritt, und des wahrscheinlichsten Zeitpunktes, an dem das Elektron ionisiert, definieren wir eine wahrscheinlichste Tunnelzeit. Darüber hinaus koppeln wir eine Quantenuhr an das Elektron, um die Dauer des Tunnelprozesses zu messen. Mithilfe der Quantenuhr berechnen wir eine durchschnittliche Tunnelzeit, die sich in Größe und Ursprung von der wahrscheinlichsten Tunnelzeit unterscheidet. Um beide Tunnelzeiten zuzuordnen und die scheinbare Differenz zu erklären, definieren wir eine Wahrscheinlichkeitsverteilung der Tunnelzeiten durch virtuelle Detektoren. Die Ergebnisse in dieser Arbeit haben allgemein einen Einfluss auf die Interpretation und Auswertung von Experimenten, welche das Impulsspektrum der tunnelionisierten Elektronen messen, weil üblicherweise Modelle mit unpräzisen Annahmen angewendet werden, um experimentelle Ergebnisse zu interpretieren. Besonders haben sie Einfluss auf die Kalibrierung der sogenannten Attoclock Experimente.

Abstract

Tunnel ionization belongs to the fundamental processes of atomic physics. It is still an open question when does the electron tunnel ionize and how long is the duration of tunneling. In this work we solve the time-dependent Schrödinger equation in one and two dimensions and use *ab initio* quantum calculations in order to answer these questions. Additionally, we determine the exit momentum of the tunnel ionized electron from first principles. We find out results that are different from the assumptions of the commonly employed two-step model, which assumes that the electron ionizes at the instant of electric field maximum with a zero momentum. After determining the quantum final momentum distribution of tunnel ionized electrons we show that the two-step model fails to predict the correct final momentum. Accordingly we suggest how to correct the two-step model. Furthermore, we determine the instant at which tunnel ionization starts, which turns out to be different from the instant usually assumed. From determining the instant at which it is most probable for the electron to enter the tunneling barrier and the instant at which it exits we determine the most probable time spent under the barrier. Moreover, we apply a quantum clock approach in order to determine the duration of tunnel ionization. From the quantum clock we determine an average tunneling time which is different in magnitude and origin with respect to the most probable tunneling time. By defining a probability distribution of tunneling times using virtual detectors we relate both methods and explain the apparent discrepancy. The results found have in general an effect on the interpretation of experiments that measure the spectra of tunnel ionized electrons, and specifically on the calibration of the so called attoclock experiments, because models with imprecise assumptions are usually employed in order to interpret experimental results.

Within the framework of this thesis, the following articles were published in refereed journals:

- ***Ionization Time and Exit Momentum in Strong-Field Tunnel Ionization***
  Nicolas Teeny, Enderalp Yakaboylu, Heiko Bauke and Christoph H. Keitel
  Physical Review Letters **116**, 063003 (2016)
- ***Virtual-detector approach to tunnel ionization and tunneling times***
  Nicolas Teeny, Christoph H. Keitel and Heiko Bauke
  Physical Review A **94**, 022104 (2016)

Articles submitted for publication in refereed journals:

- ***Salecker-Wigner-Peres quantum clock applied to strong-field tunnel ionization***
  Nicolas Teeny, Christoph H. Keitel and Heiko Bauke
  arXiv:1608.02854 (2016)

Articles in preperation:

- ***Correction of the two-step model***
  Enderalp Yakaboylu, Nicolas Teeny, Heiko Bauke and Christoph H. Keitel

„The most valuable of all education is the ability to make yourself do the thing you have to do, when it has to be done, whether you like it or not.“

—Aldous Huxley

To the memory of my beloved grandmother

Salwa Greigiry Teeny

Contents

1. Introduction **1**

2. Theoretical background and basics **7**
2.1. Quantum tunneling and time 7
2.2. Tunnel ionization in strong fields 11
2.3. Two-step model 14
2.4. Attoclock experiment 15
2.5. Virtual detector 17
2.6. Electric field pulse and gauge invariance 20
2.7. Numerical techniques 21
2.7.1. The split operator method 23
2.7.2. The Lanczos algorithm 25
2.7.3. Quantum clock numerical application 27
2.8. Conclusion 29

3. Tunnel ionization in one dimension **31**
3.1. Introduction 31
3.2. Considered system 32
3.3. Tunneling exit determination 35
3.4. Tunneling exit time 35
3.5. Exit momentum 38
3.6. Two step-model applicability 39
3.7. Modified two-step model 40
3.8. Conclusion and implications 41

4. Tunnel ionization in two dimensions **43**
4.1. Introduction 43
4.2. Considered system 45
4.3. Tunneling region determination and realization of the virtual detectors 46
4.4. Exit time and time spent under the barrier 48
4.5. Quantum and classical trajectories 52
4.6. Conclusions 55

5. Salecker-Wigner-Peres quantum clock applied to tunnel ionization **57**
5.1. Introduction 57
5.2. Considered system 58
5.3. The Salecker-Wigner-Peres quantum clock 59

5.4. Coupling of the SWP quantum Clock and its calibration 60
5.5. Measurement procedure of the SWP quantum clock in tunnel ionization 62
5.6. Results and interpretation 65
5.7. Virtual detector method and average tunneling time 67
5.8. Conclusion 71

6. Summary and outlook **73**

Appendices **77**

A. The Coulomb problem and the Strak effect in two dimensions **79**

Bibliography **83**

Acknowledgments **93**

Chapter 1.

Introduction

In quantum mechanics there are phenomena that have no classical analogs. These phenomena are interesting to study because they give us insight about the quantum world that is unreachable through common sense. In 1927 Friedrich Hund (1896–1997) was the first to notice the possibility of the phenomenon of tunneling, which he called barrier penetration, in a calculation of the ground state in a double-well potential [1, 2]. In general tunneling occurs when a particle approaches a region having a potential higher than its energy, i.e., approaches a potential barrier. According to classical mechanics the particle will either be reflected or be stopped when reaching such a region. In quantum mechanics the particle has a probability to tunnel through the potential barrier, see Fig. 1.1. Quantum tunneling is a very fundamental process which occurs in many fields of physics like tunneling diodes [3–6], or tunneling microscopy [7, 8], tunneling in Bose-Einstein condensates [9–12] and many other fields. Although quantum tunneling is very fundamental and is applied in many technologies in our everyday life there is still an important aspect of it not understood till today. Namely, what is the time associated with the tunneling process. Historically, quantum tunneling time was investigated by studying the case of a particle approaching from far away a potential box, see Fig. 1.1. Also in textbooks the phenomenon of quantum tunneling is introduced through this example, see Ref. [13]. Thus one asks the question: How long does it take for a particle to travel through the potential barrier?

The difficulty in answering such a question is two fold. First, since tunneling is a quantum phenomenon and has no classical analog, it is not possible to answer time questions by using classical arguments. Second, in quantum mechanics when one wants to measure a physical observable O, a corresponding quantum operator $\hat{O}$ is defined and the measurement of the observable is defined via $\langle\psi|\,\hat{O}\,|\psi\rangle$ where $|\psi\rangle$ is the quantum state of the system. In quantum mechanics there is no such operator $\hat{t}$, such that one could measure the time observable. In classical mechanics the generators of translations in space and time are the total momentum P and the total energy H, respectively [14, 15]. In quantum mechanics the position operator of a particle $\hat{\boldsymbol{q}}$ is conjugate to the momentum operator $\hat{\boldsymbol{p}}$ and they satisfy the commutation relations

$$[\hat{q}_i, \hat{p}_j] = i\hbar\delta_{ij}. \tag{1.1}$$

where the indexes denote the components in Cartesian coordinates. In quantum mechanics one could try to define a time operator $\hat{t}$ which is conjugate to the particle's

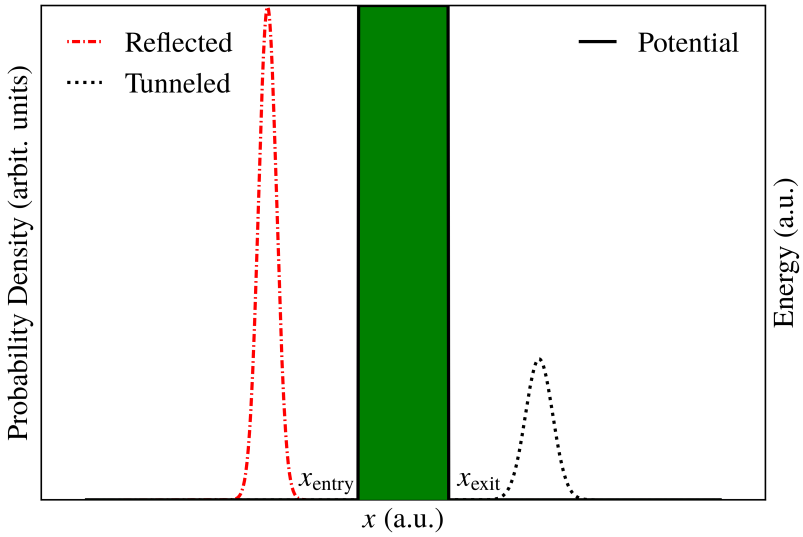

Figure 1.1.: Schematic of a wave packet which was originally incident from far left, with a kinetic energy less than the potential height, a square potential. The wave packet scatters on the square potential marked by the green shadowed area, one part is reflected (red dashed line) while the other tunnels through the barrier (black dotted line).

Hamiltonian $\hat{H}$ which is the generator of translations in time. In accordance with the space momentum relations, such an operator should also satisfy the following commutation relation

$$\left[\hat{t}, \hat{H}\right] = i\hbar. \tag{1.2}$$

As pointed out by Pauli [16], such an operator should have an unbounded spectrum $[-\infty, +\infty]$ since the time variable can take any value in the space of real numbers $\mathbb{R}$, which causes problems since the spectrum of a physically meaningful Hamiltonian is bounded from below and the operators $\hat{H}$ and $\hat{t}$ are conjugate [17]. Defining such an operator is still debated and there is no consensus on its definition [15, 17–21]. In this thesis, the existence or non existence of such an operator, which is an interesting question, is not discussed. From the above discussion, one can see that asking time questions in quantum mechanics is not straightforward and thus many approaches and techniques have been applied in the case of a particle approaching from far away a potential box in order to define tunneling times.

A possible and very intuitive approach is to determine the tunneling time by following the center of gravity of the transmitted wave packet [22]. The associated time, however, has little physical significance as argued in Ref. [23]. The second class of approaches constructs a set of dynamical paths and determines how much time each path spends under the barrier. Then, one can define the most probable time spent under the barrier, corresponding to the most probable path, or an average time spent under the barrier by taking an average over all paths. Among others, this approach is realized by three methods: the Bohm method as described in Refs. [24, 25] and references therein, the Feynman path integrals method as applied in Refs. [25–

27], and finally the Wigner distribution paths method as studied in Refs. [28–30]. Time is not only a coordinate of the universal space-time background where physical processes take place. Time can also be introduced as a dynamical variable of physical systems that clock a certain process [15]. This leads to the last category of approaches to define a tunneling time. In the so-called quantum clock approach, an additional physical system is coupled to the system which undergoes the tunneling dynamics [31–36]. Then either a dynamical variable of the coupled system acts as a clock or the accessory system may have an explicit time dependence with a given time scale, which provides a reference for time measurements [37, 38]. Depending on how temporal quantities are extracted from the clock system, the quantum clock approach gives rise to definitions of various times which characterize the tunneling dynamics. A detailed revision of these approaches is given in chapter 2, where also the fundamental ideas needed to understand this thesis are presented.

Another example which is interesting to consider for investigating tunneling times and which is experimentally accessible is tunnel ionization. Keller *et al.* have conducted experiments using the angular streaking technique aiming to measure tunneling times for ionization from a bound state, the so-called attoclock experiments [39, 40]. In the tunnel ionization case, a Coulomb-bound electron is ionized by a strong electromagnetic field, and a potential barrier can be defined via the electron's binding energy and the Coulomb potential bent by the electric field's potential. Since the attoclock experiments have been performed, many renewed efforts have been directed toward defining a tunnel ionization time, because a consensus on a suitable theoretical definition of tunneling time and the interpretation of experimental results is still lacking [17, 39–45]. The main difference between tunneling of free particles and tunnel ionization is that in the latter the particle is initially bound. In particular, there is some part of the wavefunction of the bound electron that already lies under the barrier in contrast to approaching the barrier from far away.

Though for studying tunneling times in tunnel ionization theoretically, many approaches can be adopted from tunneling of free particles. For example, the Wigner time approach [46–48] was applied to tunnel ionization in the adiabatic limit in Refs. [49, 50]. The adiabatic limit corresponds to a parameter regime where the time scale of the tunneling dynamics is short compared to the time scale of the variation of the electric field. Calculating the complex transmission amplitude as a function of the barrier height and the electron energy, various theoretical definitions of tunneling times can be introduced, often referred to as Büttiker Landauer time, Pollack Miller time, Eisenbud Wigner time, and Lamor time. These have been compared to experimental results in Ref. [51].

To my knowledge none of the above mentioned approaches has been applied dynamically to tunnel ionization, i. e., taking into account the continuous increase and decay of the external driving electric field as it is the situation in an experimental setting. Often the external field is treated as static [49] or switched on instantaneously [42, 52]. As emphasized in Ref. [42], tunneling in a continuously evolving potential is very different from the sudden turn-on case. In particular, there is no natural reference point in time which defines when tunneling begins. Furthermore,

the quantum state at the onset of tunneling is no longer the ground state of the unperturbed binding potential. When tunneling sets in, the wavefunction has already evolved in the time-dependent potential.

One of the main accomplishments in this thesis is adopting the Salecker-Wigner-Peres quantum clock [31, 34] to tunnel ionization taking into account the continuous evolution of the driving electric field to determine tunneling times, which is achieved in chapter 5. The Salecker-Wigner-Peres quantum clock is coupled to the electron in such a way that it measures the average time spent by the electron under the barrier. Where we have defined in chapter 5 through the Salecker-Wigner-Peres quantum clock an average tunnel ionization time spent under the barrier by electrons that tunnel ionize, and an average time spent by electrons that do not undergo tunneling ionization, i.e., a reflection time.

Another problem that we investigate in this thesis is when does the electron exit the tunnel ionization barrier. Experimentally the quantum dynamics in the vicinity of the tunneling barrier cannot be studied directly, i. e., it is not possible to place a detector close to the atomic tunneling barrier. Thus, information about the tunneling dynamics has to be inferred from measurable asymptotic quantities, e. g., the momentum distribution of the photo ionized electrons. In attoclock experiments, an electron is ionized by an elliptically polarized few-cycle pulse. This quasi-free electron is accelerated in the rotating electric field, and in this way the instant of ionization t_{exit} is mapped to the final angle of the momentum vector in the polarization plane. The mapping is carried out by using some theoretical model that predicts the final momentum of the tunnel ionized electrons [51, 53–55]. Thus, the interpretation of attoclock experiments requires a precise model of the electron's motion from the barrier exit to the detector. The value of a possible tunneling delay depends crucially on the theoretical model [55], which is employed to calibrate the attoclock. In the extraction of t_{exit} from attoclock experiments, it is state of the art to treat the ionized electron classically, to take into account Coulomb corrections, and to assume that the electron's initial momentum follows from some semiclassical theory [51, 53]. For a reliable reconstruction of the time t_{exit}, however, suitable initial conditions have to be identified as pointed out in Refs. [54, 55]. In particular, assumptions about the initial momentum [49, 56] bias the reconstructed value of t_{exit}.

Neither the time t_{exit} nor the initial momentum of the tunnel ionized electron are directly accessible by experiments, and it is also challenging to calculate them analytically. Thus a second accomplishment in this thesis is employing *ab initio* quantum calculations and the virtual detector [57, 58] method at the tunnel exit through which we determine directly the electron's time of arrival at the tunnel exit as well as its exit momentum. This is accomplished for a one-dimensional system that models the essential features of a three-dimensional system in chapter 3, and is also achieved for a two-dimensional system in chapter 4.

In chapter 3 we solve the time-dependent Schrödinger equation in a one-dimensional system and consider an electron bound to the soft-core potential [59–62] to model the essential features of an electron in a three-dimensional Coulomb potential. By

solving the equation and employing *ab initio* quantum calculations we find the instant when the electron exits the tunneling barrier as well as the initial momentum of the tunnel ionized electron for the considered system. Additionally, we also determine the final momentum of the tunnel ionized electron. From these three values we study the applicability and correctness of the famous and commonly employed two-step model [63, 64]. The so-called two-step model, which describes the ionization as instantaneous tunneling at the electric field maximum and classical motion afterward with zero exit momentum, is commonly employed to describe tunnel ionization in adiabatic regimes.

In the case of tunnel ionization the experimental determination of a tunneling time is complicated by the fact that it is notoriously difficult to determine the starting moment of the tunnel dynamics. There is no apparent reason to assume that the electron enters the barrier at the instant of the electric field maximum which is usually assumed in the community. A third accomplishment in this thesis is determining from first principles the instant at which the electron enters the tunneling barrier, which is achieved in chapter 4. In chapter 4 we solve the time-dependent Schrödinger equation in two dimensions and employ *ab initio* quantum calculations, and answer the question when does the electron enter the tunneling barrier. Additionally, we answer the questions: When does the electron exit the tunneling barrier in a similar manner as in chapter 3; and, accordingly, how much time does the electron spend under the barrier? Moreover, we compare the quantum trajectory of the electron to the one predicted by the two-step model [63–66]. Thus a fourth accomplishment in this thesis is showing that the tunnel ionized wave packet does not propagate according to classical equations of motion directly after the exit, this is achieved in chapter 3 for a one-dimensional system and in chapter 4 for a two-dimensional system. With the results found in chapter 4 we do not only confirm the results found for a one-dimensional system in chapter 3 but also we show that the electron does not enter the tunneling barrier at the instant of electric field maximum as usually assumed. The time spent by the electron under the barrier defined in chapter 4 should be understood as the most probable time. Where as the time spent under the barrier determined by the Salecker-Wigner-Peres quantum clock in chapter 5 should be understood as an average time. A fifth accomplishment in this thesis is that we have not only defined the most probable tunneling ionization time from first principles in chapter 4, and that we have defined an average tunneling ionization time from first principles in chapter 5, but we also show that these times are physically meaningful since they do not correspond to superluminal velocities.

Finally in chapter 6 the main results reached in this thesis and their implications are discussed and an outlook on how one can build on this work to gain more information on tunnel ionization time is given.

Chapter 2.

Theoretical background and basics

As we have seen in the introduction many approaches for defining tunneling time have been applied in the case of a free particle approaching a potential barrier. In Sec. 2.1 we briefly review most of the notable techniques that were used to investigate quantum tunneling time for the above mentioned case. In this thesis we investigate tunneling time in the strong field ionization process, because tunnel ionization is experimentally accessible. Thus strong field tunnel ionization is introduced in Sec. 2.2. Moreover, the main concept of the so called attoclock experiment [39, 40] that aims to extract tunneling times in strong field tunnel ionization is discussed in Sec. 2.4. For understanding the experimental procedure it is important before to understand the quite known two-step model of tunnel ionization which is introduced in Sec. 2.3. After understanding the fundamentals of the considered problem, it is also important to understand the techniques applied in this thesis for solving the problem. In this work a new technique is applied to examine tunneling times, the virtual detector approach technique. In Sec. 2.5 the essentials of the virtual detector approach are discussed. For simplifying the interpretation of the virtual detector approach, throughout the whole work we apply a single form of an electric field pulse, its physicality and applicability are discussed in Sec. 2.6. Last but not least, in this thesis the time dependent Schödinger equation is numerically solved, thus the algorithms and numerical techniques applied are reviewed in the last section. By reading this chapter one gains the essential knowledge necessary to understand this thesis.

2.1. Quantum tunneling and time

Although tunneling is a fundamental process in quantum mechanics, there is still no consensus on the definition and interpretation of tunneling time. Tunneling time was first studied [67] in the problem of a particle tunneling through a square potential. In this case, a particle approaches from far away a potential barrier of a height larger than the particle's energy and eventually tunnels through the barrier, see Fig. 1.1, which is a classically forbidden region.

Thus one asks the question: How long does it take for a particle to travel through the classically forbidden region? As stated, described and criticized in Ref. [23], many of the approaches applied to define tunneling times for a particle tunneling through a square potential can be listed into three categories:

Wave packet approach

The first approach invokes following some feature of the incident wave packet, like the peak or a centroid of the packet, as the wave packet goes through the barrier and eventually tunnels. An example of this approach is presented in Ref. [22], where a typical Gaussian wave packet was prepared and sent from far away through the barrier. One can define a time delay τ_{wpa} as the difference between the instant the peak of the tunneling wave packet leaves the tunneling barrier and the instant the peak of the incident wave packet reaches the tunneling barrier. This approach is criticized in [23]. As found out in Ref. [22], the high energy components of the wave packet reach the barrier first, and because of their high energy are transmitted more effectively than later proportions. As a result, one can prepare the wave packet in a such a way, that the peak of the tunneling packet leaves the barrier even before the peak of the incident packet reaches the barrier. This causes τ_{wpa} to be negative violating the law of causality. Moreover, this approach is not useful for defining a time delay in strong field tunnel ionization. In tunnel ionization the electron tunnels from a bound state to a free state, and one cannot follow some peak of a wave packet incident from far away on the barrier.

Dynamical path approach

The second class of approaches determines a set of dynamical paths and asks how much time each path spends under the barrier. From these paths one can define either the most probable time spent under the barrier, corresponding to the most probable path, or an average time spent under the barrier, corresponding to the averaged time spent by the electron through all possible paths. This approach is mainly realized by three methods:

In the Bohm method, described mainly in [24] and references therein, one writes the wave function ψ in the form $\psi = R\exp(iS/\hbar)$ where R is the amplitude. Then S would be the solution of the classical Hamilton-Jacobi equation with the original problem potential V and an additional quantum potential Q. The difference between the Bohm method and the well known Wentzel–Kramers–Brillouin (WKB) approximation is that in the later the quantum potential Q is neglected. One can see, that in the Bohm approach one has a set of classical paths following the Hamiltonian-Jacobi equation and each weighted by R^2. For each classical path one can define a time spent in the classically forbidden region. For a discussion and review of the Bohm method check Ref. [23].

The Feynman path integrals method applied by the authors of Ref. [26] follows from the Feynman path-integral approach to quantum mechanics. Each path $x(t)$ is weighted by $\exp(iS(x(t))/\hbar)$ where $S(x(t))$ is the action of the trajectory $x(t)$. The controversy in the Feynman path integral method is that the weight of each path is in general a complex number. Specifically averaging over the time each trajectory spends under the barrier with a complex weight, leads to a complex average time spent under the barrier. For more explicit discussion see Ref. [23].

The last method is the so called Wigner distribution path method based on the Wigner function is a phase-space distribution function [23, 68]. For a time-independent tunneling barrier, trajectories in phase-space can be determined by demanding that the Wigner function remains constant along these trajectories [23, 69]. These trajectories satisfy then the classical Hamilton equation with a modified quantum potential. Again for each trajectory one can define the time spent under the barrier with a weight given by the Wigner distribution function. For more detailed discussion see Ref. [23].

Clock approach

The last category which is preferred by the authors of Ref. [23] as well as by the author of this thesis, from the above listed approaches, is the clock approach. As pointed out in Ref. [15], that in quantum and classical mechanics one has to make a difference between the time parameter t as a c-number, and dynamical time variables that time a certain process. In both classical and quantum mechanics one needs clocks to time a certain process [15]. In classical mechanics one could determine at each time, the position, velocity, and acceleration of a particle. Suppose there is an analog to quantum tunneling in classical mechanics. Then one can easily define the time spent under the tunneling barrier similarly to the way done by the dynamical path approach. Since one knows when the point particle enters the barrier and when the particle exits the barrier. In classical mechanics such a problem is straight forward since there is a simple relation between time t and the particle's position x. If such a relation does not exist one has to map the position x of the point particle to some dynamical variable θ which could be mapped to time. Such a dynamical variable θ behaves like a clock. One could imagine that in classical mechanics, for timing a complex dynamical process that could not be directly mapped to time, one needs a clock. In quantum mechanics there is no simple relation between the position of the particle and time. The particle is not even point like. Thus measuring tunneling times is also not straight forward as it would be in classical mechanics. Fortunately in quantum systems one can map the dynamics of the particle under the barrier to a dynamically measurable observable $\hat{\theta}$ that could be mapped to time. In other words, one could couple the quantum particle to a quantum clock in order to time its dynamics under the barrier.

There are many ways that one could define clocks in quantum mechanics [70], i.e., map some dynamical process to some dynamical variable which could be mapped to time. Here we list the ones most known in the tunneling time community [23]; the oscillatory tunneling barrier clock [37], a clock measuring the precession of the particle's spin due to a uniform magnetic field applied in the tunneling region which is known as the Larmor clock [33, 35] (and references therein), and finally the Salecker-Wigner-Peres (SWP) quantum clock [31, 34]. Although not all clocks give the same results for a particle tunneling through a square potential, there are lot of overlaps and similarities [23].

In the oscillating barrier clock the originally static barrier is perturbed by an oscillation whose amplitude could be chosen as small as desired. If the particle interaction time with the barrier is smaller than the oscillation frequency the particle would be affected by the perturbation. While if it is much larger, the particle will experience many oscillations such that it feels effectively a static barrier. The frequency at which such a transition from experiencing the oscillation to not experiencing the oscillation occurs, defines the interaction time of the particle with the barrier.

The main idea of the Larmor clock is that due to a constant magnetic field in the tunneling region the spin will precess and one could map this precession to time. On the one hand, the Larmor clock concept is very attractive because in principle electrons have spin and their spin precession could be measured experimentally. On the other hand, in the Larmor clock approach one requires a magnetic field which has a constant value in the tunneling region and zero elsewhere, which is experimentally very challenging to achieve.

The Salecker-Wigner-Peres quantum clock is in concept very similar to the Larmor clock. In fact the Larmor clock is a special case of the more general SWP quantum clock. The Larmor clock is two dimensional whereas the SWP quantum clock could be of any integral dimensionality. This quantum clock is a quantum system that is coupled to the particle in such a way that it only evolve in time when the particle is inside the barrier. The quantum clock in structure is very similar to a classical periodic clock. The SWP quantum clock has been applied to the tunneling through square potential by Ref. [71–73].

To my knowledge none of the above methods has been applied dynamically to the tunnel ionization problem. Note that some of the above mentioned concepts cannot be even applied dynamically. For example the Wigner time approach [46–48] was applied for tunnel ionization by Ref. [49, 50] where the adiabatic limit was considered. In tunnel ionization a time-dependent electric field pulse is considered, and the adiabatic limit means that the electric field pulse changes much slower than the tunneling dynamics. Taking the adiabatic limit and considering that at the instant of electric field maximum one has the highest ionization probability, in Ref. [49, 50] the wavefunction at the instant of field maximum is considered. And many of the above listed approaches have been applied to tunnel ionization in Ref. [51]. In Ref. [51] the wavefunction was propagated till the instant of electric field maximum and considered at that instant for calculating tunneling times. In other words the approaches in [51] have been applied non dynamically. The results were compared to the experimental results of the attoclock experiments. In this thesis, we apply the SWP quantum clock to the problem of tunnel ionization in order to explore tunneling times, where a detailed description of the quantum clock is given in chapter 5.

2.2. Tunnel ionization in strong fields

Tunneling is defined as when a particle having an energy E goes through a region in space where a potential $\hat{V}(\boldsymbol{r})$ exists and such that $E < \hat{V}(\boldsymbol{r})$, where $\boldsymbol{r}$ is a vector in three dimensional space. In classical mechanics, such a process is forbidden since the particle does not possess enough energy to go through such a region and the particle would either reflect or stop when reaching such a region. While quantum mechanically there is a probability that the particle would go through the classically forbidden region. Here we illustrate how the tunneling picture can describe ionization of an electron by an electric field pulse, and under which conditions such a picture is applicable. The Schrödinger equation of an electron bound by a Coulomb potential in an electromagnetic field is written as (in atomic units)

$$i\frac{\partial\Psi(\boldsymbol{r},t)}{\partial t} = \left(\frac{1}{2}\left(-i\boldsymbol{\nabla} + \frac{1}{c}\boldsymbol{A}(\boldsymbol{r},t)\right)^2 - \frac{Z}{|\boldsymbol{r}|} - \phi(\boldsymbol{r},t)\right)\Psi(\boldsymbol{r},t) = \hat{H}\Psi(\boldsymbol{r},t)\,, \quad (2.1)$$

where $\phi(\boldsymbol{r},t)$ and $\boldsymbol{A}(\boldsymbol{r},t)$ denote the electromagnetic potentials of the pulse, $\Psi(\boldsymbol{r},t)$ the wave function of the electron, $\boldsymbol{\nabla}$ is the gradient, Z the atomic number and $-Z/|\boldsymbol{r}|$ is the Coulomb potential. In experiments, a Coulomb-bound electron is usually excited by a laser pulse with a wavelength much bigger than the atomic dimensions such that the laser pulse is nearly homogeneous over the size of the atom and the condition

$$a_0 \ll \lambda \quad (2.2)$$

is satisfied, with a_0 being the Bohr radius and λ the wavelength of the pulse. According to Maxwell's equations the relation between the electromagnetic potentials and the electric field $\boldsymbol{\mathcal{E}}$ and the magnetic field $\boldsymbol{\mathcal{B}}$, which are the physical quantities, is given by (in atomic units)

$$\boldsymbol{\mathcal{E}} = -\boldsymbol{\nabla}\phi(\boldsymbol{r},t) - \frac{1}{c}\frac{\partial\boldsymbol{A}(\boldsymbol{r},t)}{\partial t}, \quad (2.3a)$$

$$\boldsymbol{\mathcal{B}} = \boldsymbol{\nabla}\times\boldsymbol{A}(\boldsymbol{r},t)\,, \quad (2.3b)$$

where c is the speed of light. If one approximates the electromagnetic field with a space homogeneous one, which is known as the dipole approximation, the electric field as well as the magnetic field should then be position independent. This implies from Eqs. (2.3) that the electromagnetic potentials should be as well position independent. From Eqs. (2.3) one could see that applying the dipole approximation insinuates that one also approximates the electromagnetic pulse by a pulse without magnetic field, since for a homogeneous vector potential $\boldsymbol{A}(t)$ one obtains $\boldsymbol{\nabla}\times\boldsymbol{A}(t) = 0$. Nevertheless, it was shown in [74] that one could find a gauge where both electric and magnetic field are non zero even when the dipole approximation is applied. The Lorentz force on an electron in an electromagnetic field is (in atomic units)

$$\boldsymbol{F} = -\left(\boldsymbol{\mathcal{E}} + \frac{\boldsymbol{v}}{c}\times\boldsymbol{\mathcal{B}}\right)\,, \quad (2.4)$$

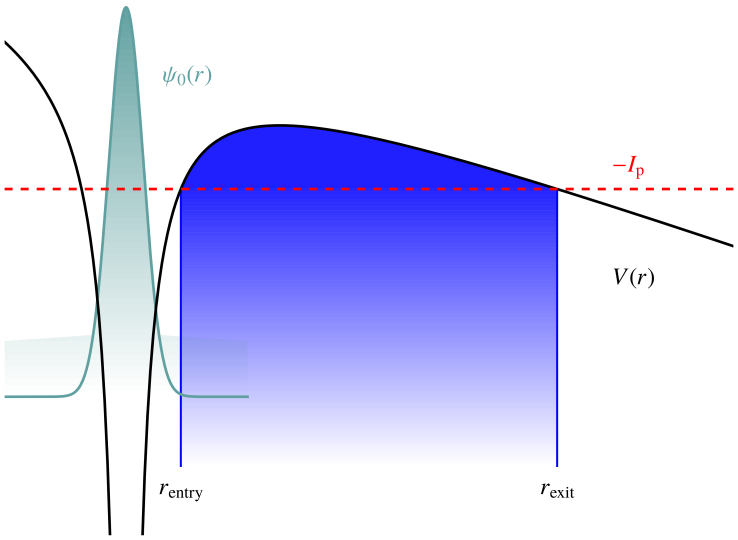

Figure 2.1.: The one dimensional representation of the tunneling barrier of an electron bound by a Coulomb potential in the radial direction. The electron is represented by the radial part of the ground state $\psi_0(r)$ of the Coulomb potential with binding energy $-I_p$. The Coulomb potential is bent by the electric field. The points r_{entry} and r_{exit} represent the entry and exit points of the tunneling barrier respectively. The figure is adopted from Ref. [75].

where $\boldsymbol{v}$ is the velocity of the electron. One can see that the force due to the magnetic field is multiplied by $1/c$ in comparison to that of the electric field $\boldsymbol{E}$ [74]. In this thesis we consider hydrogen like ions which are not highly charged. For such ions where $Z < 20$, the term $\boldsymbol{v}/c$ and hence the effect of the magnetic field [50, 74]. Relativistic effects are even of the order $(|\boldsymbol{v}|/c)^2$ and consequently can also be neglected [50, 74]. Thus we apply the dipole approximation without magnetic field. In strong field physics two gauges are commonly used within the electric dipole approximation, the length-gauge defined by the scalar potential $\phi(t) = -\boldsymbol{x} \cdot \boldsymbol{\mathcal{E}}(t)$ and vector potential $\boldsymbol{A}(t) = 0$, and the velocity gauge defined by $\phi(t) = 0$ and $\boldsymbol{A}(t) = -c \int \boldsymbol{\mathcal{E}}(t)\mathrm{dt}$. Let us consider the time-independent solution of the Schrödinger equation at static electric field $\boldsymbol{\mathcal{E}}_0$, the maximum of the applied pulse, in the length gauge. Then we have

$$\hat{H}\Psi = \left(-\frac{1}{2}\Delta - \frac{Z}{|\boldsymbol{r}|} + \boldsymbol{x} \cdot \boldsymbol{\mathcal{E}}_0\right) = -I_p\Psi \tag{2.5}$$

where $-I_p$ is the eigenenergy solution with $I_p > 0$ and $\Delta = \boldsymbol{\nabla} \cdot \boldsymbol{\nabla}$ is the Laplacian. In this gauge we see that the Coulomb potential is bent by the electric potential forming the total potential $\hat{V}(x, y, z)$ as shown in Fig. 2.1, where the electric field

direction is chosen opposite to the x-direction such that $x \cdot \boldsymbol{\mathcal{E}}_0 = -x\mathcal{E}_0$. Then the potential $\hat{V}(x, y, z)$ could be written as

$$\hat{V}(x, y, z) = -\frac{Z}{|\boldsymbol{r}|} - x\mathcal{E}_0. \tag{2.6}$$

Whereas the potential plotted in Fig. 2.1 corresponds to an electric field opposite to the $\boldsymbol{r}$ direction such that

$$\hat{V}(r) = -\frac{Z}{|\boldsymbol{r}|} - r\mathcal{E}_0. \tag{2.7}$$

The definition of the tunneling barrier in three or two dimensions is more complicated and requires a different approach that we will discuss in Chapter 4. But for the sake of understanding the tunneling ionization picture we treat the three dimensional system here like a one dimensional system and consider the potential $\hat{V}(r)$. As a result, we have an electron with energy $E = -I_p$ penetrating the potential $V(r)$, then the boundary of the classically forbidden region is defined by

$$-I_p = V(r). \tag{2.8}$$

Other than the electric dipole approximation and the one dimensional radial treatment that we used to define the tunneling picture, we have also considered the system static and applied the length gauge. Yet the electromagnetic pulse with frequency ω applied in experiments is time dependent. The semi-classical theory of Keldysh [41] defines the so called Keldysh parameter γ which determines when the tunneling picture is applicable in tunnel ionization. Keldysh considered the classical time needed by the electron to pass the barrier the so called Keldysh time $\tau_k = \sqrt{2I_p}/\mathcal{E}_0$. Then the tunneling picture applies for $\gamma = \omega\tau_k \ll 1$. In this case the period of the applied pulse is much bigger than the typical time of the tunneling process such that during tunneling the electric field could be considered static. In this case one should be careful since for very long pulses the relativistic effects set in again and the dipole approximation is not valid anymore [76]. But as a result, for long enough pulses the tunneling picture holds.

One issue remains here to consider: is the tunneling picture valid in the velocity gauge? In principle the tunneling picture should be gauge independent. Substituting the velocity gauge in Eq. (2.1) one gets the Hamiltonian $\hat{H}$:

$$\hat{H} = \frac{1}{2}\left(-i\boldsymbol{\nabla} - \int \boldsymbol{\mathcal{E}}(t)\mathrm{dt}\right)^2 - \frac{Z}{|\boldsymbol{r}|}, \tag{2.9}$$

where obviously the potential bent by the electric field is not apparent anymore as in $V(r)$. Any physical observable should be gauge invariant under a gauge transformation, which is not the case for Hamiltonian $\hat{H}$. Hence the Hamiltonian $\hat{H}$ is not a physical observable, while the quantity $\hat{H} - i\partial/\partial t$ is gauge invariant and is a physical observable. The Hamiltonian if time-independent represents the energy of the system and thus is a physical observable, otherwise if time-dependent it is responsible for translations in time and is not a physical observable [50, 77]. For the

static case one can find a time-independent gauge where the Hamiltonian is explicitly time independent and is in an observable [50, 77] of the system's total energy. As pointed out in [50, 77] defining the time-independent Hamiltonian with this time independent gauge one can define a gauge invariant tunneling picture.

In this thesis we apply the dipole approximation, i.e., we consider a homogeneous pulse in space. The frequency of the pulse is chosen such that $\gamma < 1$. After explaining what is strong field tunnel ionization, in the next section the famous two-step model of tunnel ionization that predicts the momentum of the tunneled electrons is explained.

2.3. Two-step model

Corkum *el al.* [63, 64] developed a simple and easily applicable model in order to describe the spectra of tunnel ionized electrons, the so-called two step model. This model is important to understand the attoclock experiment. Moreover in this thesis we test, for the considered physical setups, how good can the two step model predict the final momentum of the tunnel ionized electron. Additionally, we examine how good this model can be used to extract tunneling times. The main assumptions of this model are ones concerning the tunneling process. In this thesis we examine the tunneling process and question these assumptions and inquest how realistic they are.

In the first step of the model, the electron tunnels out at the instant of field maximum. This is founded on the theoretical calculations [53, 78] that results in a maximal tunnel probability for maximal electric field strength. Assuming that the electron tunnels out at the instant of field maximum means also that the electron spends no time under the barrier, i.e., instantaneous tunneling. Additionally, at the tunnel exit (the turning point) the total energy of the electron is exactly equal to the potential. It follows from classical mechanics, specifically from energy conservation $E = P^2/2 + V$ that the electron does not posses any kinetic energy and thus have zero momentum at the tunnel exit.

In the second step the electron follows Newton's equations of motion of a negatively charged particle in an electric field. Accordingly, the final momentum of the tunneled electron $\boldsymbol{p}(t_f)$ is given by (in atomic units),

$$\boldsymbol{p}(t_f) = \boldsymbol{p}(t_0) + \int_{t_0}^{t_f} \boldsymbol{\mathcal{E}}(t')\mathrm{dt}', \tag{2.10}$$

where t_0 is the instant of field maximum such that $\boldsymbol{\mathcal{E}}(t_0) = \boldsymbol{\mathcal{E}}_0$ and t_f is at the instant at which the electric field pulse vanishes. Also here the dipole approximation is applied. The initial conditions of Newton's equations of motion follow from the first step assumptions. The electron is at the tunnel exit $\boldsymbol{x}_{\text{exit}}$ at the instant t_0, i.e., $\boldsymbol{x}(t_0) = \boldsymbol{x}_{\text{exit}}$ with an initial momentum $\boldsymbol{p}(t_0) = 0$ since the electron has no kinetic energy at the tunneling exit. The two step model is usually corrected by the so called Perelomov, Popov and Terentev (PPT) theory [79]. In the PPT theory Eq. 2.1 is solved by considering the length gauge and approximating the Coulomb potential

by a short range potential. The Coulomb effect is then considered by correcting the resulting ionization rate by a prefactor calculated using a quasi-classical theory. From the ionization spectra of the PPT theory one induces that the electron exits with a non-zero transverse momentum (perpendicular to the electric field direction). In the static limit, for $\gamma \ll 1$ this exit transverse momentum goes to zero. Note that the so called Ammosov, Delone and Krainov (ADK) theory [80] is just the static limit of the PPT theory.

2.4. Attoclock experiment

Keller *et al.* have conducted experiments using the angular streaking technique aiming to measure when does the electron ionize from a bound state, the so-called attoclock experiments [39, 40]. Although the attoclock experiments try to determine when does the electron tunnel ionize, a consensus on the interpretation of the experimental results is still lacking. In the following we sketch the basic idea of the angular streaking attoclock experiment [39, 40] in order to clarify where the difficulties lei.

Consider a circularly polarized laser field applied to the Coulomb bound electron defined as (within the electric dipole approximation):

$$\boldsymbol{\mathcal{E}}(t) = \mathcal{E}_0 \left[-\sin(\omega t)\hat{\boldsymbol{x}} + \cos(\omega t)\hat{\boldsymbol{y}} \right] \tag{2.11}$$

where $\mathcal{E}_0$ is the electric field strength and ω is the angular frequency of the applied field. Consider the electron that has tunneled at electric field maximum when the field was pointing in the negative y-direction i.e., $\boldsymbol{\mathcal{E}}(t_0) = -\mathcal{E}_0\hat{\boldsymbol{y}}$ at instant $t_0 = \pi/\omega$, and that the pulse runs for one period, i.e. $t_f = 2\pi/\omega$. Using the two-step model by substituting Eq. (2.11) in Eq. (2.10) the asymptotic momentum of the tunneled electron should point only along the x-direction $\hat{\boldsymbol{x}}$ see Fig. 2.2. In the experiment one finds that the asymptotic momentum is shifted with respect to the x-direction. The origin of this shift could be of many reasons. One of the reasons could be long range Coulomb effects not considered in the two-step model. Another reason could be an initial momentum not equal to zero at the instant of electric field maximum $\boldsymbol{p_e(t_0)} \neq 0$. The initial momentum of the tunneled electron is usually corrected by a momentum perpendicular to the electric field direction due to non-adiabatic effects by the so called PPT theory [53, 79, 80] see also Sec. 2.3. Also a momentum in the electric field direction exists as pointed out in [49, 75], as we will show in this thesis. Moreover, the shift could be caused by a delay τ_{exit} with respect to the instant of electric field maximum, i.e., the electron exits the tunneling barrier either before or after the instant of electric field maximum t_0 with a negative or positive delay τ_{exit}, respectively. One can easily recognize that the interpretation of the experimental results are not straight forward and are dependent on a theoretical model that calibrates the attoclock, as done for example in [54, 55] where the analytical R-matrix theory [81] is used to develop a calibration model.

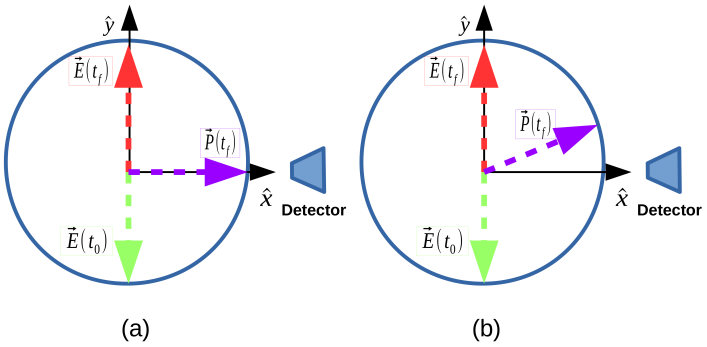

Figure 2.2.: A schematic representation of the direction of the electric field $\boldsymbol{\mathcal{E}}(t)$ at the instant of tunneling t_0 and at the instant of decay of the pulse t_f. (a) The direction of the asymptotic momentum $\boldsymbol{p}_e(t_f)$ as expected using the two-step model. (b) The direction of the asymptotic momentum $\boldsymbol{p}_e(t_f)$ as measured experimentally.

The main purpose of the attoclock angular streaking experiment is to provide information about the instant of tunnel ionization, i.e., the instant the electron leaves the tunneling barrier. According to the attoclock experimental setup this could be only determined with respect to the instant of maximum electric field strength. Such that one can define the delay

$$\tau_{\text{exit}} = t_{\text{exit}} - t_0 \tag{2.12}$$

where t_{exit} is the instant of ionization and $t_0 = \arg\max\left[|\boldsymbol{\mathcal{E}}(t)|\right]$ is the instant of maximum electric field strength.

The aim in this thesis is not to calibrate or model the attoclock experiment. The main purpose in this work is to determine the instant of ionization t_{exit} and consequently the delay τ_{exit} from first principles. Another aim is the interpretation of the delay τ_{exit}, does it represent the time spent under the barrier? Moreover, some findings of this thesis influence the modeling of attoclock experiment, although the exact parameters of the experiment are not considered here. This will be discussed thoroughly in Chpater. 3.

In conclusion, one should note that the attoclock experiment aims to determine the delay τ_{exit} , and for this purpose the final momentum of the tunnel ionized electron is measured. Accordingly, τ_{exit} is extracted from the measured final momentum using some theoretical model.

In this thesis τ_{exit} is determined from first principles via the virtual detector approach which is introduced in the next section.

2.5. Virtual detector

In this thesis we apply the virtual detector method [57, 58] to investigate tunneling ionization dynamics[1]. Ionization from a binding potential means that an electron moves away from the vicinity of the binding potential's minimum. A virtual detector allows to quantify this dynamics. More specifically, a virtual detector is a hypothetical device that determine how the probability to find a particle within some specific space region changes over time. In the following, we lay down its mathematical foundations.

The quantum mechanical evolution of an electron's wave function $\Psi(\boldsymbol{r},t)$ is governed by the Schrödinger equation (in atomic units)

$$\mathrm{i}\frac{\partial\Psi(\boldsymbol{r},t)}{\partial t} = \left(\frac{1}{2}\left(-\mathrm{i}\frac{\partial}{\partial\boldsymbol{r}} + \frac{1}{c}\boldsymbol{A}(\boldsymbol{r},t)\right)^2 - \phi(\boldsymbol{r},t)\right)\Psi(\boldsymbol{r},t)\,, \tag{2.13}$$

where $\phi(\boldsymbol{r},t)$ and $\boldsymbol{A}(\boldsymbol{r},t)$ denote the electromagnetic potentials. The probability density to find the electron at position $\boldsymbol{r}$ at time t is given by

$$\varrho(\boldsymbol{r},t) = \Psi(\boldsymbol{r},t)^*\Psi(\boldsymbol{r},t)\,, \tag{2.14}$$

where $\Psi(\boldsymbol{r},t)^*$ indicates the complex conjugate of $\Psi(\boldsymbol{r},t)$. The dynamics of the density $\varrho(\boldsymbol{r},t)$ is associated with the probability current

$$\boldsymbol{j}(\boldsymbol{r},t) = \mathrm{Re}\left(\Psi(\boldsymbol{r},t)^*\left(-\mathrm{i}\frac{\partial}{\partial\boldsymbol{r}} + \frac{1}{c}\boldsymbol{A}(\boldsymbol{r},t)\right)\Psi(\boldsymbol{r},t))\right)\,. \tag{2.15}$$

Expressing the wavefunction as

$$\Psi(\boldsymbol{r},t) = \sqrt{\varrho(\boldsymbol{r},t)}\exp(\mathrm{i}\varphi(\boldsymbol{r},t))\,, \tag{2.16}$$

the probability current may be written as a product of the probability density $\varrho(\boldsymbol{r},t)$ and some local velocity, viz.

$$\boldsymbol{j}(\boldsymbol{r},t) = \varrho(\boldsymbol{r},t)\left(\frac{\partial\varphi(\boldsymbol{r},t)}{\partial\boldsymbol{r}} + \frac{1}{c}\boldsymbol{A}(\boldsymbol{r},t)\right)\,, \tag{2.17}$$

which occurs in the framework of Bohmian mechanics [82]. The probability density and the probability current fulfill the continuity equation

$$-\frac{\partial\varrho(\boldsymbol{r},t)}{\partial t} = \boldsymbol{\nabla}\cdot\boldsymbol{j}(\boldsymbol{r},t)\,. \tag{2.18}$$

For a compact subspace V of the physical space with a piecewise smooth boundary S the continuity equation (2.18) yields by integration over the subspace

$$-\frac{\mathrm{d}}{\mathrm{d}t}\int_V \varrho(\boldsymbol{r},t)\,\mathrm{d}V = \int_S \boldsymbol{j}(\boldsymbol{r},t)\cdot\boldsymbol{n}\,\mathrm{d}S\,, \tag{2.19}$$

[1] This method was developed by the author before the knowledge of the above cited work. Nevertheless, this method is only here applied for the purpose of investigating tunnel ionization dynamics.

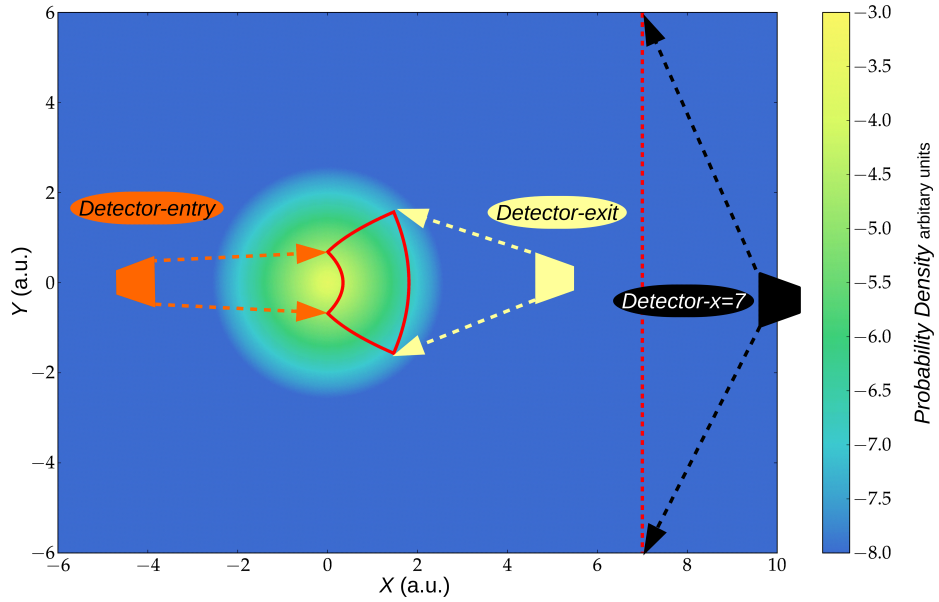

Figure 2.3.: A schematic representation of the virtual detectors in two dimensions applied for the tunneling ionization problem. The probability distribution of an electron in the ground state of a Coulomb potential in two dimensions is plotted in logarithmic scale. The parabolic red lines describe the boundaries of the tunneling barrier as calculated using parabolic coordinates for $\mathcal{E}_0 = 1.1$ in atomic units. The calculation of the tunneling barrier is described thoroughly in Chapter 4. The detector at the entry is realized by calculating $D_{\mathrm{c_{entry}}}(t)\mathrm{d}t$, see Eq. (2.22), along the entry curve as pointed out by the arrows. The arrows point to the starting and end points of the curve. Similarly the detector at the exit is realized by calculating $D_{\mathrm{c_{exit}}}(t)\mathrm{d}t$ along the exit curve as pointed out by the arrows. Calculating $D_{\mathrm{x=7}}(t)\mathrm{d}t$ over the dotted red line gives the probability that an electron passes $x = 7$ in the time window $[t, t + \mathrm{d}t]$.

where $\boldsymbol{n}$ denotes the outward pointing unit normal field of the boundary S. Equation (2.19) holds also for unbounded subspaces if $\varrho(\boldsymbol{r}, t)$ decreases fast enough when $|\boldsymbol{r}| \to \infty$. Thus, the rate of the change of the probability to find the electron within the space region V is given by the probability current through the volume's surface, which is quantified by the virtual detector. In other words, a virtual detector placed at the surface S determines how much probability passes from one side of the surface to the other per unit time. Here we explain the virtual detector method intuitively in the usual interpretation of quantum mechanics. Understanding the virtual detector method is important for interpreting the represented results in this thesis. Since in this thesis we investigate a one dimensional and two dimensional systems, the interpretation of the virtual detector is explained in both cases.

In one dimension

Suppose an experimentalist wants to measure the time of arrival of an ionized electron at a certain point in space x_d. One way would be to place an electron detector at x_d and each time the detector ticks, register the time of arrival with a time uncertainty δt. In the usual interpretation of quantum mechanics the experimentalist is expected to measure a distribution of number of electrons in time, i.e., at each time of arrival the experimentalist will measure a certain number of ticks. This is interpreted as at each arrival time window $[t, t+\delta\mathrm{t}]$ one has a certain probability of an electron arriving at the detector. The higher the probability is, the higher the number of ticks is. Summing over all the number of ticks during the whole measurement time, gives the total number of ionized electrons that have passed x_d. In the above explained way the probability current multiplied with a time interval $j(x_d,t)\mathrm{dt}$ represents a virtual electron detector in one dimension [2]. It gives us the quantity of probability that have passed x_d in the time window $[t, t+\mathrm{dt}]$, or for the experimentalist the number of ticks in the time window $[t, t+\delta\mathrm{t}]$. Integrating $j(x_d,t)\mathrm{dt}$ over time gives us the total probability that have passed x_d or for the experimentalist the total number of ionized electrons that have passed x_d.

In two dimensions

In two dimensions the probability current is a vector $\boldsymbol{j}(x,y,t) = j_x(x,y,t)\boldsymbol{x} + j_y(x,y,t)\boldsymbol{y}$ where (in atomic units)

$$j_x(x,y,t) = \frac{1}{2\mathrm{i}}\left(\Psi(x,y,t)^\dagger \frac{\partial\Psi(x,y,t)}{\partial x} - \Psi(x,y,t)\frac{\partial\Psi(x,y,t)^\dagger}{\partial x}\right), \tag{2.20}$$

$$j_y(x,y,t) = \frac{1}{2\mathrm{i}}\left(\Psi(x,y,t)^\dagger \frac{\partial\Psi(x,y,t)}{\partial y} - \Psi(x,y,t)\frac{\partial\Psi(x,y,t)^\dagger}{\partial y}\right) \tag{2.21}$$

are the probability currents in x and y directions, respectively, when $\boldsymbol{A}(\boldsymbol{r},t) = 0$. We consider this case because in this thesis the length gauge is applied. The probability current in two dimensions $\boldsymbol{j}(x,y,t)$ could not be interpreted in the same manner as the probability current in one dimension $j(x,t)$. The integral of $\boldsymbol{j}(x,y,t)$ over a curve in two dimensions

$$D_{c(x,y)}(t)\mathrm{dt} = \left[\int_{c(x,y)} \boldsymbol{j}(x,y,t)\cdot\boldsymbol{n}d\left[c(x,y)\right]\right]\mathrm{dt} \tag{2.22}$$

could be interpreted like $j(x,t)\mathrm{dt}$, where $\boldsymbol{n}$ is the unit vector normal to the curve[3] $c(x,y)$. Note, that Eq. (2.22) is equivalent to the right side of Eq. (2.19) but ex-

[2] Note that in one dimension the closed surface occurring in (2.19) is formed of two points. Also the electric field points only in one direction. As a result, it is enough to consider one point in order to calculate the probability of ionized electrons since one could choose the other point where the probability flow is null.

[3] In two dimensions the surface occurring in the integral (2.19) is a closed curve. While the entry and the exit curves shown in Fig. 2.3 are not closed. It will be shown in chapter 4 the probability flow is non-negligible only along parabolic curves that are not closed.

panded in two dimensions.$D_{c(x,y)}(t)\mathrm{d}t$ gives the amount of probability that passes the curve $c(x, y)$ in time window $[t, t + \mathrm{d}t]$. Thus calculating $D_{c(x,y)}(t)\mathrm{d}t$ resembles placing a detector along the curve $c(x, y)$. For calculating the probability that an electron exits the tunneling barrier in the interval $[t, t+\mathrm{d}t]$, $D_{c(x,y)}(t)\mathrm{d}t$ is calculated over the exit curve c_{exit}. Similarly, for calculating the probability that an electron enters the tunneling barrier in the interval $[t, t + \mathrm{d}t]$, $D_{c(x,y)}(t)\mathrm{d}t$ is calculated over the entry curve c_{entry}. For calculating the probability that an electron passes the line $x = c$ in the time window $[t, t + \mathrm{d}t]$, where c is a constant, $D_{x=c}(t)\mathrm{d}t$ is calculated, see Fig. 2.3 for an illustration.

It is also important to remark that the detectors here are virtual detectors realized by calculating the probability flow and do not affect the system in any way. On the other hand, realizing such a measurement setup experimentally if possible requires a real electron detector, which would affect the considered ionization process. Thus the simple method described above allows one to detect the electron at the tunneling barrier entry and exit without effecting the tunnel ionization process.

In order not to complicate the interpretation of the virtual detector results, a certain shape of an electric field pulse is applied throughout this thesis. The shape of the pulse and it's physicality is discussed in the next section.

2.6. Electric field pulse and gauge invariance

In this thesis the same pulse is applied for all considered physical setups. As argued in Sec. 2.2 the dipole approximation as well as the length gauge is applied in this work. Usually in experiments the applied pulse is of a sinusoidal form with a Gaussian similar envelope. Applying a pulse similar to the one applied in experiments would complicate the interpretation and analysis of the results attained in this thesis. Since a sinusoidal pulse would change direction and causes scatterings of the tunneled part of the wave function with the bound part. Thus to keep the analysis of the results clear and simple we apply an electric field pulse with a Gaussian structure of the form

$$\mathcal{E}(t) = \mathcal{E}_0 \exp\left(-\frac{\alpha^2(t - t_0)^2}{2}\right), \tag{2.23}$$

where α is constant that has to be determined. Such a pulse would mimic a half cycle sinusoidal pulse. The time $\tau_E = \sqrt{(2)}/\alpha$ is the time scale of the rise and the decay of the pulse. The constant α should be determined from the Keldysh parameter, see Sec. 2.2, by setting $\gamma < 1$. Since α determines how fast does the pulse change and the Keldysh parameter should be set in a way such that the pulse dynamics are much slower than the tunneling dynamics. But the frequency of the pulse ω given in the Keldysh parameter γ is given for a sinusoidal pulse whereas here we have a

Gaussian pulse. For this reason we expand the Gaussian pulse and a pulse of the form $\mathcal{E}(t) = \mathcal{E}_0 \cos(\omega(t - t_0))$ around the instant of field maximum t_0

$$\mathcal{E}(t) = \mathcal{E}_0 \exp\left(-\frac{\alpha^2(t-t_0)^2}{2}\right) = \mathcal{E}_0\left(1 - \alpha^2(t-t_0)^2 + O(\alpha^4)\right) \tag{2.24}$$

$$\mathcal{E}(t) = \mathcal{E}_0 \cos(\omega(t - t_0)) = \mathcal{E}_0\left(1 - \frac{\omega^2}{2}(t-t_0)^2 + O(\omega^4)\right) \tag{2.25}$$

and solve for the parameter α in terms of ω by equalizing both pulse equations. Additionally, the condition $\alpha, \omega < 1$ is satisfied for the studied systems such that one compares the pulses up to second order. Accordingly, one finds that $\alpha = \omega/\sqrt{2}$ and ω is determined from setting the Keldysh parameter γ to some constant k such that $k < 1$.

This pulse is applied in the Hamiltonian via a length gauge, the scalar potential is given by $\phi(\boldsymbol{r}, t) = -\boldsymbol{\mathcal{E}}(t)\cdot\boldsymbol{r}$, and one can write the total Hamiltonian as $\hat{H}_T(t) = \hat{H}_s + \hat{H}_I(t)$ where $\hat{H}_s$ is the system Hamiltonian and $\hat{H}_I(t)$ is the Hamiltonian describing the interaction of the pulse with the system. If one considers a physical pulse then the interaction term of the Hamiltonian should be zero at the beginning of the interaction, and goes back to zero at a certain time. Mathematically, this is satisfied by the condition $\hat{H}_T(t \to \pm\infty) = \hat{H}_s$, i.e., the interaction of the pulse with the system starts and ends at certain instants of time. In the length gauge this criteria is satisfied for an electric field described by Eq. (5.2), nevertheless such a pulse is not physical. To see this we represent the same electric field pulse but in the velocity gauge. In this case the vector potential $\boldsymbol{A}(t)$ that represents the interaction in the Hamiltonian is given by $\boldsymbol{A}(t) = -c\int_{-\infty}^{t}\boldsymbol{\mathcal{E}}(t')\mathrm{dt}'$. By a simple calculation one finds out that for a Gaussian electric field pulse $\boldsymbol{A}(-\infty) = 0$ and $\boldsymbol{A}(+\infty) \neq 0$. Thus for the considered electric field pulse in the velocity gauge the condition $\hat{H}_T(t \to +\infty) = \hat{H}_s$ is not satisfied. For this reason one questions the reality of the Gaussian electric field pulse applied in this thesis. This Gaussian pulse mimics a half cycle pulse and half cycle pulses have been achieved experimentally [83, 84]. Though the pulses achieved experimentally have a long negative tail with small absolute value compared to the positive part of the pulse [84]. For such pulses the integral of the electric field vanishes for large times because of the long negative tail and $\boldsymbol{A}(\pm\infty) = 0$ is satisfied. Applying such a realistic pulse in this work would not effect the results but requires a more numerical effort because of the long negative tail. In conclusion, although the Gaussian pulse is rigorously not realistic, it mimics realistic pulses that are generated experimentally.

After we have laid the physical foundations of the considered problems, we discuss in the next section which algorithms have been used in order to solve this problem.

2.7. Numerical techniques

In this thesis the time dependent Schrödinger equation of an electron interacting with an electric field is solved numerically. For this purpose two algorithms have

been applied, the Lanzcos algorithm, see for example [85–88], and the split operator method, see for example [89–91]. The split operator method is applied for the case when a soft core potential[4] is used. Whereas the Lanzcos algorithm is applied when a Coulomb potential is used. The reason for this is that for a Coulomb potential the split operator algorithm does not converge as later explained. The equation that has to be solved is of the form:

$$\mathrm{i}\hbar\frac{\partial\Psi(t)}{\partial t} = \hat{H}(t)\Psi(t) \tag{2.26}$$

which could be written as:

$$\Psi(t) = \hat{T}_o \exp\left(-\mathrm{i}\hbar\int_{t_0}^{t}\hat{H}(t')\mathrm{d}t'\right)\Psi(t_0) = \hat{U}(t,t_0)\Psi(t_0) \tag{2.27}$$

where $\hat{T}_o$ is the time ordering operator. The expression for $\hat{U}(t,t_0)$ used almost exclusively in physics [92],

$$\hat{U}(t,t_0) = 1 - \frac{i}{\hbar}\int_{t_0}^{t}\hat{H}(t_1)\mathrm{d}t_1 + \left(\frac{i}{\hbar}\right)^2\int_{t_0}^{t}\mathrm{d}t_1\int_{t_0}^{t_1}\mathrm{d}t_2\hat{H}(t_1)\hat{H}(t_2) + \ldots \tag{2.28}$$

which is obtained by iteration [92]. For a numerical solution the expansion (2.28) has to be terminated at a certain order, which is not convenient because then the unitary property of $\hat{U}(t,t_0)$ would be lost. A much more convenient expansion, which is in contrast unitary, is given by the Magnus formula [89, 92, 93],

$$\hat{U}(t+\Delta\mathrm{t},t) = \exp\left(-\frac{\mathrm{i}}{\hbar}\int_{t}^{t+\Delta\mathrm{t}}\hat{H}(t')\mathrm{d}t'\right) + D_3(t)\left(\mathrm{i}\Delta\mathrm{t}\right)^3 + D_5(t)(\mathrm{i}\Delta\mathrm{t})^5 + \ldots \tag{2.29}$$

where $D_3(t)$ is expressible as commutator of $\hat{H}(t)$ at two different times. Similarly $D_4(t)$ is a higher order commutation of $\hat{H}(t)$. In this thesis the series is truncated at the second order and $\hat{U}(t+\Delta\mathrm{t},t)$ is approximated by,

$$\hat{U}(t+\Delta\mathrm{t},t) = \exp\left(-\frac{\mathrm{i}}{\hbar}\int_{t}^{t+\Delta\mathrm{t}}\hat{H}(t')\mathrm{d}t'\right) + O\left(\Delta\mathrm{t}\right)^3. \tag{2.30}$$

As shown in [89–91] a fourth order approximated propagator can be obtained by a multiplication procedure of the second order approximated propagator. In the following two algorithms will be described that are used to solve the equation,

$$\Psi(t+\Delta\mathrm{t}) = \exp\left(-\frac{\mathrm{i}}{\hbar}\int_{t}^{t+\Delta\mathrm{t}}\hat{H}(t')\mathrm{d}t'\right)\Psi(t). \tag{2.31}$$

[4] A soft core potential is a potential of the form $a\sqrt{\boldsymbol{r}\cdot\boldsymbol{r}+b}$, where a and b are some constants.

2.7.1. The split operator method

The first procedure of the split operator method is factorizing the propagator $\hat{U}(t+\Delta\mathrm{t}, t)$ in it's exponential form by using the well known Trotter formula [94]. An important criteria for the applicability of this method is the ability to separate the Hamiltonian into parts, where each part has a certain eigenbasis, and it is not computationally demanding to transform from one eigenbasis to another . For example, for the Schrödinger equation the split operator method would be applied by separating the Hamiltonian into a part diagonal in the momentum space and a part diagonal in the Cartesian space. due to fast algorithms one could transform from one space to another very efficiently. Solving the Schrödinger equation of an electron interacting with a magnetic and electric field could become tricky, since the vector potential is space dependent and multiplied with the canonical momentum. Although the propagator could be factorized via the Trotter formula for any Hamiltonian, the algorithm could be only applied to Hamiltonians which could be separated into a part that is diagonal in the momentum space and a part which is diagonal in the Cartesian space. In the Schrödinger propagator this translates into separating the Hamiltonian into a kinetic part and a potential part. If this is the case then Eq. (2.31) could be written as (in atomic units),

$$\Psi(t+\Delta\mathrm{t}) = \exp\left(-\mathrm{i}\Delta\mathrm{t}(\hat{T}+\hat{V}(t,t+\Delta\mathrm{t})\right)\Psi(t), \tag{2.32}$$

Where $\hat{T}$ is the kinetic term and $\hat{V}(t,t+\Delta\mathrm{t}) = \frac{1}{\Delta\mathrm{t}}\int_t^{t+\Delta\mathrm{t}}\hat{V}(t')\mathrm{d}t'$ is the time integration of the potential part. Then according to Trotter formula this could be expanded in the following way:

$$\begin{aligned}\exp\left(-\mathrm{i}\Delta\mathrm{t}(\hat{T}+\hat{V}(t+\Delta\mathrm{t},t)\right) = \exp\left(-\frac{\mathrm{i}}{2}\Delta\mathrm{t}\hat{T}\right)\exp\left(-\mathrm{i}\hat{V}(t+\Delta\mathrm{t},t)\Delta\mathrm{t}\right)\exp\left(-\frac{\mathrm{i}}{2}\Delta\mathrm{t}\hat{T}\right)\\ +\frac{1}{24}\left[\hat{T}+2\hat{V}(t+\Delta\mathrm{t},t),\left[\hat{T},\hat{V}(t+\Delta\mathrm{t},t)\right]\right](\Delta\mathrm{t})^3+\ldots,\end{aligned} \tag{2.33}$$

where $\left[\hat{T},\hat{V}(t+\Delta\mathrm{t},t)\right]$ is the commutation between the kinetic part and the integrated potential part. In this thesis the Trotter formula is terminated at it's second order expansion i.e. the propagator is approximated by,

$$\begin{aligned}\exp\left(-\mathrm{i}\Delta\mathrm{t}(\hat{T}+\hat{V}(t+\Delta\mathrm{t},t)\right) =& \exp\left(-\frac{\mathrm{i}}{2}\Delta\mathrm{t}\hat{T}\right)\exp\left(-\mathrm{i}\hat{V}(t+\Delta\mathrm{t},t)\Delta\mathrm{t}\right)\exp\left(-\frac{\mathrm{i}}{2}\Delta\mathrm{t}\hat{T}\right)\\ &+O(\Delta\mathrm{t})^3.\end{aligned} \tag{2.34}$$

Higher order truncation can be obtained from this second order truncation as shown in [89]. An important criteria for the convergence and thus the applicability of this second order truncation is the convergence of the commutator in Eq. (2.33), i.e., it is bounded such that as Δt goes to zero the commutator multiplied by Δt also goes to

zero. For example it can be shown that for a Coulomb potential it does not converge and thus this algorithm is not applicable. Whereas for a soft-core potential the commutator converges and the algorithm is applicable. Another important criteria of factorizing the propagator as in Eq. (2.34), is the that the propagator remains unitary. To see the aim of writing the propagator as in Eq. (2.34) consider the wavefunction $\Psi(t)$ in it's momentum space representation,

$$\Psi(t) = \int_{\boldsymbol{p}} C_{\boldsymbol{p}}(t) \left|\boldsymbol{p}\right\rangle d\boldsymbol{p}, \tag{2.35}$$

where $C_{\boldsymbol{p}}$ is a complex number and $\left|\boldsymbol{p}\right\rangle$ is the eigen vector of the momentum $\boldsymbol{p}$. Then applying $\exp\left(-\frac{\mathrm{i}}{2}\Delta\mathrm{t}\hat{T}\right)$ is trivial since $\left|\boldsymbol{p}\right\rangle$ is also an eigen vector of the operator T. After this the resulting wavefunction is fourier transformed to it's cartesian space representation via,

$$\int_{\boldsymbol{p}} C_{\boldsymbol{p}}(t) \exp\left(-\frac{\mathrm{i}}{2}\Delta\mathrm{t}T_{\boldsymbol{p}}\right) \left|\boldsymbol{p}\right\rangle d\boldsymbol{p} = \int_{\boldsymbol{x}}\int_{\boldsymbol{p}} C_{\boldsymbol{p}}(t) \exp\left(-\frac{\mathrm{i}}{2}\Delta\mathrm{t}T_{\boldsymbol{p}}\right) \left\langle\boldsymbol{x}|\boldsymbol{p}\right\rangle \left|\boldsymbol{x}\right\rangle d\boldsymbol{x}d\boldsymbol{p}, \tag{2.36}$$

where $T_{\boldsymbol{p}}$ is just a c-number and $\left|\boldsymbol{x}\right\rangle$ is the eigen vector of the position $\boldsymbol{x}$ and $\left\langle\boldsymbol{x}\right\rangle \boldsymbol{p} = \exp\left(\mathrm{i}\boldsymbol{p}\boldsymbol{r}\right)$. This could be done because of the completeness of the $\left|\boldsymbol{x}\right\rangle$ basis. Now having $\exp\left(-\frac{\mathrm{i}}{2}\Delta\mathrm{t}\hat{T}\right)\Psi(t)$ represented in the $\left|\boldsymbol{x}\right\rangle$ basis it is trivial to apply $\exp\left(-\mathrm{i}\hat{V}(t+\Delta\mathrm{t},t)\Delta\mathrm{t}\right)$ to it since $\left|\boldsymbol{x}\right\rangle$ is an eigen vector for the operator $\hat{V}(t+\Delta\mathrm{t},t)$. What is left is to Fourier transform the whole thing back to the momentum space representation and apply the last exponential factor of the propagator via,

$$\begin{aligned}\int_{\boldsymbol{p}'}\int_{\boldsymbol{x}}\int_{\boldsymbol{p}} C_{\boldsymbol{p}}(t) \exp\left(-\frac{\mathrm{i}}{2}\Delta\mathrm{t}T_{\boldsymbol{p}'}\right) \exp\left(-\mathrm{i}V_{\boldsymbol{x}}(t+\Delta\mathrm{t},t)\Delta\mathrm{t}\right) \times \\ \exp\left(-\frac{\mathrm{i}}{2}\Delta\mathrm{t}T_{\boldsymbol{p}}\right) \left\langle\boldsymbol{x}|\boldsymbol{p}\right\rangle \left\langle\boldsymbol{p}'|\boldsymbol{x}\right\rangle \left|\boldsymbol{p}'\right\rangle d\boldsymbol{p}d\boldsymbol{x}d\boldsymbol{p}'.\end{aligned} \tag{2.37}$$

In the above described way the wavefunction is propagated from t_0 to t by repeating the above procedure for each iteration $\Delta\mathrm{t}$. $\Delta\mathrm{t}$ is chosen such that $\Delta\mathrm{t} \ll 1/E$ where E is the energy of the system.

The split operator method as described above is easily parallelizable. The Fourier transformation can be done by existing fast Fourier transformation routines like the FFTW [95]. The two dimensional calculations have been paralellized by using GPU (Graphic processing unit) cards. This algorithm is really suitable for graphic card simulations. In graphic cards one has a grid of threads where its geometry could be initialized before executing a certain routine. It is very convenient to form the grid dimensions as the matrix dimensions which represents the wavefunction. Since then each thread will take one matrix element and multiply it with the exponential factor of the propagator. After that there exists a Fast Fourier transformation routine implemented to GPU computing which is applied on the wavefunction matrix. As a result, the algorithm will first multiply each matrix element with the first propagator factor then fourier transform the matrix then multiply it with the second exponential

factor. Next apply a back Fourier transformation and at the end multiply each matrix element with the last factor (from right to left) of the propagator. In the next part the Lanzcos algorithm is explained.

2.7.2. The Lanczos algorithm

The description of the Lanczos algorithm presented here is based on the following material [85–88] The Lanczos algorithm is based on the Krylov subspace [85, 86]. Consider an $N \times N$ matrix $\boldsymbol{A}$ and an N-dimensional vector $\boldsymbol{b}$ then the Krylov subspace of dimension k is defined as:

$$\mathcal{K}_k\left(\boldsymbol{A}, \boldsymbol{b}\right) = \text{span}\left\{\boldsymbol{b}, \boldsymbol{A}\boldsymbol{b}, \ldots, \boldsymbol{A}^{k-1}\boldsymbol{b}\right\} \tag{2.38}$$

where $k \in [1, N]$. Thus the Krylov subspace is spanned by the successive powers of matrix $\boldsymbol{A}$ applied to vector $\boldsymbol{b}$. The dimension of the Krylov subspace cannot be larger than N, since applying $\boldsymbol{A}^N$ on $\boldsymbol{b}$ will produce a vector which is linearly dependent on the previous vectors [87]. If $\boldsymbol{A}$ is a Hermitian matrix then there exits a unitary transformation $\boldsymbol{Q}$ such that the following holds [87]:

$$\boldsymbol{Q}^\dagger \boldsymbol{A}\boldsymbol{Q} = \boldsymbol{T} = \begin{pmatrix} \alpha_1 & \beta_1 & & & \\ \beta_1 & \alpha_2 & \beta_2 & & \\ & \ddots & \ddots & \ddots & \\ & & \beta_{N-2} & \alpha_{N-1} & \beta_{N-1} \\ & & & \beta_{N-1} & \alpha_N \end{pmatrix}$$

where $\boldsymbol{T}$ is tridiagonal real matrix. The columns of the matrix $\boldsymbol{Q}$ are labeled $\boldsymbol{q}_i$ and are called the Lanzcos vectors. The vectors $\boldsymbol{q}_i$ form an orthonormal basis of the Krylov subsapce $\mathcal{K}_k\left(\boldsymbol{A}, \boldsymbol{b}\right)$, and can be constructed from the vector $\boldsymbol{b}$. The aim of the Lanzcos algorithm is to find the matrices $\boldsymbol{Q}$ and $\boldsymbol{T}$. One can easily show from the previous equation that

$$\boldsymbol{A}\boldsymbol{Q} = \boldsymbol{Q}\boldsymbol{T} \tag{2.39}$$

holds. Form Eq. (2.39) one could show the following [5]:

$$\boldsymbol{A}\boldsymbol{q}_j = \sum_{i=1}^{N} \boldsymbol{q}_i T_{ij}. \tag{2.40}$$

From the property of tridiogonality of $\boldsymbol{T}$ and the above introduced notation Eq. (2.40) reduces to:

$$\beta_i \boldsymbol{q}_{i+1} = \boldsymbol{A}\boldsymbol{q}_i - \alpha_i \boldsymbol{q}_i - \beta_{i-1}\boldsymbol{q}_{i-1}. \tag{2.41}$$

[5] First I prove the right hand side of Eq. (2.40). Let the result of matrix multiplication $\boldsymbol{A}\boldsymbol{Q}$ be the matrix $\boldsymbol{R}$. Then an element of matrix $\boldsymbol{R}$ with indexes i, j is equal to $R_{ij} = \sum_l A_{il}Q_{lj}$. Let $\boldsymbol{e}_i$ be an N dimensional column vector with zeros everywhere except at index i. Then a column of $\boldsymbol{R}$ could be expressed as $\sum_i R_{i,j}\boldsymbol{e}_i = \sum_i \sum_l A_{il}Q_{lj}\boldsymbol{e}_i$. The column with index l of matrix $\boldsymbol{A}$ is expressed as $\boldsymbol{A}_l = \sum_i A_{il}\boldsymbol{e}_i$. Inserting this to the original equation one gets $\boldsymbol{R}_j = \sum_l \boldsymbol{A}_l Q_l j$. Since in the last equation one sums over all the columns of matrix $\boldsymbol{A}$ multiplied with the elements of column $\boldsymbol{Q}_j$ one can write $\boldsymbol{R}_j = \boldsymbol{A}\boldsymbol{q}_j$. In a similar manner the right hand side can be written as $\boldsymbol{R}_j = \sum_l T_{lj} \sum_i Q_{il}\boldsymbol{e}_i$ and as a result one gets $\boldsymbol{R}_j = \sum_i \boldsymbol{q}_i T_{ij}$.

Data: The initial input is $\boldsymbol{b}$ and $\boldsymbol{A}$
Result: Calculate the matrix $\boldsymbol{Q}$ and matrix $\boldsymbol{T}$
$\boldsymbol{q}_1 = \boldsymbol{b}/\|\boldsymbol{b}\|_2$
$\boldsymbol{Z} = \boldsymbol{A}\boldsymbol{q}_1$
for $i = 1 \rightarrow i = k-1$ **do**
  $\alpha_i = \boldsymbol{q}_i \cdot Z$
  $\boldsymbol{Z} = \boldsymbol{Z} - \alpha_i \boldsymbol{q}_i$
  $\beta_i = \|\boldsymbol{Z}\|_2$
  $\boldsymbol{q}_{i+1} = \boldsymbol{Z}/\beta_i$
  $\boldsymbol{Z} = \boldsymbol{A}\boldsymbol{q}_{i+1} - \beta_i \boldsymbol{q}_i$
end
$\alpha_k = \boldsymbol{q}_k \cdot \boldsymbol{Z}$

Algorithm 1: The Lanzcos Algorithm

Since the vectors q_i are orthonormal multiplying Eq. (2.41) by $\boldsymbol{q}_i$ one gets:

$$\alpha_i = \boldsymbol{q}_i \cdot \boldsymbol{A}\boldsymbol{q}_i. \tag{2.42}$$

The Lanzcos algorithm is an iterative procedure based on Eq. (2.41) and Eq. (2.42). This corresponds to classical Gramm-Schmidt orthogonalization. It is known that this algorithm is unstable. Paige [96] suggested a modified stable algorithm by substituting Eq. (2.42) by:

$$\alpha_i = \boldsymbol{q}_i \cdot \left(\boldsymbol{A}\boldsymbol{q}_i - \beta_{i-1}\boldsymbol{q}_{i-1}\right), \tag{2.43}$$

which is arithmetically equivalent to Eq. (2.42) since the vectors $\boldsymbol{q}_i$ are orthonormal. So one has the Matrix $\boldsymbol{A}$ and needs to calculate the matrix $\boldsymbol{Q}$ and $\boldsymbol{T}$. For this one can start from a random non-zero vector $\boldsymbol{b}$ corresponding to $\boldsymbol{q}_1$, and then using Eq. (2.43) and Eq. (2.41) calculate the matrix $\boldsymbol{Q}$ and matrix $\boldsymbol{T}$ iteratively as shown in **Algorithm 1**. The Lanzcos relation:

$$\boldsymbol{A}\boldsymbol{Q}^{(k)} = \boldsymbol{Q}^{(k)}\boldsymbol{T}^{(k)} + \left[0, \ldots, 0, \beta_k \boldsymbol{q}_{k+1}\right] \tag{2.44}$$

holds for each iteration k for $1 < k < N$, where $\boldsymbol{Q}^{(k)}$ is the matrix formed of the first k Lanzcos vectors q_i and $\boldsymbol{T}^{(k)}$ is the tridiagonal matrix for α_1 till entry α_k. Since $\boldsymbol{Q}$ is unitary then the eigenvalues a_i of matrix $\boldsymbol{A}$ are the same as the eigenvalues t_i of $\boldsymbol{T}$ and the eigen vectors of both matrices are related via,

$$\boldsymbol{a}_i = \boldsymbol{Q}\boldsymbol{t}_i. \tag{2.45}$$

One can stop the iterations at k instead of N and approximate the Lanzcos relation with:

$$\boldsymbol{A} \approx \boldsymbol{Q}^{(k)}\boldsymbol{T}^{(k)}\boldsymbol{Q}^{(k)^\dagger}. \tag{2.46}$$

Accordingly the eigen vectors $\boldsymbol{a}_i$ of $\boldsymbol{A}$ could be approximated by:

$$\boldsymbol{a}_i \approx \boldsymbol{a}_i^{(k)} = \boldsymbol{Q}^{(k)}\boldsymbol{t}_i^{(k)}, \tag{2.47}$$

and the eigenvalues t_i by $t_i^{(k)}$.The error done with such an approximation is bounded by [87]:

$$\Delta \mathrm{t}_i^{(k)} = \min_j \left| t_i^{(k)} - t_j \right| \leq \left| \beta_k \boldsymbol{t}_i^{(k)}(k) \right| \tag{2.48}$$

where $\boldsymbol{t}_i^{(k)}(k)$ denotes the kth (last component) of the eigen vector $\boldsymbol{t}_i^{(k)}$. Since one could calculate the error via Eq. (2.48) it is possible to stop the calculation at a certain iteration k with the desired accuracy. Stopping at a certain iteration is what is known as the Lanzcos algorithm. A back-draw of the Lanzcos algorithm as presented here is it's numerical instability, because the unitary property of $\boldsymbol{Q}$ is lost due to floating arithmetic rounding errors. For the same reason the orthogonality of the Lanzcos vectors $\boldsymbol{q}_i$ is also lost [96]. An unconditional stable algorithm is attained by orthogonalization twice against all Lanzcos vectors $\boldsymbol{q}_i$ [97].

As said in the beginning of the section the aim is to solve the equation,

$$\Psi(t + \Delta \mathrm{t}) = \exp\left(-\mathrm{i} \int_t^{t+\Delta \mathrm{t}} \hat{H}(t') \mathrm{d}t' \right) \Psi(t) = \exp\left(-\mathrm{i}\boldsymbol{A}\right) \Psi(t), \tag{2.49}$$

where the matrix $\boldsymbol{A}$ is obtained by fourth order finite differences and time integration [85, 98]. Note that the matrix $\boldsymbol{A}$ is the representation of the operator $\int_t^{t+\Delta \mathrm{t}} \hat{H}(t')\mathrm{d}t'$ in the basis $|\boldsymbol{x}\rangle$. Then from Eq. (2.39) we get,

$$\Psi(t + \Delta \mathrm{t}) = \exp\left(-\mathrm{i}\boldsymbol{Q}\boldsymbol{T}\boldsymbol{Q}^\dagger\right) \Psi(t), \tag{2.50}$$

because $\boldsymbol{Q}$ is unitary and using Eq. (2.46) we get,

$$\Psi(t + \Delta \mathrm{t}) \approx \boldsymbol{Q}^{(k)} \exp\left(-\mathrm{i}\boldsymbol{T}^{(k)}\right) \boldsymbol{Q}^{(k)^\dagger} \Psi(t), \tag{2.51}$$

where $T^{(k)}$ and $Q^{(k)}$ are obtained by stopping the Lanzcos algorithm at some iteration k. What remains is to diagonalize $\boldsymbol{T}^{(k)}$ which is necessary in order to calculate $\exp\left(-\mathrm{i}\boldsymbol{T}^{(k)}\right)$. Since the dimension of $\boldsymbol{T}^{(k)}$ is small compared to $\boldsymbol{A}$ and it is real and tridiagonal, diagonalize it using eigendecomposition routines is not expensive.

As both algorithms applied in this thesis are explained it remains to explain how these algorithms could be applied to a system of coupled Schrödinger equations as in the case of the quantum clock.

2.7.3. Quantum clock numerical application

In this thesis a quantum clock is coupled to the electron in order to measure tunneling times. The quantum clock will be first introduced in chapter 5, but here we introduce the information needed to understand the algorithm. The technique used for this purpose when applying the split operator method and when applying the Lanzcos algorithm is explained below. When coupling the quantum clock to the electron the total Hamiltonian of the system have the form $\hat{H}_T = \hat{H}_e + \hat{H}_c P(\boldsymbol{x})$, where $\hat{H}_c$ is the clock Hamiltonian, $P(\boldsymbol{x})$ is a space dependent operator and the electron

Hamiltonian $\hat{H}_e = \hat{T} + \hat{V}(t)$. Additionally, the total wavefunction of the system could be represented as a cross product of the Clock Hamiltonian eigenbasis $|i\rangle$ and some eigenbasis of the electron $|\boldsymbol{x}\rangle$ via,

$$\Psi_T(t) = \sum_i \int_{\boldsymbol{x}} \phi_{i,\boldsymbol{x}}(t) \, |\boldsymbol{x}\rangle \, |i\rangle \, d\boldsymbol{x}, \tag{2.52}$$

where $\phi_{i,\boldsymbol{x}}(t)$ is a complex number. Since the clock Hamiltonian is time independent, the basis $|i\rangle$ remains an eigenbasis of $\hat{H}_c$ during the whole propagation. The quantum clock will be deliberately introduced in Chapter 5, for now the above given information is enough to understand the applied techniques. The propagator of the clock-electron system has the form,

$$\Psi_T(t + \Delta\mathrm{t}) = \exp\left(-\mathrm{i}\Delta\mathrm{t}(\hat{T} + \hat{V}(t, t + \Delta\mathrm{t})) + \hat{H}_c\hat{P}(\boldsymbol{x})\right) \Psi_T(t). \tag{2.53}$$

The split operator method case

In the split operator case the application of the clock is straight forward. Applying the Trotter formula [94] to Eq. (2.53) and a second order truncation will give the following approximate propagator,

$$\hat{U}(t + \Delta\mathrm{t}, t) = \exp\left(-\frac{\mathrm{i}}{2}\Delta\mathrm{t}\hat{T}\right) \exp\left(-\mathrm{i}(\hat{V}(t + \Delta\mathrm{t}, t) + \hat{H}_c\hat{P}(\boldsymbol{x}))\Delta\mathrm{t}\right) \exp\left(-\frac{\mathrm{i}}{2}\Delta\mathrm{t}\hat{T}\right), \tag{2.54}$$

which is straight forward to implement along the above explained split operator algorithm since the basis as shown in Eq. (2.52) is an eigenbasis of $\hat{V}(t + \Delta\mathrm{t}, t) + \hat{H}_c\hat{P}(\boldsymbol{x})$.

The Lanzcos algorithm case

Suppose that the quantum clock has in total N states. One can show, see chapter 5, that one can write the electron-clock Schrödinger equation as N Schrödinger equations each with a different potential. Thus the simplest way of solving this problem using the Lanzcos algorithm is solving each equation with a different Lanzcos propagator. Unfortunately, the perturbation of the original potential by the clock potential is very small such that it could not be resolved by the Lanzcos algorithm. As a result, a combination of the Lanzcos algorithm and split operator method has to be used. Applying the Trotter formula on Eq . 2.53 , then the second order truncated propagator could be written as,

$$\hat{U}(t+\Delta\mathrm{t}, t) = \exp\left(-\frac{\mathrm{i}}{2}\Delta\mathrm{t}\hat{H}_c\hat{P}(\boldsymbol{x})\right) \exp\left(-\mathrm{i}(\hat{T} + \hat{V}(t + \Delta\mathrm{t}, t))\Delta\mathrm{t}\right) \exp\left(-\frac{\mathrm{i}}{2}\Delta\mathrm{t}\hat{H}_c\hat{P}(\boldsymbol{x})\right). \tag{2.55}$$

To calculate this propagator first the exponential factor of the propagator on the most right of Eq. (2.55) is applied on the wavefunction when represented as in Eq. (2.52). This is straight forward to do since $|x\rangle \, |i\rangle$ represents an eigenbasis of

$\hat{H}_c\hat{P}(\boldsymbol{x})$. Then the middle factor is applied by using the Lanzcos algorithm on each clock eigen state $\int_{\boldsymbol{x}} \phi_{i,\boldsymbol{x}}(t)\,|x\rangle\,|i\rangle\,d\boldsymbol{x}$ separately. The matrix that is calculated using the Lanzcos algorithm from the middle exponential factor is the same for each clock state. This is because the middle factor does not depend on the clock. Finally, the first factor of the propagator is again applied by representing the wavefunction as in Eq. (2.52). Of course, the initial wavefunction is prepared in the form Eq. (2.52) and as a result the first and last step reduce to multiplication.

2.8. Conclusion

This chapter should be seen as a fundamental layout for the rest of the thesis, although the first section is only a review of tunneling time determination techniques. The other chapters discuss the fundamental ideas that one should know to understand this work. Most importantly, are the sections discussing strong-field tunnel ionization, the two step model, the attoclock experiment and the virtual detector. The section about the chosen electric field pulse is important but not necessary to understand the different chapters of this thesis. The final section, which explains the applied numerical techniques would be beneficial for someone who is interested in doing a similar work or reproducing the results represented here. In the next chapter we investigate strong field tunnel ionization of a one-dimensional system that models the essential features of an electron in a three-dimensional Coulomb potential.

Chapter 3.

Tunnel ionization in one dimension

In this chapter we investigate strong field tunnel ionization in a one-dimensional system that models the essential features of a correspondent three-dimensional system, the considered system is introduced in Sec. 3.2. As discussed in Sec. 2.4 the tunneling time delay extracted from the attoclock experiment depends on the used theoretical model, this is again briefly discussed in Sec. 3.1. The tunneling time delay that the attoclock experiment aims to measure is determined from first principles in Sec. 3.4. For determining the exit time of the ionized electron one needs to determine the position of the tunneling exit, in Sec. 3.3 we show that the exit determined from the energy conservation principle is indeed the tunneling exit. The so-called two-step model introduced in Sec. 2.3, which describes the ionization as instantaneous tunneling at the electric field maximum and classical motion afterwards with zero exit momentum, is commonly employed to describe tunnel ionization in adiabatic regimes. As found in Sec. 3.4 by solving numerically the time-dependent Schrödinger equation in one dimension and employing a virtual detector, see Sec. 2.5, at the tunnel exit that there is a nonvanishing positive time delay, between the electric field maximum and the instant of ionization. We additionally examine the exit momentum of the tunnel ionized electron in Sec. 3.5, where we find a nonzero exit momentum in the direction of the electric field. Moreover, we find that there is a difference between the asymptotic momentum predicted by the two-step model and the quantum mechanical one as shown in Sec. 3.6. As a result, in Sec. 3.6 we propose a modified two-step model that predicts the correct momentum of the tunnel ionized electron. These findings have implications on the experiments that try to measure tunneling times. Specifically, To extract proper tunneling times from asymptotic momentum distributions of ionized electrons, it is essential to incorporate the electron's initial momentum in the direction of the external electric field, as shown in Sec. 3.8.

Most of the results presented in this chapter have been published in Ref. [75].

3.1. Introduction

In attoclock experiments, electrons are ionized by elliptically polarized light, which makes the direction of the asymptotic momentum very sensitive to the ionization time $t_0 + \tau_{\text{exit}}$. In the extraction of τ_{exit} from attoclock experiments, it is state of the art to treat the ionized electron classically, to take into account Coulomb corrections,

and to assume that the electron's initial momentum follows from some semiclassical theory [51, 53]. For a reliable reconstruction of the attoclock time τ_{exit}, however, suitable initial conditions have to be identified as pointed out in Refs. [54, 55]. In particular, assumptions about the initial momentum bias the reconstructed value for τ_{exit}. The popular two-step model of tunnel ionization assumes a maximal ionization rate at the instant of maximal electric field strength, i. e., $\tau_{\text{exit}} = 0$, and that free electrons have zero initial momentum, i. e., $\boldsymbol{p}(t_0 + \tau_{\text{exit}}) = 0$. Within the two-step model, the electron's asymptotic momentum follows by solving the classical equations of motion for the electron's motion in the combined electromagnetic field of the binding potential and the ionizing external light pulse. This model, however, cannot be used as a benchmark for experiments, because a possible match or mismatch of experimental data and the theoretical prediction by the two-step model may be explained by various pairs of nonzero delay τ_{exit} [99] and nonzero initial momentum $\boldsymbol{p}(t_0 + \tau_{\text{exit}})$, which may a have nonzero component parallel to the electric field direction [49, 56].

Neither the delay τ_{exit} nor the initial momentum $\boldsymbol{p}(t_0+\tau_{\text{exit}})$ are directly accessible by experiments, and it is also challenging to calculate them analytically. Therefore, we employ *ab initio* quantum calculations and a virtual detector [57, 58] at the tunnel exit. The virtual detector technique allows us to determine directly the electron's time of arrival at the tunnel exit as well as its exit momentum.

We analyze theoretically an initially bound electron ionized by an electric field pulse. To determine the time delay τ_{exit} and the exit momentum, we solve the time-dependent Schrödinger equation and place a virtual detector at the tunneling exit. The virtual detector is realized by calculating the probability current at the exit. The most probable time delay τ_{exit} is determined by comparing the instant of maximum probability current at the potential barrier exit and the instant of maximum electric field strength. The exit momentum is determined by the space-resolved momentum distribution at the tunnel exit at the instant of ionization. By separating the wave function into a tunneled part and a bound part after the interaction with the laser pulse, we can calculate the momentum distribution of the tunneled electron, from which one can determine the most probable asymptotic momentum. We additionally find out that the quantum asymptotic momentum is different than the asymptotic momentum predicted by the two step model. As a result we propose a modified two-step model that predicts the correct asymptotic momentum.

In the next section we describe the considered system, the used parameters and the motivation behind choosing such a system and such parameters.

3.2. Considered system

As explained in 2.2 and 2.6, in experiments, a Coulomb-bound electron is usually excited by a laser pulse with a wavelength much bigger than the atomic dimensions such that the laser pulse is nearly homogeneous over the size of the atom. Furthermore, relativistic effects and effects due to the magnetic field component set in only

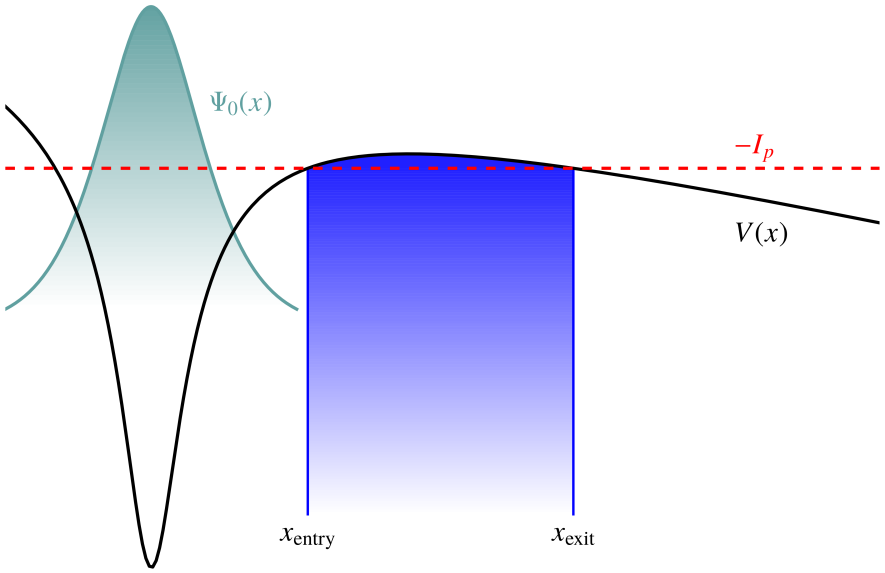

Figure 3.1.: The one dimensional tunneling barrier of a soft core potential bent by an electric field for the parameter $\mathcal{E}_0/Z^3 = 0.025$. The electron is represented by the ground state $\psi_0(x)$ of the soft core potential with binding energy $-I_p = -Z^2/2$. The points x_{entry} and x_{exit} represent the entry and exit points of the tunneling barrier respectively.

for tunneling from highly charged ions [50], see also 2.2. Thus, we will apply the electric dipole approximation. The laser pulse is modeled by a time-varying homogeneous electric field $\mathcal{E}(t) = \mathcal{E}_0 \exp(-\omega^2(t-t_0)^2/2)$, where t_0 denotes the instant of the maximum field strength $\mathcal{E}_0$ and $\tau_{\text{E}} = \sqrt{2}/\omega$ is the time scale of the rise and decay of the electric field. The linear polarization of the electric field and neglecting the magnetic field component render the motion of the electron quasi-one-dimensional allowing us to investigate general features of tunneling times in a one-dimensional scenario, see 2.6. Furthermore, tunneling in the fully three-dimensional Coulomb problem can be described by an effective one-dimensional tunneling barrier via introducing parabolic coordinates [100], see Chapter 4. Thus, we restrict ourselves to one-dimensional systems and consider an electron bound to the soft-core potential $-Z/\sqrt{x^2+\alpha(Z)}$ [59–62] to model the essential features of an electron in a three-dimensional Coulomb potential, see Fig. 3.1. Here, Z is the atomic number, and the softening parameter $\alpha(Z) = 2/Z^2$ is chosen such that the ground state energy of the soft-core potential is $-I_{\text{p}} = -Z^2/2$, which equals the ground state energy of the Coulomb potential [101]. Thus, the Schrödinger equation (in atomic units)

$$\mathrm{i}\frac{\partial\psi}{\partial t} = \hat{H}(t)\psi = \left(-\frac{1}{2}\frac{\partial^2}{\partial x^2} - \frac{Z}{\sqrt{x^2+\alpha(Z)}} - \mathcal{E}(t)x\right)\psi \tag{3.1}$$

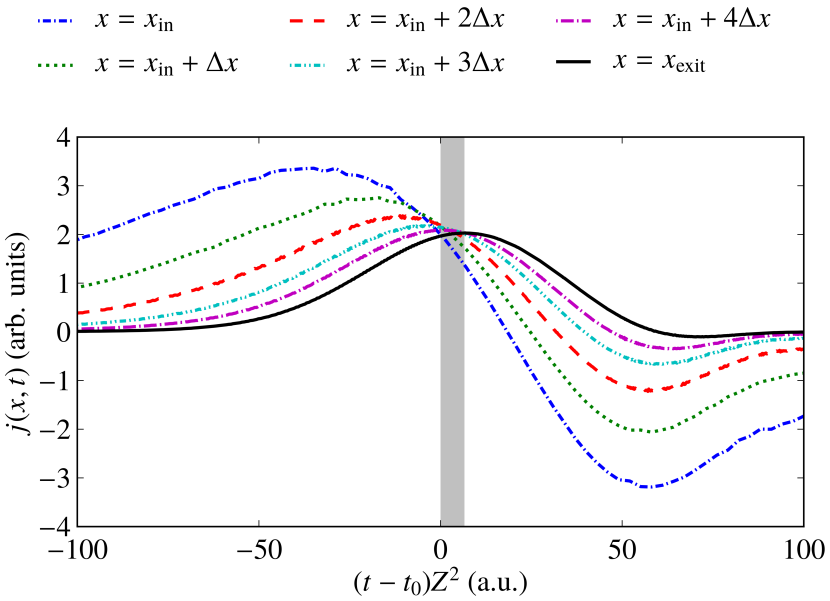

Figure 3.2.: The probability current $j(x,t)$ as a function of time at different positions x between the barrier entry $x = x_{\text{in}}$ and the barrier exit x_{exit} separated by $\Delta x = (x_{\text{exit}} - x_{\text{in}})/5$ for the parameters $\mathcal{E}_0/Z^3 = 0.048$ and $\gamma = 0.25$. The shadowed area represents the time between the instant of maximum electric field strength t_0 and the instant of maximum probability at x_{exit}. The figure is adopted from Ref. [75].

with the Hamiltonian $\hat{H}(t)$ and the effective potential $V(x,t) = -Z/\sqrt{x^2 + \alpha(Z)} - \mathcal{E}(t)x$ will be solved numerically [1], using the split operator method described in Sec. 2.7. The so-called Keldysh parameter $\gamma = \omega\sqrt{2I_{\text{p}}}/\mathcal{E}_0$ [41] characterizes the ionization process as dominated by tunneling for $\gamma \ll 1$ and by multiphoton ionization for $\gamma \gg 1$. Thus, simulation parameters will be set such that $\gamma < 1$ in the following as already discussed in 2.2.

After we have introduced the considered system, in the next section we investigate the position of the tunneling barrier exit for the above described system. The tunneling barrier exit is usually easily determined from the argument of energy conservation. But the argument of energy conservation is based on methodology of classical mechanics. One could ask does the quantum particle exit at the position determined by the energy conservation argument? Answering this question is essential for the techniques used here and for understanding tunnel ionization in general.

3.3. Tunneling exit determination

Here the tunneling barrier, and thus the tunneling exit, is determined by the classical argument of energy conservation, see 2.2. Additionally, the virtual detector method is used to verify the tunneling exit determined from the classical argument. In our one-dimensional model the probability current

$$j(x,t) = (\psi(x,t)^* \partial_x \psi(x,t) - \psi(x,t) \partial_x \psi(x,t)^*)/(2\mathrm{i}), \tag{3.2}$$

represents the average net number of electrons passing a given point at a specific time. Thus, we determine the ionization rate via the probability current at the exit x_{exit} as a function of time, where x_{exit} is defined by the maximum electric field strength $\mathcal{E}_0$ via $V(x_{\mathrm{exit}}, t_0) = -I_{\mathrm{p}}$, see Fig. 3.1. Monitoring the probability current at a fixed position is justified, because the tunnel probability is maximal for $\mathcal{E}(t) = \mathcal{E}_0$ and it is exponentially suppressed for lower electric fields. Furthermore,

$$\mathcal{E}(t) = \mathcal{E}_0(1 - \Delta t^2/\tau_{\mathrm{E}}^2 + O(\Delta t^4/\tau_{\mathrm{E}}^4)) \tag{3.3}$$

for $\Delta t = t - t_0$ with $|\Delta t| < \tau_{\mathrm{E}} = 2\sqrt{I_{\mathrm{P}}}/(\gamma \mathcal{E}_0)$. Thus the tunneling barrier does not change substantially if times close to t_0 are considered. To further ensure that the calculated exit x_{exit} is where the electron exits the barrier, we place a virtual detector at different points between x_{in} and x_{exit} and calculate $j(x,t)$ at each point as a function of time. As shown in Fig. 3.2, the probability current has a positive peak as well as a negative one for $x < x_{\mathrm{exit}}$, indicating the tunneling and reflection dynamics, respectively. This tunneling and reflection dynamics corresponds to under-the-barrier dynamics. As reflection is absent for $x \geq x_{\mathrm{exit}}$, the particle leaves the barrier at x_{exit}.

In the introduction we have introduced the two-step model that assumes that the electron exits at the instant of electric field maximum. After we have determined from first principles at which position does the electron exit, in the next section we answer the question, when does the electron exit the tunneling barrier?

3.4. Tunneling exit time

In this section we explain how to determine the time delay τ_{exit} and what discuss what does this delay mean. The time delay τ_{exit} is based on the time-dependent ionization rate.The most probable time delay τ_{exit} is calculated by subtracting the instant of maximum field strength from the instant of the maximum current, i. e., $\tau_{\mathrm{exit}} = \arg\max j(x_{\mathrm{exit}}, t) - \arg\max \mathcal{E}(t)$,see Fig. 3.3, which yields the positive time delay shown in Fig. 3.4. Note that, for the parameters used in Fig. 3.4, $\tau_{\mathrm{exit}} < \tau_{\mathrm{E}}$, and thus the electric field remains almost constant for times $|\Delta t| \lessapprox \tau_{\mathrm{exit}}$, justifying our choice for x_{exit}.

[1] The dependence on Z can be removed by suitable transformations of space, time, and the electric field strength, see [102]

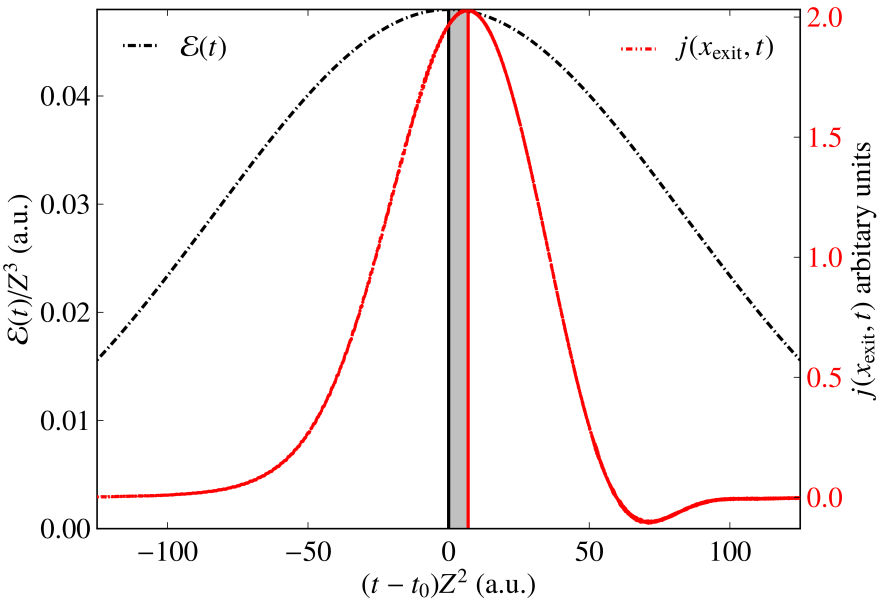

Figure 3.3.: The probability flow at the tunnel exit $j(x_{\text{exit}}, t)$ is plotted in function of time, as well as the electric field $\mathcal{E}(t)$, plotted for $\gamma = 0.25$ and $\mathcal{E}_0/Z^3 = 0.048$. Time delay τ_{exit} which is defined as the difference between the instant of maximum probability current at the exit and the instant of maximum electric field t_0 is marked by the shadowed area.

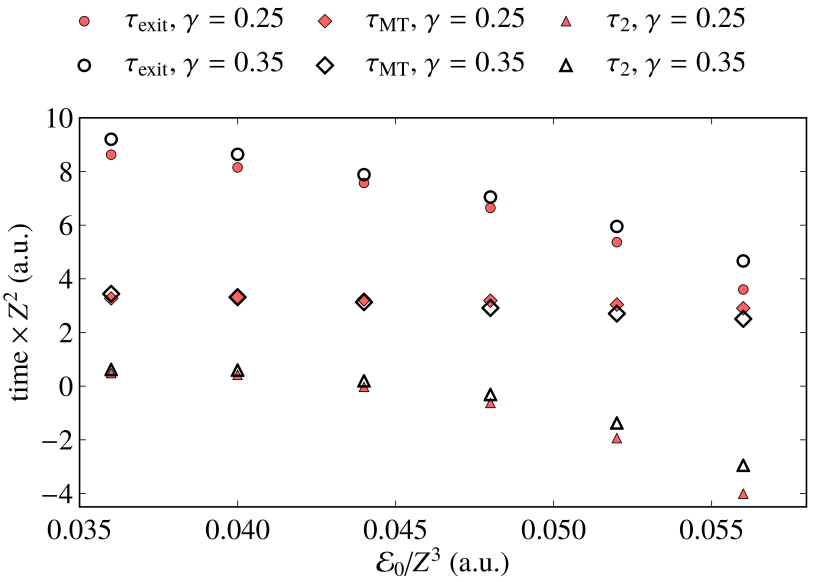

Figure 3.4.: The time delay τ_{exit}, the Mandelstam-Tamm time τ_{MT}, and the time τ_2(see 3.8) plotted for different electric field strengths $\mathcal{E}_0$ and for different Keldysh parameters γ. Definitions of the various times are given in text. The figure is adopted from Ref. [75].

The origin of the time delay τ_{exit} can be understood by considering the time-energy uncertainty principle and following its interpretation given by Mandelstam and Tamm [42, 103–105]. As a consequence of the time-energy uncertainty principle, the time, which a wave function ψ of a system with a time-independent Hamiltonian $\hat{H}$ needs to change significantly, is bounded from below by $1/(2\sigma_{\hat{H}})$, where

$$\sigma_{\hat{H}} = \sqrt{\langle\psi|\hat{H}^2|\psi\rangle - \langle\psi|\hat{H}|\psi\rangle^2}. \tag{3.4}$$

As mentioned before, the Hamiltonian in (3.1) can be considered as time-independent for times $|\Delta t| < \tau_{\text{E}}$. This allows us to define the Mandelstam-Tamm time

$$\tau_{\text{MT}} = \frac{1}{2}\left(\langle\psi(t_0)|\hat{H}(t_0)^2|\psi(t_0)\rangle - \langle\psi(t_0)|\hat{H}(t_0)|\psi(t_0)\rangle^2\right)^{-1/2}, \tag{3.5}$$

which is indeed a lower bound to the time delay τ_{exit} as indicated in Fig. 3.4. The time delay τ_{exit} is close to its lower bound τ_{MT}, which indicates that the delay τ_{exit} is a consequence of the wave function's inertia, i. e., its inability to adopt instantaneously to the field. The time delay τ_{exit} decreases as $\mathcal{E}_0$ increases at fixed Keldysh parameter γ and matches approximately τ_{MT} when the regime of over-the-barrier ionization is approached, which is for $\mathcal{E}_0/Z^3 \approx 0.06$ a.u.

The observed decrease of the delay τ_{exit} with growing electric field strength (but constant γ) is consistent with calculations for the case of a sudden turn-on of the electric field, which show that the time for the wave function to adopt to the electric field is proportional to the Keldysh time $\tau_{\text{K}} = \sqrt{2I_{\text{p}}}/\mathcal{E}_0$ [42, 105], although the functional dependence on $\mathcal{E}_0$ is different for continuously changing electric fields. For a fixed maximum electric field strength $\mathcal{E}_0$ but increasing γ, the time delay τ_{exit} increases. As γ increases, the pulse duration decreases, granting the wave function less time $\sim \tau_{\text{E}}$ to evolve and to adopt to the time-varying Hamiltonian during the rise of the electric field. Thus, the wave function has less time to develop the necessary components for tunneling and thus needs more time to reach the maximum ionization rate.

The delay τ_{exit} describes the time interval that the electron spends under the barrier *after the field maximum*. Interpreting τ_{exit} as a tunneling time [51] is justified only if the classical forbidden region is entered at the field maximum. Also, the time delay τ_{exit} is often understood as the time under the barrier , because the interpretation as under-the-barrier time is based on the assumption that tunneling starts at the instant of the maximal electric field, but the wave function could penetrate the tunneling barrier earlier. This will be examined and discussed thoroughly in the next chapter.

As we have seen the electron exits the tunneling barrier with a delay τ_{exit} which proves the assumption of the two-step model that the electron exits at the instant of electric field maximum wrong. Another assumption the two-step model makes is that the electron exit with a zero exit momentum along the electric field direction. This is investigated in the next section.

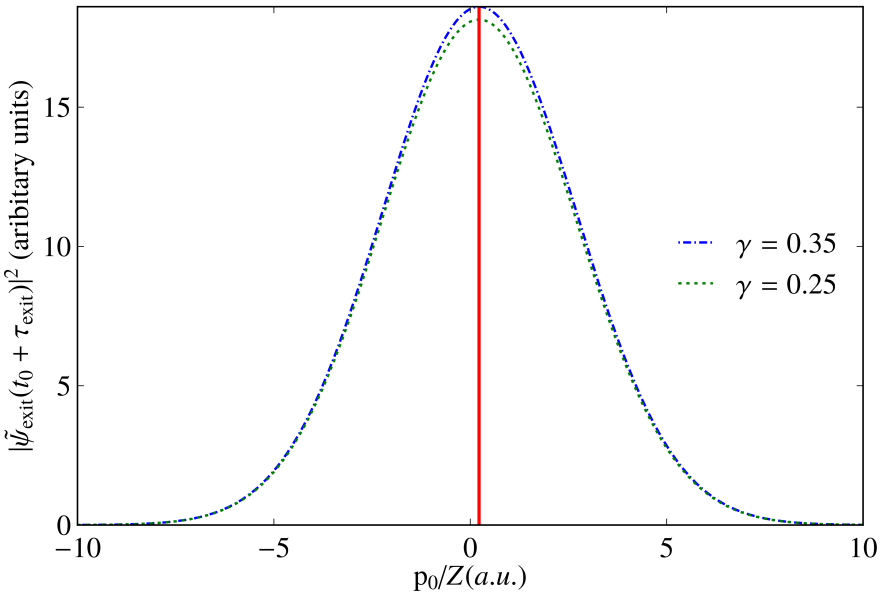

Figure 3.5.: The distribution of the exit momentum p_0 at the time $t_0 + \tau_{\mathrm{exit}}$ at the tunnel exit x_{exit} for electric field strength $\mathcal{E}_0 = 0.048$ and different Keldysh parameters γ. The distribution is obtained by Method 1 as described in text; see the main text for details. The windowing function is normal distribution of the form $1/(2\pi\sigma_w^2)\exp(-(x-x_{\mathrm{exit}})^2/2\sigma_w^2)$ and $\sigma_w = (x_{\mathrm{exit}} - x_{\mathrm{entry}})/20$.

3.5. Exit momentum

In the following, we determine the quantum mechanical exit momentum p_0 in the direction of the electric field at the tunnel exit x_{exit} at the instant of ionization $t = t_0 + \tau_{\mathrm{exit}}$ by two different methods. In the first method, we calculate a space-resolved momentum distribution around $x = x_{\mathrm{exit}}$ by multiplying the wave function $\psi(x, t_0 + \tau_{\mathrm{exit}})$ by a Gaussian window function with mean x_{exit} and width $\delta x = (x_{\mathrm{exit}} - x_{\mathrm{in}})/20$ and calculating its Fourier transform $\tilde{\psi}_{\mathrm{exit}}(t_0 + \tau_{\mathrm{exit}})$. The most probable exit momentum p_0 can be inferred by the momentum where $|\tilde{\psi}_{\mathrm{exit}}(t_0 + \tau_{\mathrm{exit}})|^2$ is maximal. In the second method, the most probable initial momentum p_0 is determined from the probability current $j(x_{\mathrm{exit}}, t_0+\tau_{\mathrm{exit}})$ at the exit at the instant of the maximum probability current. Following Refs. [57, 58], the local velocity of the wave function's probability flow at x_{exit} equals $v = j(x_{\mathrm{exit}}, t_0 + \tau_{\mathrm{exit}})/|\psi(x_{\mathrm{exit}}, t_0 + \tau_{\mathrm{exit}})|^2$. Both methods yield very similar results for the moment p_0 as shown in Fig. 3.8. The initial momentum p_0 is almost independent of the parameter γ and depends only weakly on the electric field strength $\mathcal{E}_0$.

As p_0 does not depend on the parameters of the external electric field it must result from the initial quantum state, i. e., the ground state of the binding potential. In fact, the ground state of the employed soft-core potential has in momentum space a width of about $0.38 \times Z$, which is of the same order as p_0; see Fig. 3.8. The fact that p_0 scales with the width of the ground state's momentum distribution and not

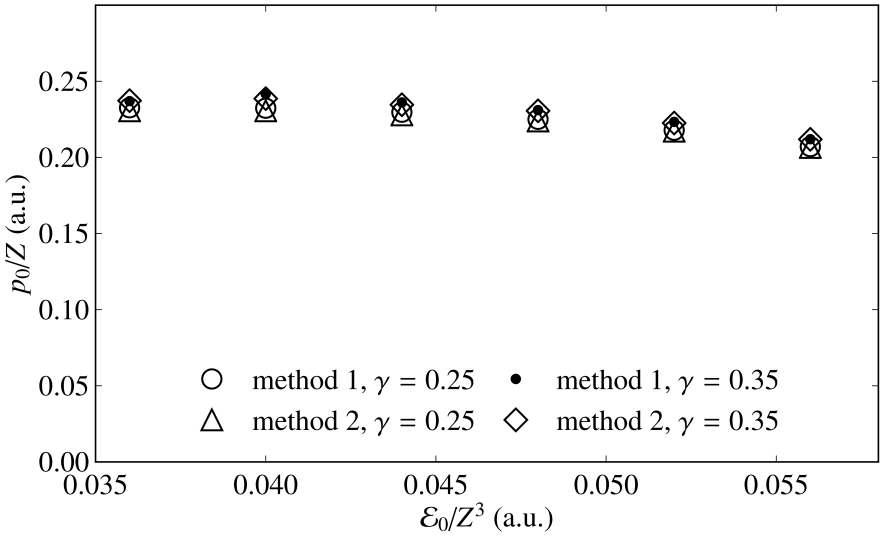

Figure 3.6.: The momentum p_0 at the time $t_0 + \tau_{\text{exit}}$ at the tunnel exit x_{exit} for different electric field strengths $\mathcal{E}_0$ and different Keldysh parameters γ as determined by two different methods. Method 1 is based on the space-resolved momentum distribution, while method 2 utilizes the velocity of the probability flow; see the main text for details on both methods. The figure is adopted from Ref. [75].

with its mean (which is zero) may be interpreted as momentum components, which propagate into the ionization direction, being ionized preferably. After we have seen in the two previous sections that the two assumptions of the two-step model are wrong, one can ask could this model still predict the correct final momentum of the tunnel ionized electron? This question is investigated in the next section.

3.6. Two step-model applicability

Applying the Wigner formalism to ionization from a zero-range potential by a static electric field it has been shown that the momentum of the tunnel-ionized electron at a far-away detector differs from the prediction of the two-step model in the so-called near-threshold-tunneling regime [49]. Our numerical solution of the time-dependent Schrödinger equation allows us now to study the final momentum by going beyond the static-field approximation.

Propagating the wavefunction till some final time t_f such that $t_\text{f} - t_0 \gg 1/\omega$ we can separate the tunneled part from the bound part of the wavefunction. The tunneled wavefunction $\psi_{\text{free}}(t_\text{f})$ is determined by projecting out all bound eigenstates of $\hat{H}$ in Eq. (3.1) for $\mathcal{E}(t) = 0$ from $\psi(t_\text{f})$. The resulting probability densities of $\psi_{\text{free}}(t_\text{f})$ and its momentum-space representation $\tilde{\psi}_{\text{free}}(t_\text{f})$ are shown in Fig. 3.7. Note that the momentum distribution of the tunneled electron is relatively sharp whereas the position distribution is very widely spread. From $\tilde{\psi}_{\text{free}}(t_\text{f})$ the most probable momentum $p_{\text{f,q}}$ can be inferred by the position where $|\tilde{\psi}_{\text{free}}(t_\text{f})|^2$ is maximal.

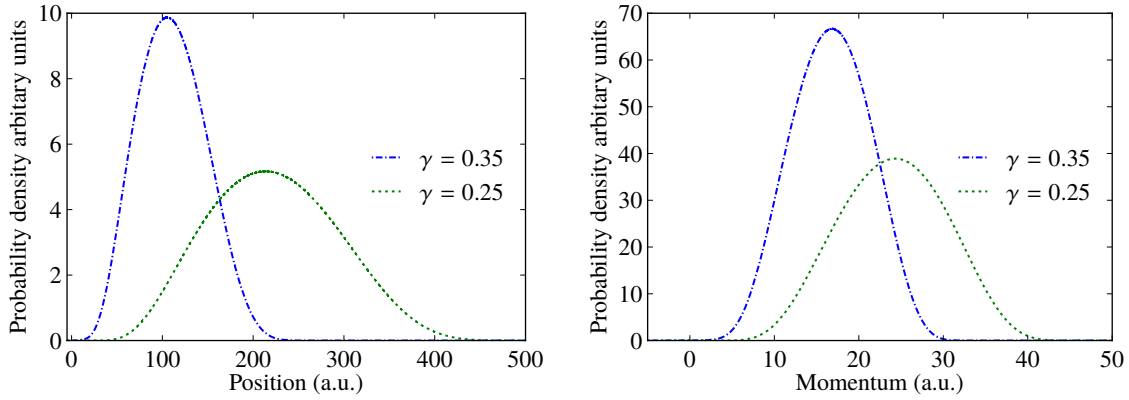

Figure 3.7.: (color online) Probability distribution in position and momentum space of the tunneled part of the electron's wavefunction for $\mathcal{E}_0/Z^3 = 0.056$ a.u. and for different Keldysh parameters γ at time $t_\mathrm{f} - t_0 = 4/\omega$, i. e., the electric field has been nearly turned off.

For the same parameters of the above quantum simulations we also calculated the final momentum $p_{\mathrm{f,c}}$ of the tunneled electron as predicted by the two-step model. This is accomplished by solving Newton's equations of motion till time t_f for the initial position $x(t_0) = x_\mathrm{exit}$ and the initial momentum $p(t_0) = 0$. The difference between the final quantum and classical momenta $\Delta p_\mathrm{f} = p_{\mathrm{f,q}} - p_{\mathrm{f,c}}$ is indicated in Fig. 3.8 by squares. In particular, the solution of the time-dependent Schrödinger equation yield a final momentum that differs from the prediction of the two-step model more the stronger the external electric field $\mathcal{E}_0$ is.

3.7. Modified two-step model

Our numerical quantum mechanical calculations point out two problems of the two-step model. The electron leaves the tunneling barrier *after* the instant of maximal electric field strength and, furthermore, there is a difference between the final momenta from the quantum theory and from the two-step model. Therefore, we suggest a modified two-step model, which allows for a nonzero initial momentum and takes into account the time delay τ_exit. In this modified two-step model the initial conditions are specified at the instant of the maximal ionization rate. The initial position equals $x(t_0+\tau_\mathrm{exit}) = x_\mathrm{exit}$ and the initial momentum is $p(t_0+\tau_\mathrm{exit}) = p_{i,e}$. This effective initial momentum $p_{i,f}$ is chosen such that the final momentum $p'_{\mathrm{f,c}}$ predicted by this modified two-step model agrees with the final quantum momentum $p_{\mathrm{f,q}}$. Note that the effective initial momentum $p_{i,f}$ is different than the initial momentum p_0. Using p_0 as an initial condition will also yield a final moemntum which is different than the quantum determined one $p_{\mathrm{f,q}}$. This can be attributed to that $p_{\mathrm{f,q}}$ originates from the motion of a broad wave packet which experiences a spatially varying soft core potential force [106]. Our numerical results yield that the effective initial mo-

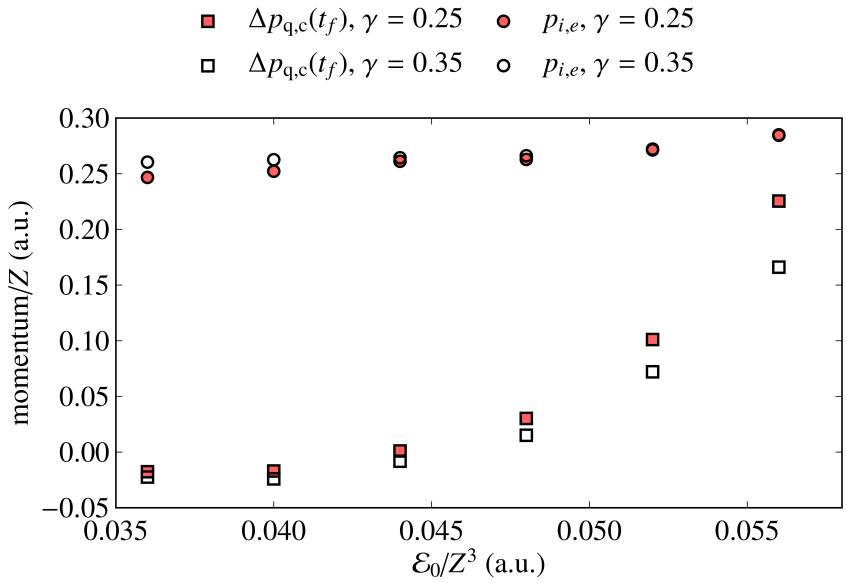

Figure 3.8.: (color online) The difference Δp_{f} between the quantum momentum $p_{\mathrm{f,q}}$ and the classical momentum $p_{\mathrm{f,c}}$ at final simulation time $t_{\mathrm{f}} - t_0 = 4/\omega$ plotted for different electric field strengths and for different Keldysh parameters γ. Additionally the plot indicates the effective initial momentum $p_{i,e}$, which is required to match the final momentum of the modified two-step model with the final quantum momentum $p_{\mathrm{f,q}}$.

mentum is almost independent of the Keldysh parameter γ and the maximal electric field strength $\mathcal{E}_0$ as indicated by the circles in Fig. 3.8.

3.8. Conclusion and implications

The above considerations are relevant for every high-precision laser-induced tunneling experiment. Here we discuss as an example attoclock measurements due to their currently high attention. Attoclock experiments aim to determine the time delay τ_{exit} between the instant of the electric field maximum and the instant of tunneling, which is not directly accessible experimentally. Instead, the asymptotic momentum of the tunneled electron is measured. As it depends on the exit momentum and on the moment at which the electron starts to propagate freely in the field, one can infer τ_{exit} from the electron's asymptotic momentum provided that the exit momentum is known. The delay τ_{exit} is commonly reconstructed by assuming zero initial momentum in the electric field direction. Our numerical simulations and the virtual detector approach, however, indicated a nonzero initial momentum in the direction of the electric field. How does the zero-initial-momentum assumption affect the reconstruction of τ_{exit} from the asymptotic momentum?

Using the Newton equations of motion for an electron in the effective potential $V(x,t)$, we can calculate at which instant of time the electron must exit the barrier at x_{exit} with zero initial momentum in the electric field direction such that its

asymptotic momentum equals $p_{\mathrm{f,q}}$. The result is the time delay τ_2, which is also shown in Fig. 3.4 and that does *not* coincide with the delay τ_{exit}. The delay τ_2 is close to zero or even negative depending on the electric field strength as found in Refs. [49, 50, 54, 55, 99]. Consequently, the delay τ_{exit} and the instant of tunneling cannot be determined on the basis of the standard assumption of zero initial momentum in the electric field direction. The exit momentum has to be included.

Similarly to the delay τ_2, also the time delays determined from measured asymptotic momenta are close to zero (of the order of experimental uncertainties) [39, 40]. As our numerical calculations indicate that the reconstruction of the delay τ_{exit} from asymptotic momenta is sensitive to the electron's exit momentum, we argue that a possible nonzero exit momentum into the electric field direction has to be included for a reliable reconstruction of τ_{exit} in attoclock experiments, not only a nonzero exit momentum in the direction perpendicular to the electric field as recently proposed [54, 107].

Furthermore, there is a discrepancy between the final momentum of the ionized electron as calculated via the Schrödinger equation and as predicted by the classical two-step model. Describing the ionization, however, by a modified two-step model, where ionization happens τ_{exit} after the electric field has reached its maximum and which allows for a suitable initial momentum into the direction of the electric field, gives the correct final momentum. The initial momentum necessary to correct the two-step model is different than the initial momentum the electron tunnel ionize with. This results probably from the width of the tunnel ionized wave packet.

In this chapter we have shown that the tunneling exit determined from energy conservation is indeed the position where the particle leaves the tunneling barrier. On one hand, it follows from the energy conservation argument that the electrons exits the tunneling barrier with zero momentum. On the other hand, we have shown that the electron exits the tunneling barrier with a non-zero momentum. thus one concludes that the tunneling exit is not the point where the particle has zero momentum, rather it is the point where the tunneling wave packet completely tunnels and does not reflect anymore.

Chapter 4.

Tunnel ionization in two dimensions

In the previous chapter we have employed the virtual detector method, see Sec. 2.5 to find out when does the electron exit the tunneling barrier. In this chapter we apply the same approach for a two-dimensional system which is described in Sec. 4.2. The motivation behind choosing a two-dimensional system is two-fold. First, the concepts introduced for the one-dimensional system could be applied for the two-dimensional system, and with this one can check if any of the qualitative behavior seen for the one-dimensional system originates from it's dimensionality. Second, there are solid state systems that can be described by a two-dimensional Hamiltonian. In Sec. 4.3 and with the help of Appendix we show that the parabolic coordinates are the natural coordinate system for tunnel ionization in two-dimensions, and that defining the tunneling barrier via parabolic coordinates is the correct method to define tunneling ionization in two dimensions. In Sec. 4.4 we investigate what is the meaning of the time delay τ_{exit} that the attoclock experiment aims to measure. Specifically, with the theoretical approach introduced in this chapter, it becomes possible to define unique moments when the electron enters and leaves with highest probability the classically forbidden region from first principles and a tunneling time can be specified unambiguously. It is shown that neither the moment when the electron enters the tunneling barrier nor when it leaves the tunneling barrier coincide with the moment when the external electric field reaches its maximum. With this information the meaning of the time delay τ_{exit} becomes clear. Apart from that, in Sec. 4.5 using virtual detectors we determine the quantum trajectory of the tunneling electron. We find out that under the tunneling barrier as well as at the exit the electron has a nonzero velocity in electric field direction as we also found out in the previous chapter. After comparing these quantum trajectories with correspondent classical ones, we find out that this nonzero exit velocity has to be incorporated when the free motion of the electron is modeled by classical equations of motion. Most of the results of this chapter have been published in Ref. [108].

4.1. Introduction

In the case of tunnel ionization, see Fig. 4.1, the experimental determination of a tunneling time is complicated by the fact that it is notoriously difficult to determine the starting (and ending) moment of the tunnel dynamics. There is no apparent reason to assume that the electron enters the barrier at the instant of the electric

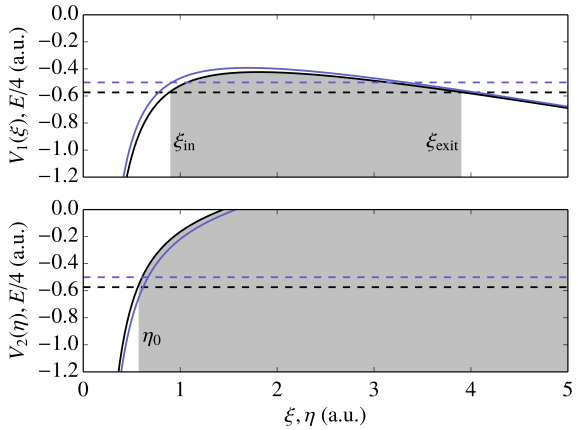

Figure 4.1.: Tunneling potentials $V_1(\xi)$ and $V_2(\eta)$ (solid lines) and the ground state energy level E (dashed lines) for the two-dimensional Coulomb problem with (black) and without (light blue) accounting for the Stark effect in parabolic coordinates ξ and η for $\mathcal{E} = 1$ a.u. Intersections between the potential lines and the energy level determine the borders between classically allowed classically forbidden regions, i. e., the tunneling entry ξ_{in}, tunneling exit ξ_{exit}, and η_0. See Appendix for details. This figure is adopted from Ref. [108].

field maximum. In fact, we are going to demonstrate that one has to carefully distinguish between the tunneling time, i. e., the time to cross the tunneling barrier, and the tunneling delay, i. e, the time delay until the electron becomes quasi-free with respect to some external reference, e. g., the moment of maximal electric field strength.

Experimentally the quantum dynamics in the vicinity of the tunneling barrier cannot be studied directly, i. e., it is not possible to place a detector close to the atomic tunneling barrier. Thus, information about the tunneling dynamics has to be inferred from measurable asymptotic quantities, e. g., the momentum distribution of the photo ionized electrons. In attoclock experiments, an electron is ionized by an elliptically polarized few-cycle pulse. This quasi-free electron is accelerated in the rotating electric field and in this way the instant of ionization t_{exit} is mapped to the final angle of the momentum vector in the polarization plane using some theoretical model. For a disccusion of the main concept of the attoclock experiment see Sec. 2.4.

In view of the difficulties of determining tunneling times from asymptotic momentum measurements, see Sec. 3.1 , we consider a complementary theoretical approach based on *ab initio* solutions of the time-dependent Schrödinger equation and virtual detectors [57, 58], which allows us to link tunneling times to observables related to the quantum dynamics in the vicinity of the tunneling barrier. The main aim of this chapter is to determine how much time does the electron spend under the barrier. With the same method used in the previous chapter we determine when does the electron enter and leave the tunneling barrier. From those two times the time spent by the electron under the barrier is determined. In the next section we introduce

the two-dimensional system considered for answering the above raised questions, and also the motivation behind choosing such a system.

4.2. Considered system

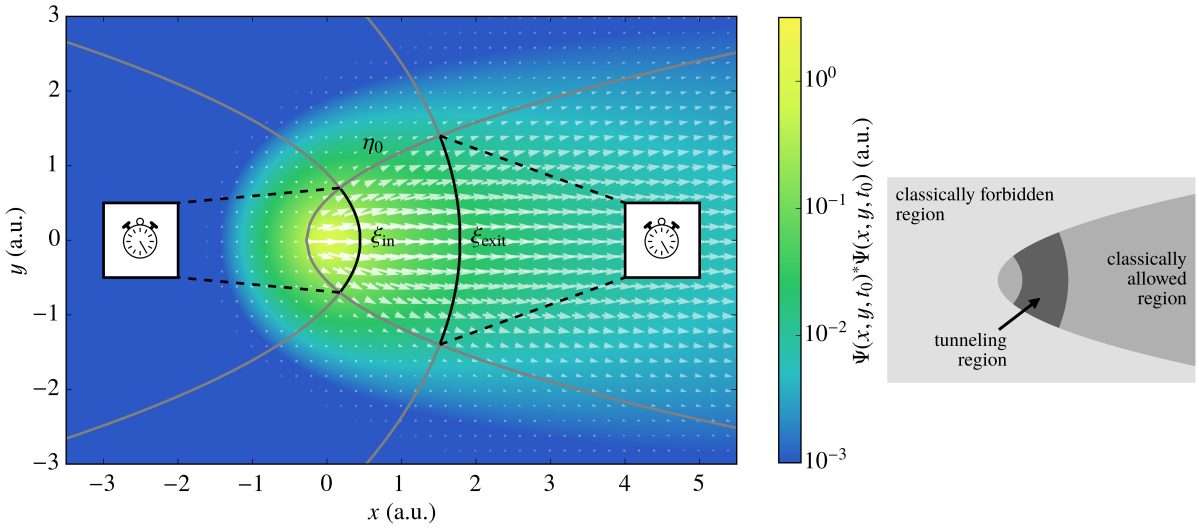

Figure 4.2.: Schematic of tunneling time determination via virtual detectors at the tunneling entry and the tunneling exit. The lines $\xi = \xi_{\text{in,out}}$ and $\eta = \eta_0$ which determine tunneling region, the classically forbidden, and the classical allowed regions are indicated by the solid lines; see Ref. [109] and Appendix for details. The black solid lines indicate the positions of the virtual detectors. The wave-function's probability density $\Psi(x,y,t)^*\Psi(x,y,t)$ at the instant of electric field maximum, i. e., $t = t_0$, is represented by colors for $\mathcal{E}_0 = 1.1$ a.u. and for the Keldysh parameter $\gamma = 0.25$. Arrows indicate the probability current $\boldsymbol{j}(x,y,t)$, where the arrows' length is proportional to the absolute value of the current and the arrows' opacity scales with the wave-function's probability density.This figure is adopted from Ref. [108].

In the following, we will study tunnel ionization from a two-dimensional Coulomb potential. The restriction to two dimensions is mainly because this system resembles tunnel ionization from hydrogen-like ions while keeping the computational demands small. In the long-wavelength limit, i. e., when the dipole approximation is applicable, see Sec. 2.2, the three-dimensional Coulomb potential with an external linearly polarized electric field has rotational symmetry which makes this system effectively two-dimensional. Furthermore, the two-dimensional Coulomb problem is of interest in its own and has been used to model some semiconductor systems [110–112]. The two-dimensional Coulomb potential can also be derived as a limit of the Hamiltonian of a three-dimensional hydrogen atom in a planar slab as the width of the slab tends to zero [113].

Applying the dipole approximation and choosing the coordinate system such that the linearly polarized external electric field $\mathcal{E}(t)$ points into the (negative) x direction, the Schrödinger equation reads in atomic units,

$$\mathrm{i}\frac{\partial\Psi(x,y,t)}{\partial t} = \hat{H}\Psi(x,y,t) = \left(-\frac{1}{2}\frac{\partial^2}{\partial x^2} - \frac{1}{2}\frac{\partial^2}{\partial y^2} - \frac{1}{\sqrt{x^2+y^2}} - x\mathcal{E}(t)\right)\Psi(x,y,t)\,. \tag{4.1}$$

In order to study the ionization dynamics without undesirable artifacts, i. e., to avoid multiple ionization and rescattering, we choose an electric field pulse with a unique maximum,

$$\mathcal{E}(t) = \mathcal{E}_0 \exp\left(-\frac{\omega^2(t-t_0)^2}{2}\right)\,, \tag{4.2}$$

where t_0 denotes the instant of maximal electric field $\mathcal{E}(t_0) = \mathcal{E}_0$ and $\tau_\mathcal{E} = \sqrt{2}/\omega$ is the time scale of the raise and decay of the electric field. In contrast to the one-dimensional case, in two dimensions it is not straight forward to define the tunneling region, and accordingly the realization of the virtual detectors is also more demanding. In the next section and with the help of the Appendix we define the tunneling region and the virtual detectors for the above described system.

4.3. Tunneling region determination and realization of the virtual detectors

Cartesian coordinates are not the most suitable choice to deal with the Coulomb problem with an external homogeneous electric field. Parabolic coordinates are the natural coordinate system for this problem. In particular, it allows to define a tunneling barrier [114]. As one can show, the Hamiltonian $\hat{H}$ in Eq. (5.1) separates in parabolic coordinates $0 \leq \xi < \infty$ and $0 \leq \eta < \infty$, which are related to the Cartesian coordinates x and y via

$$x = \frac{\xi - \eta}{2}\,, \tag{4.3a}$$

$$y = \sqrt{\xi\eta}\,, \tag{4.3b}$$

into two independent one-dimensional Schrödinger-type Hamiltonians with specific potentials $V_1(\xi)$ and $V_2(\eta)$, see Appendix for details. While $V_2(\eta)$ is purely attractive, $V_1(\xi)$ represents the tunneling barrier and, therefore, ξ denotes the tunneling direction. Intersections of the potentials with the energy value $E/4$ of the one-dimensional Hamiltonians define the borders between the classically allowed, the tunneling, and the classically forbidden regions. Here, E denotes the Stark-effect

corrected ground state energy of the two-dimensional system. The classically allowed, the tunneling, and the classically forbidden regions are characterized by

$$E/4 > V_1(\xi)\,, \qquad E/4 > V_2(\eta)\,, \tag{4.4a}$$
$$E/4 > V_1(\xi)\,, \qquad E/4 < V_2(\eta)\,, \tag{4.4b}$$
$$E/4 < V_1(\xi)\,, \qquad E/4 < V_2(\eta)\,, \tag{4.4c}$$

respectively. The tunneling barrier is confined by the three parabolas at $\xi = \xi_{\text{in}}$, $\xi = \xi_{\text{exit}}$, and $\eta = \eta_0$, which are functions of the applied electric field strength $\mathcal{E}(t)$. See Appendix for details and also Figs. 4.1 and 4.2.

As the tunneling barrier is defined we introduce how one can realize the virtual detector for this system. The virtual detectors, see Sec. 2.5, are placed at $\xi = \xi_{\text{in}}$ and $\xi = \xi_{\text{exit}}$ as given for the maximal electric field strength $\mathcal{E}_0$ at $t = t_0$. In two dimensions, the surface integral in Eq. (2.19) becomes a line integral of a vector field $\boldsymbol{j}(x, y, t)$. Thus, the probability current over the entry line $\xi = \xi_{\text{in}}$, denoted by $D_{\xi_{\text{in}}}(t)$, and the current over the exit line $\xi = \xi_{\text{exit}}$, denoted by $D_{\xi_{\text{exit}}}(t)$, are given explicitly by

$$D_\xi(t) = \int_0^{\eta_0} \boldsymbol{j}(x(\xi,\eta), y(\xi,\eta), t) \cdot \begin{pmatrix} \frac{\partial x(\xi,\eta)}{\partial \eta} \\ \frac{\partial y(\xi,\eta)}{\partial \eta} \end{pmatrix} \mathrm{d}\eta + \int_0^{\eta_0} \boldsymbol{j}(x(\xi,\eta), -y(\xi,\eta), t) \cdot \begin{pmatrix} \frac{\partial x(\xi,\eta)}{\partial \eta} \\ -\frac{\partial y(\xi,\eta)}{\partial \eta} \end{pmatrix} \mathrm{d}\eta\,, \tag{4.5}$$

where we have taken into account that Eq. (4.3) covers only the upper half of the coordinate system. Monitoring the probability current at these *fixed* entry and exit lines can be justified as follows. For static fields the tunneling probability is maximal for maximal electric fields and it is exponentially suppressed for lower fields. Furthermore, the applied electric field (5.2) is quasistatic for $|t - t_0| < \tau_{\mathcal{E}}$, i. e.,

$$\mathcal{E}(t) = \mathcal{E}_0 \left(1 - (t - t_0)^2/\tau_{\mathcal{E}}^2 + O\left((t - t_0)^4/\tau_{\mathcal{E}}^4\right)\right)\,. \tag{4.6}$$

Therefore, the tunneling barrier is also quasistatic if times close to t_0 are considered. As it will be shown later, the extracted tunneling times are short compared to $\tau_{\mathcal{E}}$ indeed.

The Schrödinger equation (5.1) is solved numerically by employing a Lanczos propagator [85, 98] and fourth-order finite differences for the discretization of the Schrödinger Hamiltonian, see Sec. 2.7 for details. The ground state of the two-dimensional Coulomb potential was chosen as an initial condition at $t - t_0 = -5\tau_{\mathcal{E}}$, i. e., when the external electric field is negligible small. The so-called Keldysh parameter $\gamma = \omega\sqrt{-2E_0}/\mathcal{E}_0$ [41] characterizes the ionization process as dominated by tunneling for $\gamma \ll 1$ and by multiphoton ionization for $\gamma \gg 1$. Here, E_0 denotes the ground state binding energy, which equals $E_0 = -2$ a.u. for the two-dimensional

Coulomb problem, see also the Appendix. In the following, the electric field amplitude $\mathcal{E}_0$ and the frequency ω are adjusted such that $\gamma = 0.25 < 1$.

Figure 4.2 illustrates the ionization dynamics in the vicinity of the tunneling barrier by presenting the electron's probability density $\Psi(x,y,t)^*\Psi(x,y,t)$ and the probability current $\boldsymbol{j}(x,y,t)$ at the instant of maximal field strength $t = t_0$. The external electric field induces a probability current opposite to the direction of the electric field. This flow is nonnegligible only in the region $\eta < \eta_0$, i. e., in the classically allowed region and the tunneling region. Thus, the shape of the probability current confirms that parabolic coordinates are the natural choice to define a tunneling barrier for the Coulomb problem.

Having defined the tunneling region and accordingly the required measurement apparatus (virtual detector), in the next section we determine when does the electron enter and exit the tunneling barrier. The obtained results are discussed and explained.

4.4. Exit time and time spent under the barrier

The action of the external electric field induces a probability current, which flows over the tunneling barrier's entry line $\xi = \xi_{\text{in}}$ and its exit line $\xi = \xi_{\text{exit}}$. This means, probability is carried over from the center region of the Coulomb potential into the tunneling barrier, from where it can escape into the classically allowed region. The quantities $D_{\xi_{\text{in}}}(t)$ and $D_{\xi_{\text{exit}}}(t)$ grow and decay over time with the applied external electric field, as shown in Fig. 4.3. As a central result of our numerical solution of the Schrödinger equation, however, the position of the maxima of $D_{\xi_{\text{in}}}(t)$, $D_{\xi_{\text{exit}}}(t)$, and the electric field $\mathcal{E}(t)$ do not coincide. The probability current over the tunneling entry $D_{\xi_{\text{in}}}(t)$ reaches its maximum before the maximum of the electric field is attained. Furthermore, the probability current over the tunneling exit $D_{\xi_{\text{exit}}}(t)$ may reach its maximum before or after the maximum of the electric field is attained depending on the electric field strength $\mathcal{E}_0$. For the rather strong electric field of the parameters of Fig. 4.3, $D_{\xi_{\text{exit}}}(t)$ reaches its maximum slightly before the electric field. Turning off the external electric field, the flow at the tunneling entry becomes negative and then oscillates rapidly around zero after switching off the electric field. These oscillations are a result of the excitation of the the bound portion of the wave function during the action of the electric field. The final bound state is a superposition of several eigenstates causing a nonsteady probability current. In contrast, the quantity $D_{\xi_{\text{exit}}}(t)$ remains positive as reflections are absent at the tunneling exit and behind the tunneling barrier [75], where this result was also obtained in the previous chapter.

Monitoring the probability current at $\xi = \xi_{\text{in}}$ and $\xi = \xi_{\text{exit}}$ allows us to determine the moments when the electrons enters or leaves the tunneling barrier with maximal probability. The probability to cross the tunneling barrier entry at $\xi = \xi_{\text{in}}$ or the exit at $\xi = \xi_{\text{exit}}$ during the small time interval $[t, t + \Delta t]$ is $\Delta t\, D_{\xi_{\text{in}}}(t)$ and $\Delta t\, D_{\xi_{\text{exit}}}(t)$,

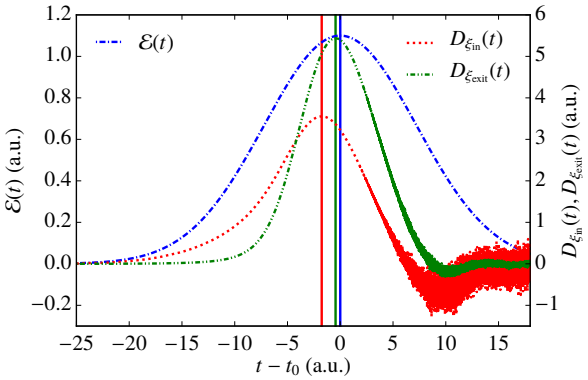

Figure 4.3.: The probability current $D_{\xi_{\mathrm{in}}}(t)$ over the entry line $\xi = \xi_{\mathrm{in}}$ and the current over $D_{\xi_{\mathrm{exit}}}(t)$ the exit line $\xi = \xi_{\mathrm{exit}}$ and the amplitude of the external electric field $\mathcal{E}(t)$ as functions of time t. The three vertical lines indicate from left to right the moments of maximal probability current over the line $\xi = \xi_{\mathrm{in}}$, of maximal electric field, and of maximal probability current over the line $\xi = \xi_{\mathrm{exit}}$. The parameters of the electric field correspond to a maximal field strengths of $\mathcal{E}_0 = 1.1$ a.u. and a Keldysh parameter $\gamma = 0.25$. This figure is adopted from Ref. [108].

respectively. This motivates us to introduce the times of maximal flow over the tunneling entry and exit as

$$t_{\mathrm{in}} = \arg\max D_{\xi_{\mathrm{in}}}(t) \tag{4.7}$$

and

$$t_{\mathrm{exit}} = \arg\max D_{\xi_{\mathrm{exit}}}(t)\,. \tag{4.8}$$

Then the delay between the instant of the maximum of the driving electric field t_0 and the exit time t_{exit}, the tunneling delay,

$$\tau_{\mathrm{exit}} = t_{\mathrm{exit}} - t_0 \tag{4.9}$$

and the tunneling time

$$\tau_{\mathrm{tsub}} = t_{\mathrm{exit}} - t_{\mathrm{in}} \tag{4.10}$$

can be introduced with the definitions above. A measurement of the delay τ_{exit} is implemented in the attoclock experiments. The time τ_{tsub} denotes the delay between the instants when the probability flow is maximal at the tunneling-barrier's entry and at the exit. Thus, τ_{tsub} may be interpreted as the typical time which an electron needs to pass the tunneling barrier.

The times τ_{exit} and τ_{tsub} are presented in Fig. 4.4 for the considered setup and varying electric field amplitudes $\mathcal{E}_0$. An increasing electric field amplitude reduces the width of the tunneling barrier. Consequently, the tunneling time τ_{tsub} decreases

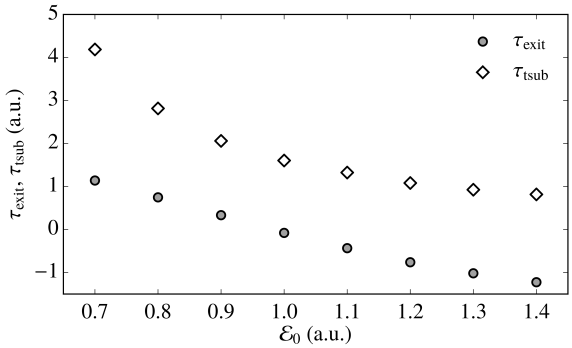

Figure 4.4.: The tunneling delay τ_{tsub} and the tunneling time τ_{exit} as functions of the electric field amplitude $\mathcal{E}_0$. The frequency ω is adjusted such that the Keldysh parameter is fixed to $\gamma = 0.25$. This figure is adopted from Ref. [108].

with increasing electric field amplitude $\mathcal{E}_0$, as shown in Fig. 4.4. The time τ_{tsub} remains, however, always positive. This means, the probability current reaches its maximum at the entry of the tunneling barrier before the current becomes maximal at the exit, i. e., the electron enters the barrier before it exits the barrier. Furthermore, it follows from the data in Fig. 4.4 that $\tau_{\mathrm{tsub}} > \tau_{\mathrm{exit}}$ and consequently $t_{\mathrm{entry}} < t_0$, because $\tau_{\mathrm{tsub}} - \tau_{\mathrm{exit}} = t_0 - t_{\mathrm{entry}}$. This means, the electron always enters the tunneling barrier before the electric field reaches its maximum.

To explain the reason for this behavior, we define in analogy to Eq. (4.5) the two integrals over the probability density

$$D_\xi^\varrho(t) \quad = \quad \int_0^{\eta_0} \varrho(x(\xi,\eta), y(\xi,\eta), t)\,\mathrm{d}\eta \;+\; \int_0^{\eta_0} \varrho(x(\xi,\eta), -y(\xi,\eta), t)\,\mathrm{d}\eta \quad (4.11)$$

and over the velocity field

$$D_\xi^{\boldsymbol{\nabla}\varphi}(t) = \int_0^{\eta_0} \boldsymbol{\nabla}\varphi(x(\xi,\eta), y(\xi,\eta), t) \cdot \begin{pmatrix} \frac{\partial x(\xi,\eta)}{\partial \eta} \\ \frac{\partial y(\xi,\eta)}{\partial \eta} \end{pmatrix} \mathrm{d}\eta$$
$$+ \int_0^{\eta_0} \boldsymbol{\nabla}\varphi(x(\xi,\eta), -y(\xi,\eta), t) \cdot \begin{pmatrix} \frac{\partial x(\xi,\eta)}{\partial \eta} \\ -\frac{\partial y(\xi,\eta)}{\partial \eta} \end{pmatrix} \mathrm{d}\eta\,, \quad (4.12)$$

which are motivated by fact that the probability current can be written as a product of the probability density and the local velocity, see Eq. (2.17). $D_{\xi_{\mathrm{in}}}^\varrho(t)$ gives the probability density integrated along the entry line $\xi = \xi_{\mathrm{in}}$ in function of time, while $D_{\xi_{\mathrm{in}}}^{\boldsymbol{\nabla}\varphi}(t)$ denotes the integrated velocity. As shown in Fig. 4.5, the velocity along the entry line $D_{\xi_{\mathrm{in}}}^{\boldsymbol{\nabla}\varphi}(t)$ increases with the electric field, reaches a maximum at the instant of electric field maximum $t = t_0$, then decreases with the electric field and it becomes even negative due to reflections from the tunneling process. Finally, the integrated velocity $D_{\xi_{\mathrm{in}}}^{\boldsymbol{\nabla}\varphi}(t)$ oscillates around zero indicating the excitation of the bound state. The probability density along the entry line $D_{\xi_{in}}^\varrho(t)$ is nonzero

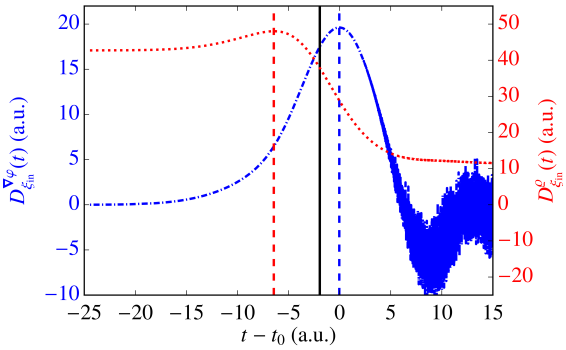

Figure 4.5.: The probability density $D^{\varrho}_{\xi_{\mathrm{in}}}(t)$ (red dashed line, right scale) and the local velocity $D^{\boldsymbol{\nabla}\varphi}_{\xi_{\mathrm{in}}}(t)$ (blue dot-dashed line, left scale) along the entry line $\xi = \xi_{\mathrm{in}}$ are plotted in function of time for the electric field strength $\mathcal{E}_0 = 1.3\,\mathrm{a.u.}$ The solid black line denotes the instant of maximal $D_{\xi_{\mathrm{in}}}(t)$, vertical dashed lines indicate the position of the maxima of $D^{\varrho}_{\xi_{\mathrm{in}}}(t)$ and $D^{\boldsymbol{\nabla}\varphi}_{\xi_{\mathrm{in}}}(t)$. This figure is adopted from Ref. [108].

even at $t \ll t_0$ because the wave function penetrates tunneling barrier even for $\mathcal{E} = 0$. Increasing the electric field, the probability density flow from the core into the barrier increases the probability density along the entry line. Although the local velocity at the tunneling entry is maximal at $t = t_0$ in sync with the electric field, the probability flow along the entry line $D^{\varrho}_{\xi_{\mathrm{in}}}(t)$ reaches its maximum earlier. The quantity $D^{\varrho}_{\xi_{\mathrm{in}}}(t)$ goes asymptotically to a constant value less than the initial value because some of the total probability has tunneled. Because the probability flow is the product of the probability density and the local velocity, the maximum of the integrated probability flow $D_{\xi_{\mathrm{in}}}(t)$ is reached between the instants of the maxima of the integrated density $D^{\varrho}_{\xi_{\mathrm{in}}}(t)$ and the integrated velocity $D^{\boldsymbol{\nabla}\varphi}_{\xi_{\mathrm{in}}}(t)$, this means $t_{\mathrm{in}} < t_0$. The time t_{exit} is usually larger than t_0, i. e., $\tau_{\mathrm{exit}} > 0$, especially for weak external fields.

After the electron has passed the entry line of the tunneling barrier, it needs some time to cross the barrier and to reach the tunneling exit. This means, $t_{\mathrm{exit}} > t_{\mathrm{in}}$, but not necessarily $t_{\mathrm{exit}} > t_0$. The latter may be understood by realizing that the above explanation for $t_{\mathrm{in}} < t_0$ is not specific to the coordinate $\xi = \xi_{\mathrm{in}}$. In particular, it also applies to $\xi = \xi_{\mathrm{exit}}$. Consequently, also the integrated flow at the exit coordinate $D^{\varrho}_{\xi_{\mathrm{exit}}}(t)$ may reach its maximum before the maximum of the electric field, as for example for the parameters in Fig. 4.3. In general, however, we find that $D^{\boldsymbol{\nabla}\varphi}_{\xi_{\mathrm{exit}}}(t)$ is maximal at an instant very close to t_0.

Taking the results above into consideration, the time t_{in} should be regarded as a reference for the tunneling time, but not t_0 which leads to the delay τ_{exit}. Choosing t_0 as a reference can lead to negative delays τ_{exit} for large electric field strengths, e. g., for $\mathcal{E}_0 \geq 1.0\,\mathrm{a.u.}$ for the setup that was applied for Fig. 4.4. This, however, should not be misinterpreted as a negative tunneling time because τ_{exit} is not related to the time which an electron needs to pass the tunneling barrier. This time is given by τ_{tsub}. As τ_{tsub} is always larger than τ_{exit}, the delay τ_{exit} may be used as a lower

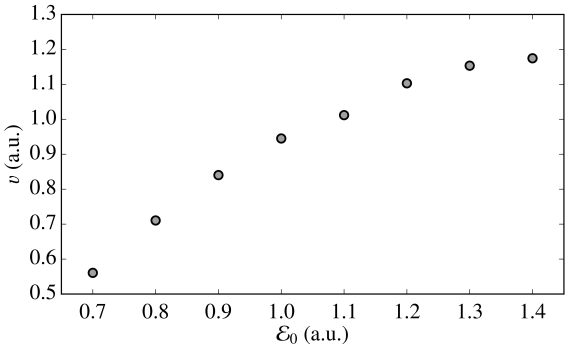

Figure 4.6.: Average velocity v of the motion of the probability-current's maximum from the tunneling barrier entry to the exit as a function of the applied maximal electric field strength $\mathcal{E}_0$. This figure is adopted from Ref. [108].

bound of the tunneling time.

It has been speculated that tunnel ionization may be instantaneous [39, 55], which would be associated with a superluminal traversal of the tunneling barrier. Our results, however, clearly indicate that there is a nonvanishing tunneling time τ_{tsub}. This leads to a finite average velocity of the motion of from $\xi = \xi_{\mathrm{in}}$ to $\xi = \xi_{\mathrm{exit}}$

$$v = \frac{\xi_{\mathrm{exit}} - \xi_{\mathrm{in}}}{2\tau_{\mathrm{tsub}}} \,. \tag{4.13}$$

Here we have taken into account that the lines of constant ξ are parabolas in the x-y plane and the probability current flows mainly at $y \approx 0$. As shown in Fig. 4.6, there is a monotonous relation between the applied maximal electric field strength $\mathcal{E}_0$ and the velocity v. The velocity presented in Fig. 4.6, however, is more than two orders of magnitude below the speed of light. Identifying the tunneling motion of the electron over the tunneling barrier with the motion of the probability-current's maximum, it is justified to say that tunneling ionization is neither instantaneous nor moves the electron at superluminal speed.

The virtual detector technique does not only allow us to define tunneling times. As in the previous chapter here we also discuss the applicability of the famous two-step model, see Sec. 2.3. For this we define a quantum trajectory with the help of the virtual detector method, and compare this trajectory to the classical two-step model trajectory. The obtained results agree with the ones of the one-dimensional system, obtained in the previous chapter.

4.5. Quantum and classical trajectories

The probability currents over different lines of constant ξ reaches their maxima at different times, which allows us to define a quantum trajectory $\xi^q(t)$ by inverting

$$t_\xi = \arg\max D_\xi(t) \,. \tag{4.14}$$

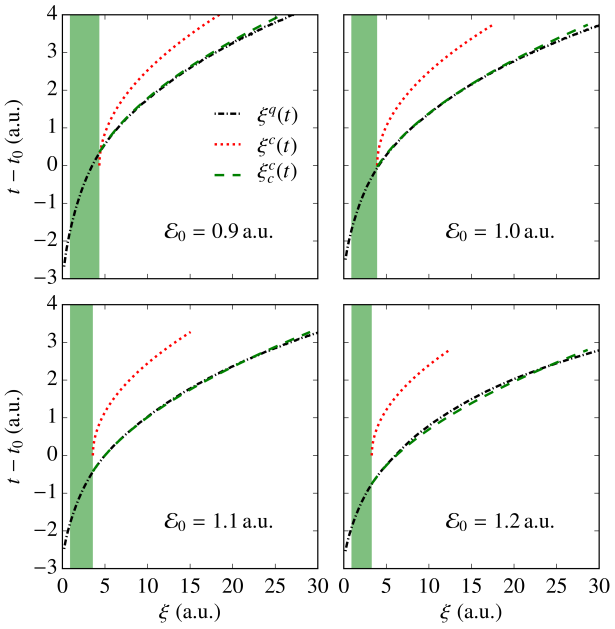

Figure 4.7.: The quantum trajectory of the electron in the ξ coordinate $\xi^q(t)$, compared to the classical trajectory according based on the two-step model $\xi^c(t)$. Both are also compared to the classical trajectory corrected according to quantum initial conditions $\xi^c_c(t)$. For more information see text. The shadowed area marks the positions ξ corresponding to under the barrier. This figure is adopted from Ref. [108].

The quantum trajectory $\xi^q(t)$ defined by Eq. (4.14) can be compared to the trajectory predicted by a Coulomb corrected two-step model $\xi^c(t)$. This classical trajectory is determined by the Newton equation

$$\frac{\mathrm{d}^2\xi^c(t)}{\mathrm{d}t^2} = -\frac{8}{\xi^c(t)^2} + 2\mathcal{E}(t)\,, \tag{4.15}$$

where the reduction to one dimension is justified as the most probable trajectory is along the x direction at $y \approx 0$. The initial conditions for the two-step model are

$$\xi^c(t_0) = \xi_{\mathrm{exit}}\,, \tag{4.16a}$$

$$\left.\frac{\mathrm{d}\xi^c(t)}{\mathrm{d}t}\right|_{t=t_0} = 0 \tag{4.16b}$$

meaning that the electron exits at the instant of electric field maximum $t = t_0$ with zero initial momentum at the turning point $x = \xi_{\mathrm{exit}}/2$. As shown in Fig. 4.7 for different electric field strengths, the classical trajectory $\xi^c(t)$ deviates from the quantum trajectory $\xi^q(t)$ not only near the barrier exit but also at a far away detector, i. e., for $\xi \gg \xi_{\mathrm{exit}}$.

From the above studies we have seen that the electron exits the tunneling barrier at t_{exit}, which differs from t_0. It has been shown in the previous chapter by using

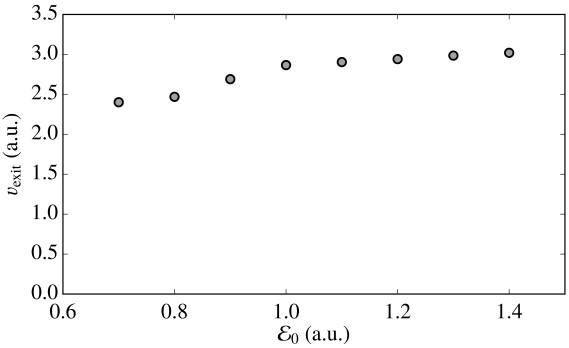

Figure 4.8.: The quantum trajectory's initial velocity v_{exit} plotted for different electric field strengths $\mathcal{E}_0$ for Keldysh parameter $\gamma = 0.25$. This figure is adopted from Ref. [108].

quantum mechanical calculations [75] that the electron exits also with an initial momentum in the electric field direction. This initial velocity can be inferred from the quantum trajectory, via

$$v_{\mathrm{exit}} = \left.\frac{\mathrm{d}\xi^q(t)}{\mathrm{d}t}\right|_{t=t_{\mathrm{exit}}} , \tag{4.17}$$

which yields results that are consistent with the results of of the previous chapter, see also Ref. [75]. The classical trajectory $\xi^c(t)$ can be corrected by the quantum initial conditions

$$\xi_c^c(t_{\mathrm{exit}}) = \xi_{\mathrm{exit}} , \tag{4.18a}$$

$$\left.\frac{\mathrm{d}\xi_c^c(t)}{\mathrm{d}t}\right|_{t=t_{\mathrm{exit}}} = v_{\mathrm{exit}} . \tag{4.18b}$$

As shown in Fig. 4.7 the corrected classical trajectory $\xi_c^c(t)$ agrees well with the quantum trajectory $\xi^q(t)$. Nevertheless, there is still a slight discrepancy between both trajectories at a far away detector, which can be attributed to that $\xi^q(t)$ originates from the motion of a broad wave packet which experiences a spatially varying Coulomb force [106]. The initial velocity v_{exit} is plotted in Fig. 4.8 for different electric field strengths. In agreement with the previous chapter, the initial momentum is slightly dependent on the electric field strength also in the considered two-dimensional system. The initial momentum is of the order of width of the ground state distribution in momentum space.

The initial velocity v_{exit} is difficult to measure directly in an experiment. But is also affects the asymptotic velocity of the ionized electron. Note that one can choose an electric field strength such that the quantum trajectory is at $\xi^q = \xi_{\mathrm{exit}}$ at $t = t_0$, i. e., the electron leaves the tunneling barrier at the moment of electric-field maximum, which is one assumption of the two-step model. In this case, the difference between the electron's actual asymptotic momentum and the prediction of the classical Coulomb-corrected two-step model is just the electron's initial momentum at the barrier exit. For the two-dimensional model as considered in Fig. 4.7 the condition $\xi^q(t_0) = \xi_{\mathrm{exit}}$ is fulfilled for an electric field strength $\mathcal{E}_0 = 1.0\,\mathrm{a.u.}$

4.6. Conclusions

We studied the dynamics of tunnel ionization by analyzing the quantum mechanical wave-function's probability current via virtual detectors. By calculating the probability current flow at all points of the considered space grid and at a fixed point in time we show that parabolic coordinates are the natural choice of coordinates in tunnel ionization. Moreover, virtual detectors are a capable concept for determining tunneling times because they allow to identify well-defined moments when the ionized electron enters and leaves the tunneling barrier.

The numerical solutions of the time-dependent Schrödinger equation and the dynamics of the probability current at the tunneling barrier indicate that the electron spends a nonvanishing time under the potential barrier. This corresponds to a crossing velocity that is much lower than the speed of light. Furthermore, the electron enters the classical forbidden region on average before the instant of the maximum of the driving electric field. Therefore, the instant of electric field maximum should not be considered as an initial reference time of the tunneling process. Nevertheless, for electric field strengths well below the threshold regime the electron exits the barrier after the instant of electric field maximum. For such strengths a nonvanishing delay τ_{exit} between the electric field maximum and the emergence of the electron behind the tunneling barrier exists as a signature of the time spent under the barrier. The actual time span that the electron has spent in the classically forbidden region, however, will be larger than τ_{exit}. Vanishing or negative time delays τ_{exit} should not be interpreted as instantaneous tunneling.

Under the barrier as well at the tunneling exit, the electron has a nonzero velocity in electric field direction. After the tunneling exit, the quantum trajectory, which is induced by the wave-function's probability current, agrees well with a trajectory as given by classical equations of motion when the electron's initial velocity at the tunneling exit is taken into account properly.

Having defined a most probable tunneling time using the virtual detector technique in the next chapter we define an average tunneling time for the above considered system. For this purpose we apply the quantum clock approach. It will be shown in the next chapter that using virtual detector method we can also define an average time spent under the barrier. This average time is compared to the average time obtained by the quantum clock approach.

Chapter 5.

Salecker-Wigner-Peres quantum clock applied to tunnel ionization

In chapter 2 we have introduced many techniques that where developed in order to define tunneling time in the case of tunneling through a potential barrier. For studying tunneling time in strong field tunnel ionization one can implement these techniques to the case of tunnel ionization. As mentioned in chapter 2 some of these techniques have been applied to the case of strong field tunnel ionization, where for calculating tunneling times the wavefunction at the instant of electric field maximum was considered. In this chapter we apply a method which was to our knowledge not applied before to strong field ionization, namely the Salecker-Wigner-Peres(SWP) quantum clock. Additionally, instead of considering only the wavefunction at the instant of electric field maximum we apply the SWP quantum clock dynamically through the whole pulse duration. In the introduction we argue why we apply this method instead of other techniques. Next we introduce the structure and the basic concept of the SWP quantum clock in Sec. 5.3. Of course for this clock to measure tunneling times of strong field tunnel ionization it has to be coupled to the system in a specific way, as explained in Sec. 5.4. After propagating the Hamiltonian of the coupled systems till the end of the pulse duration, in Sec. 5.5 we explain how one can determine the tunneling time from the measurement of the SWP quantum clock. The determined values and their physical interpretations are presented and discussed in Sec. 5.6. As we will see in this chapter the SWP quantum clock determines an average tunneling time. In the previous chapter we have determined a most probable time by using the virtual detector method. In Sec 5.7 we define an average tunneling time based on the virtual detector method and compare it to the average tunneling time determined by the SWP quantum clock. Most of the results presented in this chapter have been submitted for publication [115].

5.1. Introduction

Although tunneling is a fundamental process in quantum mechanics, there is still no consensus on the definition and interpretation of tunneling time. Tunneling time was first studied [67] in the problem of a particle tunneling through a square potential. In this case a particle approaches from far away a potential wall higher than it's energy. Many approaches and methods were proposed to define tunneling time [23]

in the case of tunneling through a potential barrier as discussed in Sec. 2.1. From the discussed approaches the clock approach is preferred by the authors of [23]. The reason for this preference is given in Sec. 2.1.

Another example of quantum tunneling where also tunneling time could be studied is tunnel ionization. Tunnel ionization is specifically attractive to study tunneling times because it is experimentally accessible. In the tunnel ionization case, a Coulomb-bound electron is ionized by a strong electromagnetic field, and a potential barrier can be defined via the electron's binding energy and the Coulomb potential bent by the electric field's potential. Keller et al.have conducted experiments using the angular streaking technique aiming to measure tunneling times for ionization from a bound state, the so-called attoclock experiments [39, 40]. For studying tunneling times in tunnel ionization many approaches could be applied from the ones used in the case of a particle tunneling through a square potential. Many of these approaches have been applied to Strong field tunnel ionization as discussed in Sec. 2.1. To our knowledge none of the above mentioned approaches has been applied dynamically to tunnel ionization, i.e., taking into account the continuous increase and decay of the external driving electric field as it is the situation in an experimental setting. Often the external field is treated as static [49] or switched on instantaneously [42, 52]. As emphasized in Ref. [42], tunneling in a continuously evolving potential is very different from the sudden turn-on case. In particular, there is not natural reference point in time which defines when tunneling begins. Furthermore, the quantum state at the onset of tunneling is no longer the ground state of the unperturbed binding potential. When tunneling sets in, the wavefunction has already evolved in the time-dependent potential.

In this thesis, we apply the Salecker-Wigner-Peres quantum clock to tunnel ionization taking into account the continuous evolution of the driving electric field to determine tunneling times. The Salecker-Wigner-Peres quantum clock is coupled to the electron in such a way that it measures the average time spent by the electron under the barrier. The obtained results are compared to the virtual detector method described in the previous chapter.

In the next section we describe the system and the electric field pulse that we consider in order to measure tunneling ionization times.

5.2. Considered system

Similar to chapter 4 we also study tunnel ionization from a two-dimensional Coulomb potential. The restriction to two dimensions is mainly because this system resembles tunnel ionization from hydrogen-like ions while keeping the computational demands small. In the long-wavelength limit, i. e., in the dipole approximation, the three-dimensional Coulomb potential with an external electric field has rotational symmetry which makes this system effectively two-dimensional. Furthermore, the two-dimensional Coulomb problem has been used to model some semiconductor systems [110–112].

Applying the dipole approximation and choosing the coordinate system such that the linearly polarized external electric field with the amplitude $\mathcal{E}(t)$ points into the x direction, the Schrödinger equation reads in atomic unit,

$$\mathrm{i}\frac{\partial \Psi_E(x,y,t)}{\partial t} = H_E \Psi_E(x,y,t) = \left(-\frac{1}{2}\frac{\partial^2}{\partial x^2} - \frac{1}{2}\frac{\partial^2}{\partial y^2} - \frac{1}{\sqrt{x^2+y^2}} - x\mathcal{E}(t)\right)\Psi_E(x,y,t)\,. \quad (5.1)$$

Applying an electric field pulse with a unique maximum allows us to study the ionization dynamics without undesirable artifacts, i. e., to avoid multiple ionization and rescattering see Sec. 2.6. Therefore, we employing a Gaussian pulse and the electric field is given by

$$\mathcal{E}(t) = \mathcal{E}_0 \exp\left(-\frac{\omega_{\mathcal{E}}^2 (t-t_0)^2}{2}\right), \quad (5.2)$$

where t_0 denotes the instant of maximal electric field $\mathcal{E}_0$ and $\tau_{\mathcal{E}} = \sqrt{2}/\omega_{\mathcal{E}}$ is the time scale of the raise and decay of the electric field. After we have determined the system that we consider in order to measure tunnel ionization time using the SWP quantum clock, we introduce the clock in the next section.

5.3. The Salecker-Wigner-Peres quantum clock

Salecker-Wigner-Peres [31, 34] introuced a quantum system that could serve as a clock, the so called SWP Quantum Clock. The system has the Hamiltonian $\hat{H}_c = \omega\hat{J}$ where $\hat{J} = -i\hbar\frac{\partial}{\partial\theta}$ is an angular momentum operator and the operator $\hat{\theta}$ is an angular operator, and consequently ω is the angular frequency. Solving the time-independent Schrödinger equation of the clock Hamiltonian $H_c\psi(\theta) = E_c\psi(\theta)$ and requiring that the clock angular wave functions to be periodic via $\psi(\theta) = \psi(\theta + 2\pi)$, results in the energy quantization of the system, i.e., $E_c = n\hbar\omega$. Clearly, this also means that the angular momentum is also quantized via:

$$\hat{J}\psi_n(\theta) = n\hbar\psi_n(\theta) \quad (5.3)$$

From now on we use the Dirac's bra-ket notation and denote $\psi_n(\theta) = |J_n\rangle$. The vector space $\{\,|J_n\rangle\,\}$ represents a complete orthonormal eigenbasis of $\hat{J}$ and $\hat{H}_c$ consequently. From the hamiltonian eigenbasis we can define another complete orthonormal eigen basis $\{\,|V_k\rangle\,\}$ via

$$\langle V_k|J_n\rangle = \frac{1}{\sqrt{N}}\exp\left(i\frac{2\pi nk}{N}\right) \quad (5.4)$$

where N is the dimension of the eigen basis and $k \in [0, N-1]$. The clock state Ψ can be described by either basis, and the transformation from one basis to the other

is defined by Eq. (5.4). It is convenient though not necessary to assume that we have an odd number N of the angular momentum eigen states such that the integer $n \in [-j, j]$ [34]. One can define ω, the angular frequency, in terms of a time interval τ such that $\omega = 2\pi/N\tau$. To see why this system behaves as a clock, we prepare the clock state in a state $|V_k\rangle$ at t_0 such that

$$|\Psi(t_0)\rangle = |V_k\rangle = \sum_n \langle J_n|V_k\rangle \, |J_n\rangle \, . \tag{5.5}$$

By propagating the wavefunction $|\Psi(t_0)\rangle$ using the time-dependent Schrödinger equation till time t such that $t - t_0 = \tau$, we get

$$\exp\left(-i\frac{\hat{H}_c\tau}{\hbar}\right)|\Psi(t_0)\rangle = \sum_n \frac{1}{\sqrt{N}} \exp\left(-i\frac{2\pi n(k+1)}{N}\right)|J_n\rangle = |V_{k+1}\rangle \, . \tag{5.6}$$

According to equation Eq. (5.6), setting the clock in state $|V_0\rangle$ at time $t = 0$ then applying the evolution operator, the clock will pass successively through the states $|V_0\rangle, \ldots, |V_{N-1}\rangle$ in time intervals τ. The quantum clock is cyclic as a normal clock, i.e., If $t - t_0 = N\tau$ and $\Psi(t_0) = |V_k\rangle$ the clock will be again in state $|V_k\rangle$ at time t. Thus for time intervals $t - t_0 \leq (N-1)\tau$ one can define an unambiguous mapping from the clock state to time via measuring the expectation value of the operator

$$\hat{T} = \sum_k k\tau \hat{P}_k, \tag{5.7}$$

where $\hat{P}_k$ is the projection operator on the states $|V_k\rangle$.The bahviour of the SWP quantum clock in time is illustrated in Fig. 5.1. The precision of the quantum clock is the time τ. Since propagating the clock for time intervals $t - t_0$ that are not integer multiples of τ will cause the quantum clock state Ψ to be in a coherent state in the basis $\{\, |V_k\rangle \,\}$. This means that for such intervals there is not a well defined mapping to real time from these coherent states through the expectation value of the time operator $\langle\hat{T}\rangle$. Thus any time measurement by the clock should be read with an error bar $\pm\tau/2$. In order to measure time using the SWP quantum clock, the clock has to be coupled to the system of interest. This procedure is discussed in the next section.

5.4. Coupling of the SWP quantum Clock and its calibration

As in the case of a normal clock, in order to time the dynamics of some system we have to couple the clock to the system. Like measuring the duration that a runner needs to run one lap. In this case one needs to know two times the instant the runner starts running and the instant the runner finishes the lap, thus the coupling is done by measuring when does the runner starts and finishes his lap. Suppose we want to measure the time of flight of a free particle. One way to couple the quantum clock to the free particle would be via the Hamiltonian [34],

$$\hat{H}_T = \frac{\hat{P}^2}{2M} + \hat{P}(\boldsymbol{x} \in R)\hat{H}_c, \tag{5.8}$$

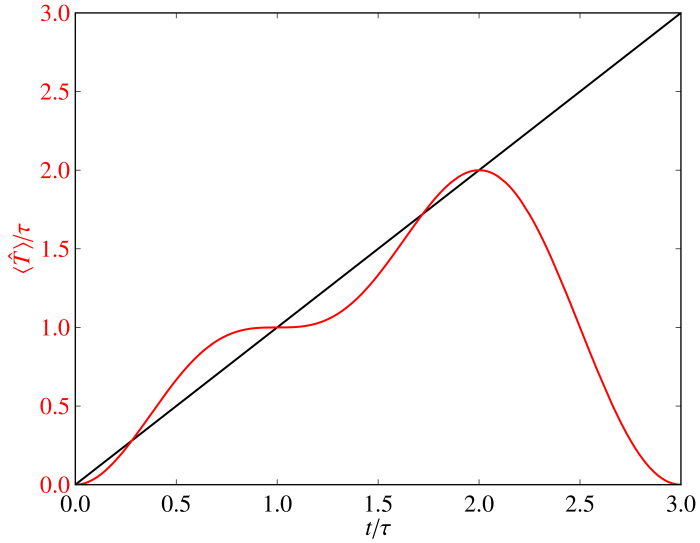

Figure 5.1.: The bahviour of $\langle\hat{T}\rangle$ in time t is plotted for a free running clock for $N = 3$ in terms of the time interval τ.

where $\hat{P}$ and M are the particle's momentum operator and mass respectively, $\hat{P}(\boldsymbol{x} \in R)$ is the projection operator on the $\boldsymbol{x}$-eigen states in the region R, and $\hat{H}_c$ is the clock Hamiltonian. The projection operator $\hat{P}(\boldsymbol{x} \in R) = \mathbb{1}$ when $\boldsymbol{x} \in R$ and zero otherwise. Using the Hamiltonian Eq. (5.8) one is able to measure the time of flight of a free particle in region R. From $\hat{H}_T$ one could see that the clock would run only when the particle is in region R. One should remark that in contrast to the runner example the quantum clock does not measure the time of starting and time of arrival, the quantum clock measures only the time spent in a certain region R when coupled via the projection operator $\hat{P}(\boldsymbol{x} \in R)$.

In the classical limit the system is not influenced by the measurement of the clock. But in the quantum limit coupling any measurement device will influence the dynamics of the studied system. The wavefunction of the Hamiltonian $\hat{H}_T$ is the cross product of the particle's state and the clock state, i.e. , $|\Psi_T\rangle = |\Psi_p\rangle\,|\Psi_c\rangle$. Expressing $|\Psi_c\rangle$ in the eigen basis $\{\,|J_n\rangle\,\}$ would result in N Schrödinger equations of a particle approaching a potential in region R of height $n\hbar\omega$ where $n \in [-j, j]$ and $j = (N-1)/2$. For more details see [34], where this problem is solved and as expected the time required for the free particle to pass region R is shown to be $t_{tf} = |R|\,M/\langle\hat{P}\rangle$. The free particle with energy $E_{fp} = \langle\hat{P}^2/2M\rangle$ feels the influence by the quantum clock via experiencing a potential of maximum height/depth $|j\hbar\omega|$. Thus to minimize this influence one has to set the clock such that $j\hbar\omega \ll E_{fp}$. But this also restricts the possible measurable time of fight. This is a general characteristic of SWP quantum clock. In general $j\hbar\omega$ must be much smaller than the energy of the studied system E_s. This directly implies that the condition $\tau \gg (j\hbar\omega)/E_sN$ must be satisfied. This means that as one decreases the effect of the quantum clock on the studied system the clock precision deteriorates. Note that increasing the

number of states of the clock N does not improve the precision of the clock since j also increases linearly with N. Indeed this fact restricts the applicability of the quantum clock. This problem is solved by Leavens [72], where the quantum clock is utilized to measure the tunneling time of a particle approaching from far away a potential barrier.

Leavens suggests that one could prepare a free running clock and measure it's behavior in time. For each time t one could measure the expectation value of the time operator $F_{\text{free}}(t) = \langle \hat{T}_{\text{free}} \rangle$ for the free running clock. For $t \ll \tau$ the function $\langle \hat{T} \rangle(t)$ is monotonically increasing see Fig. 5.1. Such that one could define in the domain $t \ll \tau$ an inverse function F^{-1}_{free}. When coupling the quantum clock to some quantum system one could calibrate it's measurement by the function F^{-1}_{free}. Such that the coupled quantum clock final measurement would be $F^{-1}_{\text{free}}\left(\langle \hat{T} \rangle\right)$. In this case the clock precision τ has lost it's meaning and one could now operate in the opposite regime $|j\hbar\omega| \ll E_s$. This condition is not only necessary to decrease the quantum clock influence on the studied system but also to insure that the would be measured dynamics occur on a time order $t \ll \tau$. In the next section we present the procedure of implementing the SWP quantum clock for measuring tunneling ionization times.

5.5. Measurement procedure of the SWP quantum clock in tunnel ionization

In order to measure the tunneling ionization time using the quantum clock one has to couple the quantum clock to the electron in the tunneling region. This is done by the Hamiltonian

$$H_T = H_E + \hat{P}(\boldsymbol{x} \in R)\hat{H}_c \tag{5.9}$$

where H_E is the Hamiltonian of a tunnel ionizing electron. Here R is the tunneling region defined by parabolic coordinates for $\mathcal{E}(t) = \mathcal{E}_0$ as described in chapter 4 and in the Appendix, see Fig. 5.2 . Coupling the clock to the electron in a fixed tunneling region is justified because for static fields the tunneling probability is maximal for maximal electric fields and it is exponentially suppressed for lower fields [79, 80]. We can see form Eq. (5.9) that the clock will run only when the electron is in the tunneling region see Sec. 5.3. In contrast to the time of flight measurement not all of the electron will enter the tunneling region. Moreover, from the part that enters the tunneling region one part will tunnel and the other will be reflected. Since the clock cannot differentiate between reflected electrons and tunneled electrons, it measures the average time spent in region R irrespective if the electron has been reflected or transmitted. This average time is known as the dwell time τ_D and is originally postulated by Büttiker [35]. An expression for the dwell time

$$\tau_D(R) = \int_0^\infty dt \int_R dxdy |\Psi_E(x, y, t)|^2 \tag{5.10}$$

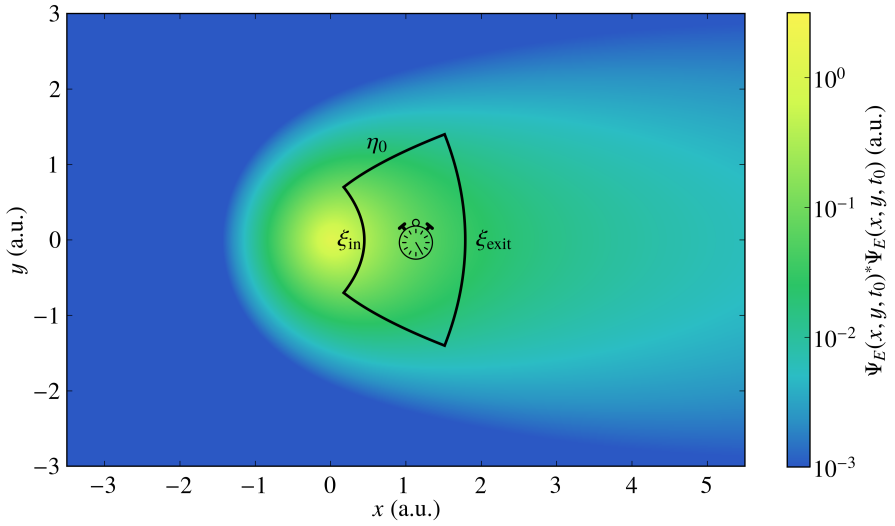

Figure 5.2.: Schematic of tunneling time determination via SWP quantum clock measurment in the tunneling region R, which is marked by the black solid lines. The lines $\xi = \xi_{\text{in,exit}}$ and $\eta = \eta_0$ which determine the tunneling region, are indicated by the solid lines; see Appendix. The wavefunction's probability density $|\Psi_E(x,y,t)|^2$ at the instant of electric field maximum, i. e., $t = t_0$, is represented by colors for $\mathcal{E}_0 = 1.1$ a.u. and $\gamma = 0.25$. This figure has been adopted from Ref. [115].

is derived within conventional [46] and casual [116] interpretations of quantum mechanics and is accepted by almost all workers in the tunneling time field [117].Since the expression in Eq. (5.10) and the quantum clock measure the same physical quantity their values should agree [72]. In other words the expression Eq. (5.10) should be considered as a check to weather if the quantum clock is implemented correctly to the studied system.

To measure the dwell time of tunnel ionization using the quantum clock we propagate the wave function $|\Psi_T(t_i)\rangle = |\Psi_E(t_i)\rangle \otimes |\Psi_c(t_i)\rangle$ till t_f via the Schrödinger equation:

$$\mathrm{i}\frac{\partial\,|\Psi_T(t)\rangle}{\partial t} = H_T\,|\Psi_T(t)\rangle\,. \tag{5.11}$$

The initial time t_i is chosen such that $(t_i - t_0) = -5\tau_{\mathcal{E}}$. Moreover at instant t_i the initial state of the electron is the ground state of H_E such that $H_E(t_i)\,|\Psi_E(t_i)\rangle = E_E\,|\Psi_E(t_i)\rangle$. While the clock is set in the state corresponding to a zero expectation value of the time operator $\hat{T}$, i.e., $|\Psi_c(t_i)\rangle = |V_0\rangle$. After propagating till time t_f, determined by $(t_f - t_0) = 5\tau_{\mathcal{E}}$, one could measure the expectation value of the time operator of the clock $\langle\hat{T}\rangle_{t_f}$. This expectation value is rigorously measured by taking the tensor of the clock density operator $\hat{\rho}_c$. The total density matrix of the system is given by

$$\hat{\rho}_T = \sum_{k,k'}\int dxdydx'dy'\phi^*_{k'}(x',y')\phi_k(x,y)\,|x;y\rangle\,\langle x';y'|\otimes|V_k\rangle\,\langle V_{k'}|\,. \tag{5.12}$$

Then the clock density operator $\hat{\rho}_c$ is defined by tracing out the electron degrees of freedom from $\hat{\rho}_T$ viz

$$\hat{\rho}_c = \int dx''dy'' \langle x''; y''| \hat{\rho}_T |x''; y''\rangle = \sum_{k,k'} \left(\int dxdy \phi^*_{k'}(x,y)\phi_k(x,y) \right) |V_k\rangle \langle V_{k'}| . \quad (5.13)$$

Then the expectation value of the time operator at the instant t_f, $\langle \hat{T} \rangle_{t_f}$ is given by

$$\langle \hat{T} \rangle_{t_f} = \sum_{k''} \langle V_{k''}| \hat{T} \hat{\rho}_c(t_f) |V_{k''}\rangle . \quad (5.14)$$

As explained in the previous section this measurement still needs calibration, and the final clock measurement is then $F^{-1}_{\text{free}}\left(\langle \hat{T} \rangle_{t_f}\right)$, and if everything is implemented correctly this should be in agreement with τ_D.

The main aim of implementing the quantum clock is to measure the time a tunneled electron spends under the barrier. In the following we will show that the time spent under the barrier by an electron that has tunneled is related to the Dwell time τ_D similarly as shown in [71]. At t_f the electric field has almost vanished and the wavefunction is well separated in space into a bound part and a tunneled part such that we can write the time operator expectation value as

$$\langle \hat{T} \rangle_{t_f} = \sum_k \left(\int_{\text{bd}} dxdy \phi^*_k(x,y)\phi_k(x,y) \right) k\tau + \sum_k \left(\int_{\text{tn}} dxdy \phi^*_k(x,y)\phi_k(x,y) \right) k\tau. \quad (5.15)$$

The bound part is the part of the wavefunction that has been reflected or did not undergo the tunneling process at all, while the tunneled part is part that entered the tunneling barrier and tunneled through it. If the system is not coupled to the quantum clock the sums $\int_{\text{bd}} dxdy\phi^*(x,y)\phi(x,y)$ and $\int_{\text{tn}} dxdy\phi^*(x,y)\phi(x,y)$ correspond to the reflection probability R and tunneling probability T respectively, where $R+T=1$. Since in each state $|V_k\rangle$ the electron experiences a slightly different tunneling barrier, the reflection R_k and tunneling T_k coefficients will be different in each state $|V_k\rangle$. Where $R_k = \int_{\text{bd}} dxdy\phi^*_k(x,y)\phi_k(x,y)$ and $T_k = \int_{\text{tn}} dxdy\phi^*_k(x,y)\phi_k(x,y)$. We can express the reflection and tunneling coefficients in terms of the reflection and tunneling coefficients of the non-coupled electron via, $R_k = R\Delta^R_k$ and $T_k = T\Delta^T_k$. Substituting these coefficients in $\langle \hat{T} \rangle_{t_f}$ gives

$$\langle \hat{T} \rangle_{t_f} = R\tau_R + T\tau_T \quad (5.16)$$

where $\tau_R = \sum_k \Delta^R_k k\tau$ is the reflection time and $\tau_T = \sum_k \Delta^T_k k\tau$ is the tunneling time. Expression (5.16) which satisfy the sum rule of reflection and tunneling time

is well known; it is identical to the spin-precession result [33], and to the real-part of the complex-valued Feynman-path [46] results [71]. On one hand we know that the clock needs calibration and that the calibrating function F_{free}^{-1} is not linear. Thus $F_{\text{free}}^{-1}\left(\langle\hat{T}\rangle_{t_f}\right)$ would not be equal to $RF_{\text{free}}^{-1}(\tau_R)+TF_{\text{free}}^{-1}(\tau_T)$. On the other hand, for one measurement one needs to calibrate three values $\langle\hat{T}\rangle_{t_f}$, τ_R and τ_T. These values are included in a small domain of F_{free}^{-1} , Δt. Since we are operating in the regime $t \ll \tau$, the function F_{free}^{-1} is almost linear in the small domain Δt. Thus as will see in the next section, that the following holds

$$\tau_D^C = F_{\text{free}}^{-1}\left(\langle\hat{T}\rangle_{t_f}\right) \approx RF_{\text{free}}^{-1}(\tau_R) + TF_{\text{free}}^{-1}(\tau_T)\,. \tag{5.17}$$

Finally, the calibrated tunneling time is defined by $\tau_T^C = F_{\text{free}}^{-1}(\tau_T)$ and the calibrated reflection time τ_R^C is determined by $\tau_R^C = F_{\text{free}}^{-1}(\tau_R)$. To understand the separation of dwell time into tunneling and reflection time intuitively, one can imagine that there is a far away detector that does not disturb the system and can differentiate between tunneled electrons and reflected electron. This detector is realized by the integral which can separate between reflected part and tunneled part. Additionally the measurement of the tunneled electrons is then normalized by the tunneling probability T, while the measurement of the reflected electrons is normalized by the reflection probability R.

Although the splitting (5.16) has been employed in many works, it has also be criticized [23, 118, 119]. One point of criticism that was put forward is that the dwell time (5.10) adds up probability density rather than probability amplitudes and therefore neglects possible interferences between transmitted and reflected portions of the wave packet. This argument, however, does not apply to the clock approach taken here. The clock Hamiltonian couples to the wave function, not to the density. For the quantum clock approach it is not required to separate the wave function under the barrier into tunneling and reflecting parts, which would be problematic indeed. Furthermore, the expectation value (5.14) is calculated when the tunneled and the bound parts of the wave function are well separated and therefore there is no interference between both parts.

Having defined the coupling, measurement and calibration procedure of the SWP quantum clock in the next section the obtained results are discussed and interpreted.

5.6. Results and interpretation

The Schrödinger equation with the Hamilton operator (5.9) is solved numerically by employing a Lanczos propagator [85, 98] and a fourth-order finite differences scheme for the discretization of the Hamilton operator in order to investigate tunneling times in strong-field tunnel ionization see Sec. 2.7. The so-called Keldysh parameter $\gamma = \omega_{\mathcal{E}}\sqrt{-2E_E m}/(e\mathcal{E}_0)$ [41] characterizes the ionization process as dominated by tunneling for $\gamma \ll 1$ and by multiphoton ionization for $\gamma \gg 1$ see also Sec. 2.2. Here, E_E denotes the ground state binding energy, which equals $E_0 = -2\,\text{a.u.}$ for

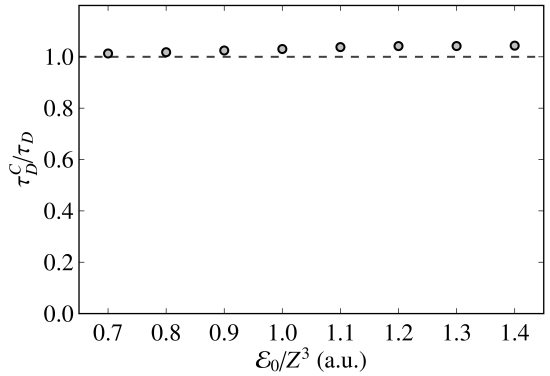

Figure 5.3.: The ratio of the dwell time τ_D determined by integrating the probability density in the tunneling barrier to the (corrected) dwell time τ_D^C as given by the quantum clock for different electric field strengths $\mathcal{E}_0$ and for a constant Keldysh parameter $\gamma = 0.25$. To guide the eye, the horizontal dashed line indicates the ratio one, i. e., when both dwell times exactly agree. This figure has been adopted from Ref. [115].

the two-dimensional Coulomb problem [120]. In the following, the electric field amplitude $\mathcal{E}_0$ and the frequency $\omega_\mathcal{E}$ are adjusted such that $\gamma = 0.25 < 1$. The clock parameters $\tau = 200\,\text{a.u.}$ and $N = 3$ are chosen such that $|j\hbar\omega/E_E| = 0.0104 \ll 1$, i. e., the quantum clock Hamiltonian is coupled weakly to the Coulomb Hamiltonian. This ensures that the distribution of Coulomb Hamiltonian by the quantum clock Hamiltonian is negligible. This has been tested by repeating numerical calculations with $\tau = 400\,\text{a.u.}$, i. e., even weaker coupling, which yields results that are almost equal to the results obtained for $\tau = 200\,\text{a.u.}$ Note that choosing the clock parameter τ arbitrary large such that the influence of the clock on the studied system becomes infinitely small leads to numerical difficulties because then also transitions between various clock states $|V_k\rangle$ becomes small and therefore difficult to resolve numerically. As explained in Sec. 5.4 increasing the number of states of the clock does not improve the clock precision, and thus we choose the smallest non trivial odd number of states $N = 3$. A larger number of states N would increase the required numerical effort without providing any advantage.

The two definitions of the dwell time τ_D defined in Eq. (5.10) and τ_D^C defined in Eq. (5.17) , respectively, provide us a valuable consistency check of the quantum clock approach. To be consistent, the dwell time as determined by the quantum clock (5.17) must agree with the dwell time (5.10), which does not rely on the concept of a quantum clock. Our numerical results shown in Fig. 5.3 confirm this property. For the chosen parameters, both dwell times agree up to a discrepancy of about 4 %. For larger field strengths $\mathcal{E}_0$ this small discrepancy tends to be systematically larger than for small field strengths. This can be attributed to the fact that the dwell time becomes small for large field strengths and therefore the relative accuracy of the dwell-time determination is reduced.

The tunneling time τ_T^C, the reflection time τ_R^C, as well as the dwell time τ_D^C are presented in Fig. 5.4. Furthermore, the figure shows the weighted sum $T\tau_T^C + R\tau_R^C$,

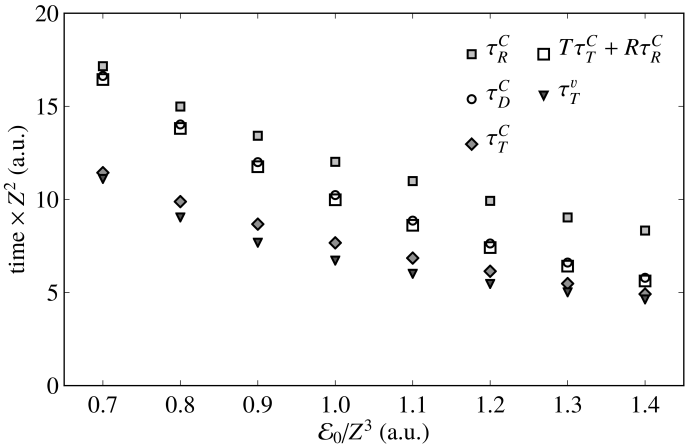

Figure 5.4.: Refection time τ_R^C, dwell time τ_D^C, tunneling time τ_T^C, the weighted sum $T\tau_T^C + R\tau_R^C$, and tunneling time τ_T^v for different electric field strengths $\mathcal{E}_0$ at a fixed Keldysh parameter $\gamma = 0.25$. For specific definitions of the various times see main text. This figure has been adopted from Ref. [115].

which is close to the dwell time τ_D^C but does not strictly agree with the latter due to the non-linearity of the function F_{free}^{-1}. Because τ_D^C is close to the weighted average $T\tau_T^C + R\tau_R^C$ it lies always between the tunneling time τ_T^C and the reflection time τ_R^C. As one can also see in Fig. 5.4, the reflection time τ_R^C is always larger than the tunneling time τ_T^C. The ratio of the reflection time τ_R^C and the tunneling time τ_T^C is close to 1.6 almost independently of the strength of the applied electric field as shown in Fig. 5.6. This can be intuitively understood as tunneling electrons enter the barrier and then leave the barrier at the exit while reflected electrons move under the barrier until they get reflected at the barrier exit and then travel back into the direction of the atomic core.

The tunneling time as well as the reflection time decrease with increasing electric field strength $\mathcal{E}_0$. In fact, we find a power-law behavior for τ_T^C as well as for τ_R^C, $\tau_T \sim \mathcal{E}_0^{-1.2}$ and $\tau_R \sim \mathcal{E}_0^{-1}$ as shown in Fig. 5.5.

In this section we have represented the results of tunneling time measured via the SWP quantum clock τ_D^C. In Sec. 4.4 we have also defined and represented the tunneling time τ_{tsub} based on the virtual detector method. In the following section we explain what is the difference between both times and how we can define an average tunneling time based on virtual detectors.

5.7. Virtual detector method and average tunneling time

In chapter 4 we studied tunneling times for the same kind of system and the same parameter regime as in this chapter by a different approach, the so-called virtual detector method. In this section we are going to relate the virtual detector approach to the quantum clock approach.

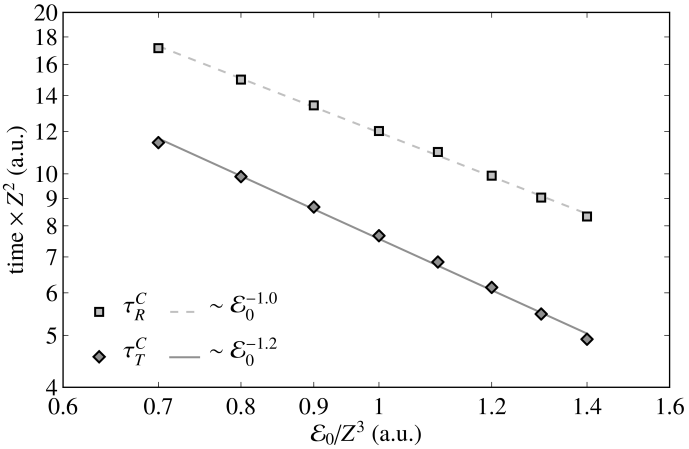

Figure 5.5.: Reflection time τ_R^C and tunneling time τ_T^C on a double logarithmic scale. For specific definitions of the various times see the main text. This figure has been adopted from Ref. [115].

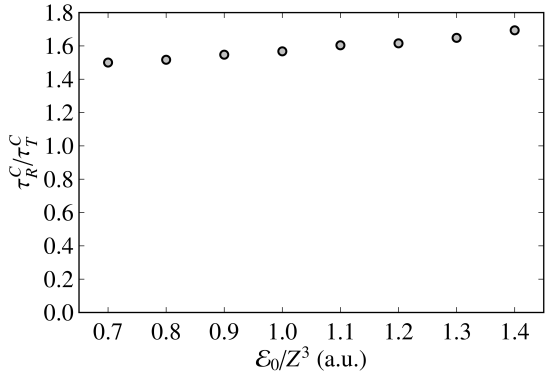

Figure 5.6.: Ratio of the reflection time τ_R^C and the tunneling time τ_T^C as a function of the electric field strengths $\mathcal{E}_0$ at a fixed Keldysh parameter $\gamma = 0.25$. This figure has been adopted from Ref. [115].

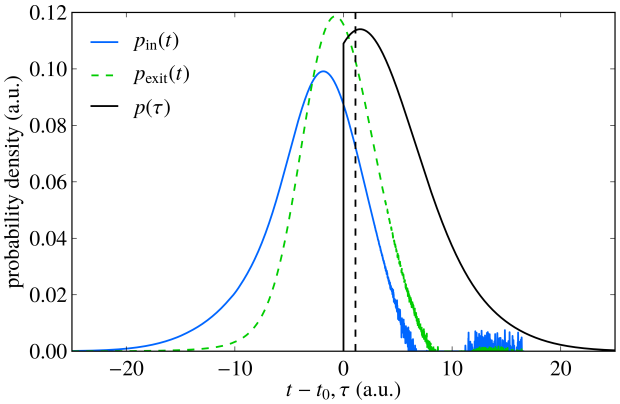

Figure 5.7.: Probability distributions $p_{\mathrm{in}}(t)$ and $p_{\mathrm{exit}}(t)$ to enter or to leave the tunneling barrier into the direction away from the atomic core as functions of time t and probability distribution $p(\tau)$ of the tunneling time as derived from $p_{\mathrm{in}}(t)$ and $p_{\mathrm{exit}}(t)$ for $\mathcal{E}_0 = 1.2\,\mathrm{a.u.}$ and $Z = 1$. The vertical black dashed line indicates the time τ_{tsub}, which is the distance between the positions of the maxima of the distributions $p_{\mathrm{in}}(t)$ and $p_{\mathrm{exit}}(t)$. This figure has been adopted from Ref. [115].

The central idea of the virtual detector approach is to determine the electron's probability density flow at the entry line and the exit line of the tunneling barrier at the parabolic coordinates $\xi = \xi_{\mathrm{in}}$ and $\xi = \xi_{\mathrm{exit}}$ as functions of the time t. Integrating the probability density flow along these lines gives the quantities $D\xi_{\mathrm{in}}(t)$ and $D\xi_{\mathrm{exit}}(t)$. Furthermore, $D_{\xi_{\mathrm{in}}}(t)\Theta(D_{\xi_{\mathrm{in}}}(t))\,\Delta t$ is proportional to the probability that the electron crosses the entry line of the tunneling barrier into the direction away from the atomic core. Here $\Theta(x)$ denotes the Heaviside step function. Similarly, $D_{\xi_{\mathrm{exit}}}(t)\Theta(D_{\xi_{\mathrm{exit}}}(t))\,\Delta t$ is proportional to the probability that the electron crosses the exit line of the tunneling barrier into the direction away from the atomic core. It is convenient to introduce the normalization constants N_{in} and N_{exit} and the distributions $p_{\mathrm{in}}(t)$ and $p_{\mathrm{exit}}(t)$ such that

$$p_{\mathrm{in}}(t) = \frac{1}{N_{\mathrm{in}}} D_{\xi_{\mathrm{in}}}(t)\Theta(D_{\xi_{\mathrm{in}}}(t))\,, \tag{5.18a}$$

$$p_{\mathrm{exit}}(t) = \frac{1}{N_{\mathrm{exit}}} D_{\xi_{\mathrm{exit}}}(t)\Theta(D_{\xi_{\mathrm{exit}}}(t))\,, \tag{5.18b}$$

and

$$\int_{-\infty}^{\infty} p_{\mathrm{in}}(t)\,\mathrm{d}t = 1\,, \tag{5.19a}$$

$$\int_{-\infty}^{\infty} p_{\mathrm{exit}}(t)\,\mathrm{d}t = 1\,. \tag{5.19b}$$

The functions $D_{\xi_{\mathrm{in}}}(t)$ and $D_{\xi_{\mathrm{exit}}}(t)$ have both a unique global maximum; see Fig. 4.3. In sec. 4.4, we defined the distance of the positions of these maxima as the tunneling time τ_{tsub}.

Comparing τ_{tsub} and τ_T^C, one finds that τ_{tsub} is smaller than τ_T^C by a factor of about three. This discrepancy is a direct consequence of the different definitions of τ_{tsub} and τ_T^C. It does not necessarily indicate a conflict between the quantum clock approach and the virtual detector approach. As we will show in the following, the discrepancy arises essentially because taking the difference between two expectation values of two times is not equivalent to determining the expectation value of a time delay. Due to the approximate symmetry of $p_{\text{in}}(t)$ and $p_{\text{exit}}(t)$ around their maxima, τ_{tsub} equals approximately the difference between the expectation values for the moments of entering and leaving the tunneling barrier. The tunneling time τ_T, however, is derived from an expectation value of a clock operator which determines directly the time spend in the tunneling barrier. As a quantum mechanical observable, the time that corresponds to this operator has some distribution. Neglecting possible quantum correlations between entering and leaving the tunneling barrier, one can reconstruct this distribution from $p_{\text{in}}(t)$ and $p_{\text{exit}}(t)$ by assuming that the probability to spend the nonnegative time τ in the tunneling barrier is proportional to the product of $p_{\text{in}}(t)$ at the entry time t and $p_{\text{exit}}(t+\tau)$. Integrating over all possible entry times yields the probability distribution

$$p(\tau) = \frac{1}{N} \int_{-\infty}^{\infty} p_{\text{in}}(t) p_{\text{exit}}(t+\tau)\, \mathrm{d}t\,, \tag{5.20}$$

where N is a normalization constant such that

$$\int_0^{\infty} p(\tau)\, \mathrm{d}\tau = 1\,. \tag{5.21}$$

Note that due to causality reasons, $p(\tau)$ vanishes for $\tau < 0$. The corresponding expectation value of the tunneling time of the virtual detector approach is then

$$\tau_T^v = \int_0^{\infty} \tau p(\tau)\, \mathrm{d}\tau\,. \tag{5.22}$$

For comparison with the tunneling time τ_T^C of the quantum clock approach, the time τ_T^v is also indicated in Fig. 5.4. In contrast to tunneling delay τ_{tsub}, τ_T^v is very close to the tunneling time τ_T^C of the quantum clock approach. As one can see in Fig. 5.7, the distribution $p(\tau)$ has a maximum approximately at τ_{tsub}. Due to the distribution's asymmetry that results from the causality condition $p(\tau) = 0$ for $\tau < 0$, the expectation value of $p(\tau)$ is shifted away from the position of the maximum to larger values, which explains the factor-3 discrepancy between τ_{tsub} and τ_T^C. For calculating τ_T^v we have made the assumption that there is no correlation between the probability of entering the barrier and the probability of exiting the barrier. Since the numerical values of τ_T^v and τ_T^C[1] agree then we can conclude that there is no correlation between when the electron enters the barrier and when does the electron exit the barrier.

[1] Note that for the calculation of τ_T^C a pure quantum approach was used and no assumptions about entry and exit probability distribution correlations were made.

5.8. Conclusion

In this chapter we have applied the SWP quantum clock in order to determine tunnel ionization times. We have defined through the quantum clock an average tunneling time and an average reflection time. We have seen that the reflection time is almost 1.6 times the tunneling time. This is due to the fact that the electrons that enter the barrier and reflect spend more time under the barrier in comparison to electrons that tunnel. The SWP quantum clock in its structure measures an average tunneling time while through the virtual detector method used in the previous chapter we defined a most probable tunneling time. By defining a probability distribution of tunneling times based on the virtual detector approach we find that the maximum of this distribution is the time defined in sec. 4.4 and the expectation value of this distribution is very close to the tunneling time defined by the quantum clock. The difference between the maximum of the distribution and its expectation value, i.e., between the magnitude of both times is due to the unsymmetrical probability distribution of tunneling times.

Realizing a structure similar to the quantum clock and coupling it to the tunnel ionizing electron is very hard to realize experimentally, since one needs to couple both systems only under the tunneling barrier. Nevertheless, it is very interesting to calculate expectation values of tunneling times from first principles by using the SWP quantum clock.

Chapter 6.

Summary and outlook

We started this work in chapter 3 by studying tunnel ionization of an electron bound in a soft-core potential in a one-dimensional system that models the essential features of a three-dimensional Coulomb system. Using the virtual detector method we have shown that the electron exits the tunneling barrier after the instance of electric field maximum. Furthermore, by resolving the momentum distribution of the tunnel ionized electron at the instant of ionization, we find out that the electron exits the tunnel barrier with a non-zero initial momentum. These two results are different from the assumptions of the commonly employed two-step model, which assumes ionization at the instant of electric field maximum with zero momentum. For this reason we have also investigated the applicability of the two-step model by determining the final momentum of the tunnel ionized electron. We have found out that not only the assumptions of the two step model are not correct but also its predictions of the final momentum deviate from the quantum mechanical one. Furthermore, correcting the assumptions of the two-step model by the correct instant of ionization and correct exit momentum does not result in a correct prediction of the final momentum. This is a hint that propagation of the wave packet after tunnel ionization is not classical. Nevertheless, we have shown that the two-step model can be corrected by changing its initial parameters. These results have an effect on the interpretation of tunnel ionization experiments in general and specifically on the calibration of the attoclock experiment that aims to determine the instant of ionization, because theoretical models with false assumptions are usually employed in order to interpret experimental results.

In chapter 4 we studied tunnel ionization of an electron bound by a Coulomb potential in two dimensions. We did not only determine the instant of ionization but also we have determined the instant when the electron enters the tunneling barrier. From these two instants we have determined the most probable duration spent by an electron under the tunneling barrier. We found out that the determined tunneling time is meaningful because it does not correspond to superluminal speeds. Most importantly we have found out that tunnel ionization does not start at the instant of electric field maximum as often assumed. Furthermore, we have shown that also in two dimensions the assumptions and predictions of the two-step model are incorrect. Namely, the electron exits the tunneling barrier not at the instant of electric field maximum with a non-zero exit momentum. We have also seen that the trajectory of the electron predicted by the two-step model deviates from the

quantum trajectory, and that this deviation increases with increasing electric field strength. Moreover, we have shown that the trajectory of the two-step model can be corrected by changing the initial conditions.

Finally, in chapter 5 we have applied the Salecker-Wigner-Peres (SWP) quantum clock on tunnel ionization. From the SWP quantum clock we have determined an average tunneling time corresponding to an average time spent under the barrier by electrons which tunnel. Also we have determined an average reflection time spent under the barrier by the electrons which do not tunnel. We have seen that both times do not correspond to superluminal speeds, and that the ratio between reflection and tunneling time is greater than one. This could be understood as electrons which are reflected penetrate the barrier to some point and then return back, while electrons which tunnel just go through the barrier. In chapter 4 we defined a most probable tunneling time based on the virtual detector method, while in chapter 5 we determined an average tunneling time; these two tunneling times are different in magnitude and origin. To understand this discrepancy we have defined an average tunneling time based on the virtual detector method by defining a probability distribution of tunneling times. The expectation value of tunneling time taken over the probability distribution matches very well the tunneling time defined by the quantum clock, while the maximum of the probability distribution matches very well the tunneling time defined in chapter 4. The discrepancy between the magnitude of the most probable time and the average time is attributed to the unsymmetrical probability distribution of tunneling times.

Outlook

The present work may stimulate further studies in the field. In chapter 3 and chapter 4 we have found out that the two-step model should be corrected. The attoclock experiments measure the final momentum of the tunnel ionized electrons and map from it the instant of ionization using some theoretical model. Many works propose theoretical models to calibrate the attoclock. A direct measurement of the instant of ionization is experimentally very hard to achieve. In the present work we have directly determined the instant of ionization by simulations and by using numerical quantum calculations for systems that model the essential features of Coulomb potential in three dimensions. This has the advantage of simplicity of solving the system with full quantum mechanical numerical calculations and finding the correct qualitative behavior of exit time and exit momentum from first principles. Additionally many methods that has been used in this thesis to determine the exit time and the exit momentum are applied for the first time for tunnel ionization and it would be convenient to apply them first to simple systems and understand them before applying them to more complex systems. Though the considered system in this work is not exactly the same as the experimentally used one. Thus one can repeat the above presented simulations and calculations but for a three dimensional system and by considering experimental parameters. This has the advantage of determining the instant of ionization not only qualitatively but also quantitatively. In experiments usually a Helium atom is ionized by an elliptically polarized pulse.

Thus one needs to consider an electron in an effective potential which models the Coulomb potential of a Helium atom screened by the first electron. Additionally, one should consider an electrically polarized sinusoidal pulse with an envelope as considered in experiments. Even nowadays three dimensional calculations are still very demanding. As shown in Ref. [78] the three dimensional time-independent tunnel ionization problem in the absence of a magnetic field can be reduced via coordinate transformation two a two dimensional problem. This hints that the important dynamics of the electron in the time-dependent problem is rendered in two dimensions. Thus for the three dimensional time-dependent tunnel ionization problem one could choose a grid where the third dimension is modeled by a thin layer, which is numerically feasible.

Moreover, the two-step model is commonly employed in order to determine tunnel ionization spectra and we have shown that it fails to predict the correct final momentum. It would be interesting to study the effect of correcting the two-step model on the tunnel ionization spectra. For example, in tunnel ionization recombination spectra, i.e., when an electron tunnel ionize and propagate away from the atom by the driving field and then recombines with the atom after the driving field changes sign. This problem could be studied via semi-classical calculations. Recently, it was shown in [121] that high harmonic generation (HHG) spectra could not be reconstructed using the two-step model. Particularly, it was shown that a non-zero initial momentum in the electric field direction was necessary to describe the HHG experimental spectra. In this work we have shown that the electron has a certain distribution of exit time as well as a distribution of exit momentum. These distributions could be used as initial conditions for the classical equations of motion in order to calculate the spectrum. By comparing the results of the semi-classical calculations to experimental or quantum calculated spectra one could study the effect of the time delay at the exit as well as the effect of the non-zero initial momentum.

Furthermore, in this work we have introduced for the first time the virtual detector approach in order to determine tunnel ionization times. It would be interesting to employ this method on tunneling of free particles, when free particles approach from far away a potential barrier. In this case most of tunneling time definitions in literature lead to a tunneling time value corresponding to superluminal velocities. Employing the virtual detector method for this problem would be straight forward, and very promising based on the results found in this thesis.

Another field where these methods could be applied is in the field of trapped Bose-Einstein condensates. Recently, in an experimental work, tunneling time of Bose-Einstein condensates trapped in optical lattices was measured [122]. The techniques applied in this work could also be used to determine tunneling times of Bose-Einstein condensates which could be compared to experimental results. For achieving this, one has to consider a particle (Bose-Einstein Condensate) in an effective potential that models the potential of the particle as well as the effect of neighboring potentials. Additionally, one has to consider the effect of the interaction with neighboring particles caused by lattice vibrations. For these one could use the already developed techniques of condensed matter physics.

Appendices

Appendix A.

The Coulomb problem and the Strak effect in two dimensions

The eigen equation of the two-dimensional Coulomb problem [111, 120] with some additional homogeneous electric field of strength $\mathcal{E}$ is given in Cartesian coordinates x and y and employing atomic units by

$$\left(-\frac{1}{2}\frac{\partial^2}{\partial x^2} - \frac{1}{2}\frac{\partial^2}{\partial y^2} - \frac{1}{\sqrt{x^2+y^2}} - \mathcal{E}x\right)\Psi(x,y) = E\Psi(x,y)\,, \tag{A.1}$$

where $\Psi(x,y)$ denotes an eigen function with energy E. This eigen equation separates in parabolic coordinates ξ and η [120, 123, 124], which are related to the Cartesian coordinates x and y via Eq. (4.3). This coordinate system is particularly useful because here the two-dimensional Schrödinger equation can be separated into two one-dimensional Schrödinger equations, which allows to define a one-dimensional tunneling barrier. The calculations in this section follow Ref. [78], where the three-dimensional Coulomb problem is considered in a similar way.

The Laplacian becomes in the new coordinate system

$$\frac{\partial^2}{\partial x^2} + \frac{\partial^2}{\partial y^2} = \frac{1}{\xi+\eta}\left(4\xi\frac{\partial^2}{\partial \xi^2} + 2\frac{\partial}{\partial\xi} + 4\eta\frac{\partial^2}{\partial\eta^2} + 2\frac{\partial}{\partial\eta}\right)\,. \tag{A.2}$$

Expressing (A.1) in parabolic coordinates yields after some algebraic transformations

$$\left(\xi\frac{\partial^2}{\partial\xi^2} + \frac{1}{2}\frac{\partial}{\partial\xi} + \frac{E}{2}\xi + \frac{\mathcal{E}}{4}\xi^2\right)\Psi(\xi,\eta) + \left(\eta\frac{\partial^2}{\partial\eta^2} + \frac{1}{2}\frac{\partial}{\partial\eta} + \frac{E}{2}\eta - \frac{\mathcal{E}}{4}\eta^2\right)\Psi(\xi,\eta) = -\Psi(\xi,\eta)\,. \tag{A.3}$$

Substituting the ansatz $\Psi(\xi,\eta) = f_1(\xi)f_2(\eta)$ into the last equation end separating the variables ξ and η we obtain the two equations

$$\left(\xi\frac{\partial^2}{\partial\xi^2} + \frac{1}{2}\frac{\partial}{\partial\xi} + \frac{E}{2}\xi + \frac{\mathcal{E}}{4}\xi^2 + \beta_1\right)f_1(\xi) = 0\,, \tag{A.4a}$$

$$\left(\eta\frac{\partial^2}{\partial\eta^2} + \frac{1}{2}\frac{\partial}{\partial\eta} + \frac{E}{2}\eta - \frac{\mathcal{E}}{4}\eta^2 + \beta_2\right)f_2(\eta) = 0\,, \tag{A.4b}$$

where the separation constants β_1 and β_2 are related by

$$\beta_1 + \beta_2 = 1\,. \tag{A.5}$$

The tunneling barriers are obtained by substituting $f_1(\xi) = g_1(\xi)/\xi^{1/4}$ and $f_2(\eta) = g_2(\eta)/\eta^{1/4}$, which gives the equations for the new functions as

$$-\frac{1}{2}\frac{\partial^2 g_1(\xi)}{\partial\xi^2} + \left(-\frac{3}{32\xi^2} - \frac{\beta_1}{2\xi} - \frac{\xi}{8}\mathcal{E}\right) g_1(\xi) = \frac{E}{4} g_1(\xi)\,, \tag{A.6a}$$

$$-\frac{1}{2}\frac{\partial^2 g_2(\eta)}{\partial\eta^2} + \left(-\frac{3}{32\eta^2} - \frac{\beta_2}{2\eta} + \frac{\eta}{8}\mathcal{E}\right) g_2(\eta) = \frac{E}{4} g_2(\eta)\,. \tag{A.6b}$$

These two equations represent Schrödinger-type eigen equations with potentials

$$V_1(\xi) = -\frac{3}{32\xi^2} - \frac{\beta_1}{2\xi} - \frac{\xi}{8}\mathcal{E}\,, \tag{A.7a}$$

$$V_2(\eta) = -\frac{3}{32\eta^2} - \frac{\beta_2}{2\eta} + \frac{\eta}{8}\mathcal{E} \tag{A.7b}$$

and the energy $E/4$.

For a vanishing external electric field, i. e., $\mathcal{E} = 0$, Eqs. (A.4a) and (A.4b) are identical. Introducing the variable transformation $\xi = \eta = \zeta/\sqrt{-2E}$ gives in this case

$$\left(\zeta\frac{\partial^2}{\partial\zeta^2} + \frac{1}{2}\frac{\partial}{\partial\zeta} + \frac{\beta_{1,2}}{\sqrt{-2E}} - \frac{\zeta}{4}\right) f_{1,2}(\zeta) = 0\,. \tag{A.8}$$

Making the ansatz $f_{1,2}(\zeta) = \exp(-\zeta/2) g_{1,2}(\zeta)$ this differential equation yields the equation

$$\left(\zeta\frac{\partial^2}{\partial\zeta^2} + \left(\frac{1}{2} - \zeta\right)\frac{\partial}{\partial\zeta} - \left(\frac{1}{4} - \frac{\beta_{1,2}}{\sqrt{-2E}}\right)\right) g_{1,2}(\zeta) = 0 \tag{A.9}$$

for $g_{1,2}(\zeta)$, which can be identified as the confluent hypergeometric equation [125] with

$$a = \frac{1}{4} - \frac{\beta_{1,2}}{\sqrt{-2E}}\,, \qquad\qquad b = \frac{1}{2}\,. \tag{A.10}$$

The nonsingular solution of the confluent hypergeometric equation is usually called confluent hypergeometric function and denoted by ${}_1F_1(a;b;\zeta)$ or $M(a;b;\zeta)$. Thus we have found the solution

$$f_1(\xi) \sim \exp\left(-\frac{\xi}{2}\sqrt{-2E}\right) M\left(\frac{1}{4} - \frac{\beta_1}{\sqrt{-2E}}; \frac{1}{2}; \xi\sqrt{-2E}\right) \tag{A.11}$$

and similar for $f_2(\eta)$. These functions $f_1(\xi)$ and $f_2(\eta)$ can be normalized only if the first argument of the confluent hypergeometric function is a negative integer or zero. In this case the confluent hypergeometric function coincides (up to normalization) with the associated Laguerre polynomials. Thus, the quantization conditions

$$\frac{1}{4} - \frac{\beta_{1,2}}{\sqrt{-2E}} = -n_{1,2} \tag{A.12}$$

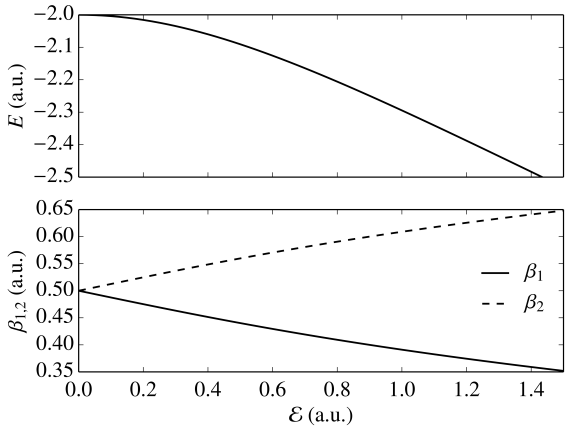

Figure A.1.: The ground state energy E of the two-dimensional Coulomb problem with an external electric field and the separation parameters β_1 and β_2 as functions of the electric field strength $\mathcal{E}$. This figure is adopted from Ref. [108].

with $n_{1,2} = 0, 1, 2, \ldots$ with have to be fulfilled. Together with the relation (A.5) the quantization conditions yield

$$E = -\frac{1}{2(n_1 + n_2 + 1/2)^2} \,, \tag{A.13}$$

$$\beta_{1,2} = \left(n_{1,2} + \frac{1}{4}\right)\sqrt{-2E} \,. \tag{A.14}$$

Normalizing $f_1(\xi)$ and $f_2(\eta)$ to unity finally gives the bound eigen states of the two-dimensional Coulomb problem $\Psi_{n_1,n_2}(\xi,\eta) = f_{1;E,n_1}(\xi) f_{2;E,n_2}(\eta)$ with

$$f_{1;E,n_1}(\xi) = \sqrt{\frac{\sqrt{-2E}}{1+4n_1}} \exp\left(-\frac{\xi}{2}\sqrt{-2E}\right) M\left(-n_1; \frac{1}{2}; \xi\sqrt{-2E}\right) \,, \tag{A.15a}$$

$$f_{2;E,n_2}(\eta) = \sqrt{\frac{\sqrt{-2E}}{1+4n_2}} \exp\left(-\frac{\eta}{2}\sqrt{-2E}\right) M\left(-n_2; \frac{1}{2}; \eta\sqrt{-2E}\right) \tag{A.15b}$$

and the energy E given by (A.13).

Taking into account the Stark effect, i. ,e., $\mathcal{E} > 0$, leads to a modification of the eigen states, of the eigen energies E, as well as of the separation constants β_1 and β_2. In this way, also the tunneling potential (A.7a) changes. The resulting values for β_1, β_2, and E can be calculated via perturbation theory [78]. In case of the ground state with $n_1 = n_2 = 0$, we get in second order

$$\beta_{1,2} = \beta_{1,2}^{(0)} + \beta_{1,2}^{(1)} + \beta_{1,2}^{(2)} \tag{A.16}$$

with

$$\beta_{1,2}^{(0)} = \sqrt{-E/8} \,, \tag{A.17a}$$

$$\beta_{1,2}^{(1)} = \int f_{1,2;E,0}(\xi) \left(\mp \frac{\xi}{4} \mathcal{E} \right) f_{1,2;E,0}(\xi) \, \mathrm{d}\xi = \mp \frac{\mathcal{E}}{4E} \,, \tag{A.17b}$$

$$\begin{aligned} \beta_{1,2}^{(2)} &= \frac{1}{\sqrt{-2E}} \times \\ &\qquad \sum_{n=1}^{\infty} \frac{1}{\frac{1}{4} - \left(n + \frac{1}{4} \right)} \left| \int f_{1,2;E,n}(\xi) \left(\mp \frac{\xi}{4} \mathcal{E} \right) f_{1,2;E,0}(\xi) \, \mathrm{d}\xi \right|^2 \\ &\approx 0.2004642410 \sqrt{-2E} \frac{\mathcal{E}^2}{E^3} \,. \end{aligned} \tag{A.17c}$$

The Eqs. (A.16) and (A.5) determine the parameters β_1, β_2, and E uniquely and the results of a numerical solution of these equations is shown in Fig. A.1.

Bibliography

[1] G. Nimtz and A. Haibel, *Zero Time Space: How Quantum Tunneling Broke the Light Speed Barrier* (Wiley, 2008).

[2] F. Hund, "Zur Deutung der Molekelspektren. I," Z. Physik **40**, 742–764 (1927).

[3] A. Slobodskyy, C. Gould, T. Slobodskyy, C. R. Becker, G. Schmidt, and L. W. Molenkamp, "Voltage-controlled spin selection in a magnetic resonant tunneling diode," Physical Review Letters **90**, 246601 (2003).

[4] T. Koga, J. Nitta, H. Takayanagi, and S. Datta, "Spin-filter device based on the Rashba effect using a nonmagnetic resonant tunneling diode," Physical Review Letters **88**, 126601 (2002).

[5] J. M. Seminario, A. G. Zacarias, and J. M. Tour, "Theoretical study of a molecular resonant tunneling diode," Journal of the American Chemical Society **122**, 3015–3020 (2000).

[6] N. C. Kluksdahl, A. M. Kriman, D. K. Ferry, and C. Ringhofer, "Self-consistent study of the resonant-tunneling diode," Physical Review B **39**, 7720–7735 (1989).

[7] G. Binnig and H. Rohrer, "Scanning tunneling microscopy-from birth to adolescence," Rev. Mod. Phys. **59**, 615–625 (1987).

[8] G. Binnig and H. Rohrer, "Scanning tunneling microscopy," Surface Science **126**, 236–244 (1983).

[9] G. J. Milburn, J. Corney, E. M. Wright, and D. F. Walls, "Quantum dynamics of an atomic bose-einstein condensate in a double-well potential," Physical Review A **55**, 4318–4324 (1997).

[10] A. Smerzi, S. Fantoni, S. Giovanazzi, and S. R. Shenoy, "Quantum coherent atomic tunneling between two trapped bose-einstein condensates," Physical Review Letters **79**, 4950–4953 (1997).

[11] D. M. Stamper-Kurn, H.-J. Miesner, A. P. Chikkatur, S. Inouye, J. Stenger, and W. Ketterle, "Quantum tunneling across spin domains in a Bose-Einstein condensate," Physical Review Letters **83**, 661–665 (1999).

[12] M. Ueda and A. J. Leggett, "Macroscopic quantum tunneling of a Bose-Einstein condensate with attractive interaction," Physical Review Letters **80**, 1576–1579 (1998).

[13] A. Messiah, *Quantum Mechanics*, Dover books on physics (Dover Publications, 1961).

[14] H. Goldstein, *Classical Mechanics* (Narosa Publishing House, 1980).

[15] J. Hilgevoord, "Time in quantum mechanics," American Journal of Physics **70**, 301 (2002).

[16] W. Pauli, *General principles of quantum mechanics* (Springer-Verlag, 1980).

[17] A. Maquet, J. Caillat, and R. Taïeb, "Attosecond delays in photoionization: time and quantum mechanics," Journal of Physics B: Atomic, Molecular and Optical Physics **47**, 204004 (2014).

[18] V. S. Olkhovsky, E. Recami, and A. J. Gerasimchuk, "Time operator in quantum mechanics," Nuov Cim A **22**, 263–278 (1974).

[19] E. Galapon, "Pauli´s theorem and quantum canonical pairs: the consistency of a bounded, self-adjoint time operator canonically conjugate to a hamiltonian with non-empty point spectrum," Proceedings of the Royal Society A: Mathematical, Physical and Engineering Sciences **458**, 451–472 (2002).

[20] A. Ivanov, "Energy-time uncertainty relations and time operators," J Math Chem **43**, 1–11 (2006).

[21] Z. Y. Wang, B. Chen, and C. D. Xiong, "Time in quantum mechanics and quantum field theory," Journal of Physics A: Mathematical and General **36**, 5135 (2003).

[22] T. Martin and R. Landauer, "Time delay of evanescent electromagnetic waves and the analogy to particle tunneling," Phys. Rev. A **45**, 2611–2617 (1992).

[23] R. Landauer and T. Martin, "Barrier interaction time in tunneling," Rev. Mod. Phys. **66**, 217–228 (1994).

[24] C. R. Leavens and G. C. Aers, "Scanning tunneling microscopy III: Theory of STM and related scanning probe methods," (Springer Berlin Heidelberg, Berlin, Heidelberg, 1996) Chap. Bohm Trajectories and the Tunneling Time Problem, pp. 105–140.

[25] C. R. Leavens, "Bohm trajectory and Feynman path approaches to the "Tunneling time problem"," Found. Phys. **229–268**, 229–268 (1995).

[26] D. Sokolovski and L. M. Baskin, "Traversal time in quantum scattering," Phys. Rev. A **36**, 4604–4611 (1987).

[27] H. A. Fertig, "Traversal-time distribution and the uncertainty principle in quantum tunneling," Phys. Rev. Lett. **65**, 2321–2324 (1990).

[28] K. L. Jensen and F. A. Buot, "Numerical calculation of particle trajectories and tunneling times for resonant tunneling barrier structures," Appl. Phys. Lett. **55**, 669–671 (1989).

[29] N. L. Balazs and A. Voros, "Wigner's function and tunneling," Ann. Phys. (N.Y.) **199**, 123–140 (1990).

[30] M. S. Marinov and B. Segev, "Quantum tunneling in the Wigner representation," Phys. Rev. A **54**, 4752–4762 (1996).

[31] H. Salecker and E. P. Wigner, "Quantum limitations of the measurement of space-time distances," Phys. Rev. **109**, 571–577 (1958).

[32] A. I. Baz', "Lifetime of intermediate states," Sov. J. Nucl. Phys. **4**, 182–188 (1967).

[33] V. F. Rybachenko, "Time of penetration of a particle through a potential barrier," Sov. J. Nucl. Phys. **5**, 635–639 (1967).

[34] A. Peres, "Measurement of time by quantum clocks," Am. J. Phys. **48**, 552–557 (1980).

[35] M. Büttiker, "Larmor precession and the traversal time for tunneling," Physical Review B **27**, 6178–6188 (1983).

[36] P. A. Martin and M. Sassoli de Bianchi, "On the theory of the Larmor clock and time delay," J. Phys. A: Math. Gen. **25**, 3627–3647 (1992).

[37] M. Büttiker and R. Landauer, "Traversal time for tunneling," Phys. Rev. Lett. **49**, 1739–1742 (1982).

[38] M. Büttiker and R. Landauer, "Traversal time for tunneling," Physica Scripta **32**, 429–434 (1985).

[39] P. Eckle, A. N. Pfeiffer, C. Cirelli, A. Staudte, R. Dörner, H. G. Muller, M. Büttiker, and U. Keller, "Attosecond ionization and tunneling delay time measurements in helium," Science **322**, 1525–1529 (2008).

[40] P. Eckle, M. Smolarski, P. Schlup, J. Biegert, A. Staudte, M. Schöffler, H. G. Muller, R. Dörner, and U. Keller, "Attosecond angular streaking," Nat. Phys. **4**, 565–570 (2008).

[41] L. V. Keldysh, "Ionization in the field of a strong electromagnetic wave," Sov. Phys.-JETP **20**, 1307–1314 (1965).

[42] G. Orlando, C. R. McDonald, N. H. Protik, G. Vampa, and T. Brabec, "Tunnelling time, what does it mean?" J. Phys. B: At., Mol. Opt. Phys. **47**, 204002 (2014).

[43] M. Klaiber, E. Yakaboylu, H. Bauke, K. Z. Hatsagortsyan, and C. H. Keitel, "Under-the-barrier dynamics in laser-induced relativistic tunneling," Phys. Rev. Lett. **110**, 153004 (2013).

[44] A. S. Landsman and U. Keller, "Attosecond science and the tunnelling time problem," Phys. Rep. **547**, 1–24 (2015).

[45] J. Zhao and M. Lein, "Determination of ionization and tunneling times in high-order harmonic generation," Phys. Rev. Lett. **111**, 043901 (2013).

[46] D. Sokolovski and L. M. Baskin, "Traversal time in quantum scattering," Physical Review A **36**, 4604–4611 (1987).

[47] E. P. Wigner, "Lower limit for the energy derivative of the scattering phase shift," Phys. Rev. **98**, 145–147 (1955).

[48] F. T. Smith, "Lifetime matrix in collision theory," Phys. Rev. **118**, 349–356 (1960).

[49] E. Yakaboylu, M. Klaiber, and K. Z. Hatsagortsyan, "Wigner time delay for tunneling ionization via the electron propagator," Phys. Rev. A **90**, 012116 (2014).

[50] E. Yakaboylu, M. Klaiber, H. Bauke, K. Z. Hatsagortsyan, and C. H. Keitel, "Relativistic features and time delay of laser-induced tunnel ionization," Phys. Rev. A **88**, 063421–063442 (2013).

[51] A. S. Landsman, M. Weger, J. Maurer, R. Boge, A. Ludwig, S. Heuser, C. Cirelli, L. Gallmann, and U. Keller, "Ultrafast resolution of tunneling delay time," Optica **1**, 343 (2014).

[52] Y. Ban, E. Y. Sherman, J. G. Muga, and M. Büttiker, "Time scales of tunneling decay of a localized state," Phys. Rev. A **82**, 062121 (2010).

[53] N. B. Delone and V. P. Krainov, "Energy and angular electron spectra for the tunnel ionization of atoms by strong low-frequency radiation," J. Opt. Soc. Am. B **8**, 1207–1211 (1991).

[54] J. Kaushal and O. Smirnova, "Nonadiabatic coulomb effects in strong-field ionization in circularly polarized laser fields," Phys. Rev. A **88**, 013421 (2013).

[55] L. Torlina, F. Morales, J. Kaushal, I. Ivanov, A. Kheifets, A. Zielinski, A. Scrinzi, H. G. Muller, S. Sukiasyan, M. Ivanov, and et al., "Interpreting attoclock measurements of tunnelling times," Nat. Phys. **11**, 503–508 (2015).

[56] A. N. Pfeiffer, C. Cirelli, A. S. Landsman, M. Smolarski, D. Dimitrovski, L. B. Madsen, and U. Keller, "Probing the longitudinal momentum spread of the electron wave packet at the tunnel exit," Phys. Rev. Lett. **109**, 083002 (2012).

[57] X. Wang, J. Tian, and J. H. Eberly, "Extended virtual detector theory for strong-field atomic ionization," Phys. Rev. Lett. **110**, 243001 (2013).

[58] B. Feuerstein and U. Thumm, "On the computation of momentum distributions within wavepacket propagation calculations," J. Phys. B: At., Mol. Opt. Phys. **36**, 707–716 (2003).

[59] R. L. Hall, N. Saad, K. D. Sen, and H. Ciftci, "Energies and wave functions for a soft-core coulomb potential," Phys. Rev. A **80**, 032507 (2009).

[60] C. W. Clark, "Closed-form solutions of the schrödinger equation for a class of smoothed coulomb potentials," J. Phys. B: At., Mol. Opt. Phys. **30**, 2517–2527 (1997).

[61] W.-C. Liu and C. W. Clark, "Closed-form solutions of the schrodinger equation for a model one-dimensional hydrogen atom," J. Phys. B: At., Mol. Opt. Phys. **25**, L517–L524 (1992).

[62] Q. Su and J. H. Eberly, "Model atom for multiphoton physics," Phys. Rev. A **44**, 5997–6008 (1991).

[63] P. B. Corkum, "Plasma perspective on strong field multiphoton ionization," Phys. Rev. Lett. **71**, 1994–1997 (1993).

[64] P. B. Corkum, N. H. Burnett, and F. Brunel, "Above-threshold ionization in the long-wavelength limit," Physical Review Letters **62**, 1259–1262 (1989).

[65] T. F. Gallagher, "Above-threshold ionization in low-frequency limit," Phys. Rev. Lett. **61**, 2304–2307 (1988).

[66] K. J. Schafer, B. Yang, L. F. DiMauro, and K. C. Kulander, "Above threshold ionization beyond the high harmonic cutoff," Phys. Rev. Lett. **70**, 1599–1602 (1993).

[67] L. A. MacColl, "Note on the transmission and reflection of wave packets by potential barriers," Phys. Rev. **40**, 621–626 (1932).

[68] E. Wigner, "On the quantum correction for thermodynamic equilibrium," Physical Review **40**, 749–759 (1932).

[69] H.-W. Lee and M. O. Scully, "The wigner phase-space description of collision processes," Found Phys **13**, 61–72 (1983).

[70] R. Landauer, "Traversal time in tunneling," Berichte der Bunsengesellschaft für physikalische Chemie **95**, 404–410 (1991).

[71] C. Leavens and W. McKinnon, "An exact determination of the mean dwell time based on the quantum clock of Salecker and Wigner," Physics Letters A **194**, 12 – 20 (1994).

[72] C. R. Leavens, "Application of the quantum clock of Salecker and Wigner to the "tunneling time problem"," Solid State Communications **86**, 781–788 (1993).

[73] P. C. W. Davies, "Quantum tunneling time," American Journal of Physics **73**, 23 (2005).

[74] H. R. Reiss, "Dipole-approximation magnetic fields in strong laser beams," Physical Review A **63**, 013409 (2000).

[75] N. Teeny, E. Yakaboylu, H. Bauke, and C. H. Keitel, "Ionization time and exit momentum in strong-field tunnel ionization," Physical Review Letters **116**, 063003 (2016).

[76] H. R. Reiss, "The tunnelling model of laser-induced ionization and its failure at low frequencies," Journal of Physics B: Atomic, Molecular and Optical Physics **47**, 204006 (2014).

[77] E. Yakaboylu, *Relativistic features and time delay of laser-induced tunnel-ionization*, dissertation, Ruperto-Carola-University of Heidelberg (2014).

[78] L. Landau and E. Lifshitz, *Quantum Mechanics: Non-relativistic Theory*, Butterworth Heinemann (Butterworth-Heinemann, 1977).

[79] A. M. Perelomov, V. S. Popov, and M. V. Terent'ev, "Ionization of atoms in an alternating electrical field," Sov. Phys.-JETP **23**, 924–934 (1966).

[80] M. Ammosov, N. Delone, and V. Krainov, "Tunnel ionization of complex atoms and of atomic ions in an alternating electromagnetic field," Sov. Phys.-JETP **64**, 1191–1194 (1986).

[81] L. Torlina and O. Smirnova, "Time-dependent analytical R -matrix approach for strong-field dynamics. I. One-electron systems," Physical Review A **86**, 043408 (2012).

[82] X. O. Pladevall and J. Mompart, *Applied Bohmian Mechanics: From Nanoscale Systems to Cosmology* (Pan Stanford, Singapore, 2012).

[83] B. I. Greene, J. F. Federici, D. R. Dykaar, R. R. Jones, and P. H. Bucksbaum, "Interferometric characterization of 160 fs far-infrared light pulses," Applied Physics Letters **59**, 893 (1991).

[84] R. R. Jones, D. You, and P. H. Bucksbaum, "Ionization of rydberg atoms by subpicosecond half-cycle electromagnetic pulses," Physical Review Letters **70**, 1236–1239 (1993).

[85] R. Beerwerth and H. Bauke, "Krylov subspace methods for the Dirac equation," Computer Physics Communications **188**, 189–197 (2015).

[86] A. Krylov, "On the numerical solution of the equation by which in technical questions frequencies of small oscillations of material systems are determined," Izv. Akad. Nauk SSSR, ser. fis.-mat. **VII**, 491–539 (in Russian) (1931).

[87] J. Demmel, *Applied Numerical Linear Algebra*, Miscellaneous Bks (Society for Industrial and Applied Mathematics, 1997).

[88] R. Beerwerth, *The Lanczos Algorithm in Relativistic Quantum Dynamics*, Master thesis, Ruperto-Carola-University of Heidelberg (2014).

[89] A. D. Bandrauk and H. Shen, "Exponential split operator methods for solving coupled time-dependent Schrödinger equations," The Journal of Chemical Physics **99**, 1185–1193 (1993).

[90] A. D. Bandrauk and H. Shen, "Improved exponential split operator method for solving the time-dependent Schrödinger equation," Chemical Physics Letters **176**, 428–432 (1991).

[91] A. D. Bandrauk and H. Shen, "Higher order exponential split operator method for solving time-dependent Schrödinger equations," Can. J. Chem. **70**, 555–559 (1992).

[92] P. Pechukas, "On the exponential form of time-displacement operators in quantum mechanics," J. Chem. Phys. **44**, 3897 (1966).

[93] S. Blanes, F. Casas, J. Oteo, and J. Ros, "The Magnus expansion and some of its applications," Physics Reports **470**, 151–238 (2009).

[94] H. F. Trotter, "On the product of semi-groups of operators," Proc. Amer. Math. Soc. **10**, 545–545 (1959).

[95] "Fftw fast fourier transform in the west," http://www.fftw.org/, accessed: August 10, 2016.

[96] C. C. Paige, "Error analysis of the Lanczos algorithm for tridiagonalizing a symmetric matrix," IMA J Appl Math **18**, 341–349 (1976).

[97] B. N. Parlett, *The Symmetric Eigenvalue Problem* (Society for Industrial & Applied Mathematics (SIAM), 1998).

[98] T. J. Park and J. C. Light, "Unitary quantum time evolution by iterative Lanczos reduction," J. Chem. Phys. **85**, 5870 (1986).

[99] M. Lein, "Streaking analysis of strong-field ionisation," J. Mod. Opt. **58**, 1188–1194 (2011).

[100] L. D. Landau and E. M. Lifshitz, *Quantum Mechanics: Non-Relativistic Theory* (Butterworth-Heinemann, Oxford, 1981).

[101] S. Weinberg, *Lectures on Quantum Mechanics* (Cambridge University Press, Cambridge, England, 2012).

[102] H. Bauke, H. G. Hetzheim, G. R. Mocken, M. Ruf, and C. H. Keitel, "Relativistic ionization characteristics of laser-driven hydrogenlike ions," Phys. Rev. A **83**, 063414 (2011).

[103] L. Mandelstam and I. Tamm, "The uncertainty relation between energy and time in nonrelativistic quantum mechanics," J. Phys. (Moscow) **9**, 249–254 (1945).

[104] J. G. Muga, R. S. Mayato, and Í. L. Egusquiza, eds., *Time in Quantum Mechanics*, Lecture Notes in Physics (Springer, Heidelberg, 2007).

[105] C. R. McDonald, G. Orlando, G. Vampa, and T. Brabec, "Tunnel ionization dynamics of bound systems in laser fields: How long does it take for a bound electron to tunnel?" Phys. Rev. Lett. **111**, 090405 (2013).

[106] P. Ehrenfest, "Bemerkung Über die angenöherte Gültigkeit der klassischen Mechanik innerhalb der Quantenmechanik," Z. Physik **45**, 455–457 (1927).

[107] M. Klaiber, K. Z. Hatsagortsyan, and C. H. Keitel, "Tunneling dynamics in multiphoton ionization and attoclock calibration," Phys. Rev. Lett. **114**, 083001 (2015).

[108] N. Teeny, C. H. Keitel, and H. Bauke, "Virtual-detector approach to tunnel ionization and tunneling times," Physical Review A **94**, 022104 (2016).

[109] G. Lantoine and R. P. Russell, "Complete closed-form solutions of the Stark problem," Celestial Mechanics and Dynamical Astronomy **333–366**, 333–366 (2011).

[110] T. Ando, A. B. Fowler, and F. Stern, "Electronic properties of two-dimensional systems," Rev. Mod. Phys. **54**, 437–672 (1982).

[111] K. Tanaka, M. Kobashi, T. Shichiri, T. Yamabe, D. M. Silver, and H. J. Silverstone, "LoSurdo-Stark effect for a hydrogenic impurity in a thin layer: Two-dimensional model," Phys. Rev. B **35**, 2513–2516 (1987).

[112] S. Glutsch, D. S. Chemla, and F. Bechstedt, "Numerical calculation of the optical absorption in semiconductor quantum structures," Phys. Rev. B **54**, 11592–11601 (1996).

[113] P. Duclos, P. Šťovíček, and M. Tušek, "On the two-dimensional Coulomb-like potential with a central point interaction," J. Phys. A: Math. Theor. **43**, 474020 (2010).

[114] A. N. Pfeiffer, C. Cirelli, M. Smolarski, D. Dimitrovski, A.-s. Mahmoud, L. B. Madsen, and U. Keller, "Attoclock reveals natural coordinates of the laser-induced tunnelling current flow in atoms," Nat. Phys. **8**, 76–80 (2011).

[115] N. Teeny, C. H. Keitel, and H. Bauke, "Salecker-Wigner-Peres quantum clock applied to strong-field tunnel ionization," arXiv:1608.02854 (2016).

[116] C. Leavens, "Transmission, reflection and dwell times within Bohm's causal interpretation of quantum mechanics," Solid State Communications **74**, 923 – 928 (1990).

[117] V. S. Olkhovsky and E. Recami, "Recent developments in the time analysis of tunneling processes," Physics Reports **214**, 339 – 356 (1992).

[118] C. R. Leavens, "The "tunneling time problem": fundamental incompatibility of the Bohm trajectory approach with the projector and conventional probability current approaches," Phys. Lett. A **197**, 88–94 (1995).

[119] M. Goto, H. Iwamoto, V. M. d. Aquino, V. C. Aguilera-Navarro, and D. H. Kobe, "Relationship between dwell, transmission and reflection tunnelling times," J. Phys. A: Math. Gen. **37**, 3599–3606 (2004).

[120] X. L. Yang, S. H. Guo, F. T. Chan, K. W. Wong, and W. Y. Ching, "Analytic solution of a two-dimensional hydrogen atom. I. Nonrelativistic theory," Phys. Rev. A **43**, 1186–1196 (1991).

[121] O. Pedatzur, G. Orenstein, V. Serbinenko, H. Soifer, B. D. Bruner, A. J. Uzan, D. S. Brambila, A. G. Harvey, L. Torlina, F. Morales, O. Smirnova, and N. Dudovich, "Attosecond tunnelling interferometry," Nat. Phys. **11**, 815–819 (2015).

[122] A. Fortun, C. Cabrera-Gutiérrez, G. Condon, E. Michon, J. Billy, and D. Guéry-Odelin, "Direct tunneling delay time measurement in an optical lattice," Physical Review Letters **117**, 010401 (2016).

[123] V. Aquilanti, S. Cavalli, and C. Coletti, "The *d*-dimensional hydrogen atom: hyperspherical harmonics as momentum space orbitals and alternative sturmian basis sets," Chemical Physics **214**, 1–13 (1997).

[124] L. Sælen, R. Nepstad, J. P. Hansen, and L. B. Madsen, "The *N*-dimensional Coulomb problem: Stark effect in hyperparabolic and hyperspherical coordinates," J. Phys. A: Math. Theor. **40**, 1097–1104 (2007).

[125] G. B. Arfken and H. J. Weber, *Mathematical Methods for Physicists* (Academic Press, Oxford, 2013).

Acknowledgments

First of all I would like to thank my supervisor Christoph H. Keitel for giving me the opportunity to do my doctoral work at his group. Additionally, I would like to thank him very much for his openness and for making it very easy to talk to him. Such a relation between a doctoral student and his supervisor is essential for a healthy research environment. Most importantly, I would like to thank him for trusting me and allowing me to follow my ideas and for giving me the necessary advice for staying on track and not getting lost.

Second, I would like to thank my second supervisor Heiko Bauke for being patient with me and supporting me throughout my doctoral studies. This work has benefited a lot from his improvement suggestions. Additionally, I would like to thank him not only for the advice he gave me for solving physics problems, but also for sharing his wide knowledge of performing numerical calculations.

I would like also to thank Enderalp Yakaboylo for the fruitful discussions that quickened my understanding of the tunnel ionization topic. I would like to thank him very much for being always there to listen to my ideas and help me develop them and for pointing out what would be interesting to research because of his wide knowledge in the topic.

I would like to thank Prof. Dr. Andreas Mielke for kindly accepting to be the second referee of this thesis. Additionally, I thank Prof. Dr. Werner Aeschbach and PD. Dr. Robert Moshammer for accepting to be on my doctoral exam committee.

I am very thankful to all my colleagues for creating the nice and friendly environment and especially for my office colleagues Niklas Michel, Jonas Gunst, Shikha Bhadoria, Anton Wöllert and Jiri Danek. I am specifically thankful to Jonas Gunst and Niklas Michel for proofreading this thesis and for the good times .

This work is dedicated to my beloved grandmother Salwa Greigiry Teeny who I am indebted to for being who I am and who passed away while I was writing this thesis.

I am very thankful to all my family (including aunts, uncles and cousins) and specifically to my father Walid, mother Bernadette, sister Pamela, brother Elias and aunt Nada for their constant support and help.

I am thankful to my roommate Enrico Brehm for interesting discussions, motivation and good times. I am also very thankful to my neighbors Walter and Helga Bernhard for always taking care of me during my stay in Heidelberg.

Last but not least, I am thankful to all my friends for good memories and times when most needed, especially to my lifelong friends Faisal Savaya, Farid Maalouf, John Teeny, Charbel Ghossain, Hassan Said and Ayman Akil not only for amazing times but also for their support especially during my doctoral studies.